2011

Viscosity of Sulfur at 4.5 GPa in the L and L' Liquid Regions

Reynold E. Sukara

Viscosity of Sulfur at 4.5 GPa in the L and L' Liquid Regions

(Spine title: Viscosity of Liquid Sulfur at High Pressure)

(Thesis format: Monograph)

by

Reynold E. Sukara

Department of Earth Sciences

Graduate Program in Geophysics

A thesis submitted in partial fulfillment
of the requirements for the degree of
Master of Science

The School of Graduate and Postdoctoral Studies
The University of Western Ontario
London, Ontario, Canada
August 2011

THE UNIVERSITY OF WESTERN ONTARIO
SCHOOL OF GRADUATE AND POSTDOCTORAL STUDIES

CERTIFICATE OF EXAMINATION

Supervisor	Examiners
Dr. Richard A. Secco	Dr. Zhifeng Ding
Supervisory Committee	Dr. Robert Linnen
Dr. Sean Shieh	Dr. Robert Shcherbakov

The thesis by

Reynold E. Sukara

entitled:

Viscosity of Liquid Sulfur at 4.5 GPa in the L and L' Liquid Regions

is accepted in partial fulfillment of the
requirements for the degree of
Master of Science

Date _____

_____
Chair of the Thesis Examination Board

Abstract

Sulfur is an element with the most complex phase diagram, both in solid and liquid form, of any element. Unique to liquid sulfur is the λ-transition, characterized by a sharp jump in specific heat and almost four orders of magnitude increase in viscosity in the narrow temperature range from 159°C to 187°C at room pressure. As a likely constituent of the Earth's outer core, the behavior of sulfur under high pressure is important as it can elucidate the potential effect of sulfur on the dynamics and the viscosity of the Earth's outer core. The viscosity of liquid sulfur was measured at 4.5 GPa and at 726°C and 1100°C, which corresponds to the L and L' liquid regions of the phase diagram, respectively. The falling sphere and quench and recover method using a 1000 ton cubic anvil press was utilized to evaluate viscosity under indicated pressure and temperatures. The results show that the viscosity of liquid sulfur decreases with temperature and is in line with the results from Terasaki et al. (2004) at lower temperatures. The presence of polymer was established at 4.5 GPa and 726°C and subsequently measured to be 17.8% using CS_2 solution method. Evidence from Raman spectroscopy on recovered samples, and experiments at isothermal temperature (800°C) and pressures ranging from 3.5 GPa to 4.5 GPa indicate that polymerization increases with temperature. Additionally, a density driven phase transition was observed at 726°C along with three distinct and time dependent phases coexisting at 1100°C. The existence of the second order liquid-liquid phase transition in liquid sulfur at reported pressure and below 726°C is discussed in the light of recent publications. Moreover, evidence supporting the proposed λ-transition, suppressed by the high pressures and shifted significantly upward in the temperature range above the melting curve is presented.

Key words: liquid sulfur, viscosity, phase transition, high pressure, high temperature, polymerization, phase equilibria, λ-transition, polymer chains, liquid-liquid phase transition

Dedication

To my greatest family,

without whose love and support I would have not accomplished this.

Acknowledgments

I would like to express my deepest gratitude to my supervisor, Dr. Richard Secco, for his guidance and leadership, which were instrumental in the success of this work. His patience and continuous support were invaluable during my graduate project.

A great success is always a reflection of a great team of people who made it happen. My colleagues and fellow students in the lab deserve a collective praise for their willingness to always help and assist, whenever necessary, and as importantly, for their positive attitude. Many thanks go to Dr. Wenjun Yong for his assistance in running the 1000 ton press. I am very grateful to Jon Jacobs for teaching me the basics of the machine shop trade and helping in fabricating parts. I would like to extend my great appreciation to Dr. Sean Shieh, to whom I am indebted for his willingness to help, selflessly dedicate his time to talk, teach and be of assistance.

My thanks go to Dr. Roberta Fleming who was willing to expedite the analysis of my experiments even when it seemed impossible. I am grateful to Dr. Zhifeng Ding for his time and willingness to help and assist when I needed his advice and instruction. Moreover, I would like to extend my great thanks to Dr. James Wisner and Dr. Robert Hudson for volunteering their lab facilities to assist in my experiments.

I would like to humbly apologize to all who I did not mention but who contributed directly or indirectly to my success; I would need many more pages to list the names of all people who deserve credit. Finally, in conclusion, I can just say that I am honored to have worked shoulder to shoulder with so many great and amazing people.

Table of Contents

List of Tables

List of Figures

List of Appendices

1. Introduction

Sulfur is an incredibly complex element whose properties and behavior under high pressure and temperature conditions still remain partially unresolved despite the continuous efforts in a wide scientific community, totaling more than a hundred years of intensive research and a vast number of scientific publications (Nehb and Vydra, 2006).

As one of the common elements in nature, sulfur has been known and used in variety of ways throughout history, from ancient Egyptians to Greeks and Romans, and had special significance in religious texts such as the Bible (Nehb and Vydra, 2006). During the period when alchemy was the most sophisticated form of science, attempts were made to study sulfur and among other things use it as a transmutation agent, but it was not until the later part of the 19^{th} and beginning of the 20^{th} century that a serious and successful attempt was made to study and understand sulfur and its properties (Kirk-Othmer, 1998).

Moreover, the significance of sulfur extends beyond its current numerous uses and applications in a wide range of fundamental industries. Sulfur played the key role in biogeochemistry in the early Earth, (see Ohmoto and Goldhaber, 1997; Canfield and Raiswell, 1999; Canfield, 2001; Farquhar and Wing, 2003; Seal, 2006; and Mojzisis, 2007, for comprehensive reviews of the subject). More recently Metrich and Mandeville (2010) investigated the sulfur evolution and dynamics in terrestrial magmas.

The primary interest of this work is broadly directed toward illuminating the role of sulfur in the evolution of planetary interiors (Hauck et al., 2006; Campbell, 2009), effects of the sulfur on the dynamics of the Earth's outer core (Campbell et al., 2007) and understanding of the extraterrestrial phenomena such as sulfur flows on Io (Lopes and

Spencer, 2007) through experimental study of viscosity of liquid sulfur under pressures of 4.5 GPa and temperatures up to 1373 K.

Sulfur is considered to be a light element constituent of the Earth's outer core (e.g. Mason, 1966; Murthy and Hall, 1970; Usselman, 1975; Ringwood, 1977; and Poirier, 1994 for comprehensive treatments of the topic). Therefore, it is important to understand its effect on the outer core dynamics and viscosity. Whereas a large body of papers has been published covering the subject of sulfur effect on the viscosity of Fe-FeS systems, no complete consensus has been reached. For example, while Terasaki et al. (2001) showed that sulfur content contributes to the decrease in viscosity of Fe-FeS melts under high pressure and temperature conditions, the work done by Funakoshi (2010) seems to indicate that the contribution of sulfur to the viscosity of Fe-FeS melts under similar conditions is almost nonexistent, which would conform to the earlier theoretical estimates of Poirier (1988). Additionally, density of Fe-FeS melts have been studied under high pressure and temperature by a number of authors (Sanloup et al., 2000; Balog et al., 2001; Secco et al. 2002; Balog et al., 2003; Chen et al., 2005; Nishida et al., 2011). Secco et al. (2002) and Balog et al. (2003) developed a method whereby a composite sphere was used as a modifiable density marker, in addition to preventing a reaction between the Fe-S alloy and the sphere, to measure viscosity. Furthermore, Nishida et al. (2008), using the sink and float method with a modifiable density marker, showed that density of liquid Fe-S alloys decrease non-linearly with increasing sulfur content at 4 GPa and 1923 K (Figure 1.1). The consequence of increasing sulfur content in Fe-S is decreased bulk modulus of the Fe-S liquid (Katayama, 1996; Chen and Yu, 2008). It has been long established that density of the Earth's core is ~10% less than the density of a core with a

pure iron composition (Birch, 1952). Additionally, there have been suggestions that the Martian core is primarily composed of Fe-S alloys (Dreibus and Waenke, 1985; Yoder et al., 2003). Such effects of sulfur on the density of Fe-S melts require further investigation, not only within liquid Fe-FeS systems, but also in pure sulfur under high temperature and conditions. The viscosity is relatively easy tool to elucidate structural properties of liquid sulfur at instrumentally achievable pressures and temperatures, with intent to infer the extent of the role sulfur plays in the Earth's outer core environment.

Moreover, the recently reported complex liquid-liquid phase transitions in FeS at extreme pressures (Sata, 2008; Ono et al., 2008; Ishikawa and Tsuchiya, 2010) could be potentially illuminated through the study of liquid-liquid phase transitions, under lower to medium pressures, which are considered to exist in liquid sulfur.

It is appropriate first to review the properties of sulfur along with the current and historical review of the literature. Note that a comprehensive review of published material on sulfur, at least in this thesis, is impossible due to the sheer volume of published material over the past century and a half. Papers which will have been left out, are omitted not because of their lack of relevance, but because of an attempt to condense the published material into a coherent, logical and space limited review.

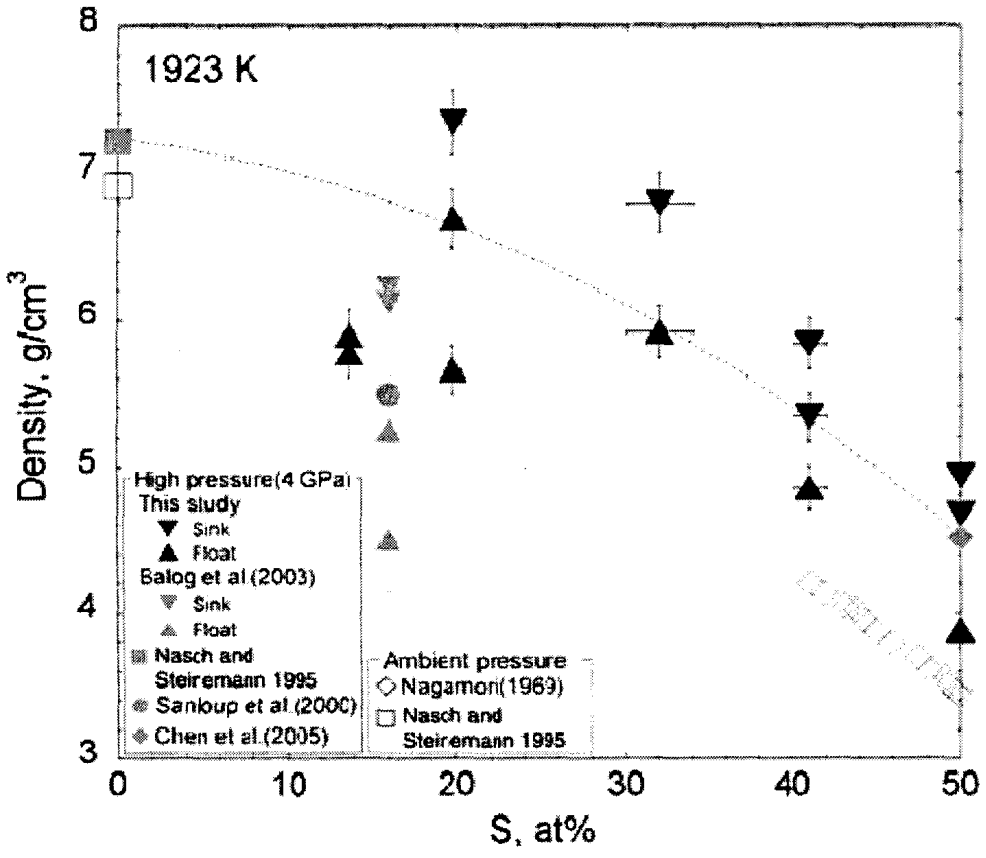

Figure 1.1: (from Nishida et al. 2008) Sulfur content versus density of liquid Fe–S diagram. Black downward- and upward-pointing triangles represent the densities of the sinking and floating of the density markers, respectively. The densities of the Fe–S samples are in the range between these triangles. The dotted bold line in this area shows the density of Fe–S liquids with various sulfur contents as monotone decreasing. The open diamonds represent the density of liquid Fe–S at ambient pressure and 1,923 K derivative (dρ/dT) of $8x10^{-4}$ from 1,473 K (Nagamori 1969). The open squares represent the density at ambient pressure and 1,923 K (Nasch and Steinemann 1995). The gray square represents the calculated values at 4 GPa and 1,923 K based on the elastic parameters of liquid Fe obtained by Nasch and Steinemann (1995). The gray circle is the density of liquid Fe84S16 at 4 GPa and 1,923 K using dρ/dT = $5.72x10^{-4}$ data for iron (Nasch and Steinemann 1995; Sanloup et al. 2000). The gray downward- and upward-pointing triangles bracket represent the density of liquid using sink/float method at 3.6–4.0 GPa and 1,923 K (Balog et al., 2003). The gray diamond represents the density of liquid FeS measured by Chen et al. (2005) at 4.1 GPa and 1,923 K using dq/dT = $8x10^{-4}$ data (Nagamori 1969).

1.1 Structure of Solid Sulfur

Sulfur belongs to the chalcogens group of elements along with selenium and tellurium (Bouroushian, 2010). Since Guy-Lussac established in1809 that sulfur is an element, much effort has been devoted to resolve and understand the structure of sulfur and subsequently the structure of its many allotropes following the discovery of the monoclinic allotrope by Mouthmann in 1890 (Smith and Holmes, 1905). Atoms of sulfur

have an s^3p^4 outer shell electron configuration thus enabling S-S bonds to be formed from two unpaired electrons in the $3p$ orbitals. Based on that configuration the optimum bond angle should be 90°, however experimentally observed values are 106°, which can be explained by repulsion of non-bonded sulfur atoms or possible *s-p* hybridization (Tuinstra, 1964; Steudel and Eckert, 2003). The same reasoning can therefore explain an absence of non-planar configuration in S-S chains, which are experimentally observed as a three-dimensional zig-zag configuration (Tuinstra, 1964).

At room temperature and pressure conditions, the most stable crystalline form of pure sulfur is the orthorhombic structure, consisting of crown shaped S_8 ring molecules (Figure 1.2) with an average bond length of 2.037 Å (Abrahams, 1955). Rettig and Trotter (1987) further refined the orthorhombic S_8 sulfur lattice parameters. The melting temperature of orthorhombic sulfur allotrope is about 115°C at room pressure at 1 atm. One should note the intentional use of the word about, hereforth used when the literature on the subject offers varying values that might be due to a multitude of factors such as experimental conditions and instrumental errors, the presence of impurities and thermal and aging history of the studied samples, all of which contribute to the behavioural complexities of this element.

The reversible transformation of the orthorhombic structure to monoclinic geometry occurs at about 95°C and monoclinic sulfur allotrope (Figure 1.3) is stable above this temperature until its melting point of 119°C and 1 atm (Sands, 1965). Further refinement of the structure of monoclinic sulfur was done by Templeton et al. (1976), where they obtained the value for average bond length of 2.045Å.

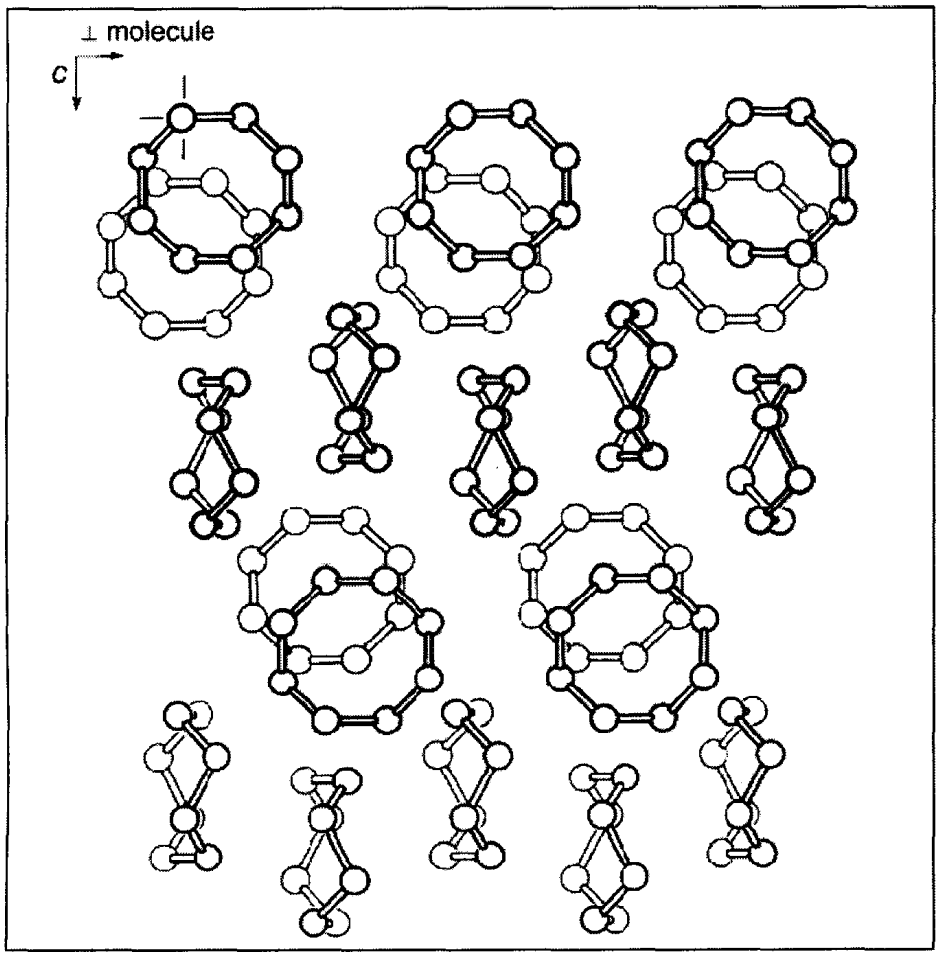

Figure 1.2: The crystal structure of orthorhombic S_8 projected parallel to the c-axis showing the so-called 'crankshaft' structure. The direction of the a- and b-axis of the crystal includes an angle of about 45° to the mean plane of the molecules in each layer (Donohue, 1974)

Among all known elements in solid form, sulfur has the highest number of allotropes. Most of the allotropes of S are highly unstable and difficult to synthesize because of high sulfur reactivity or because of necessity to employ high pressures and temperatures. Recently Steudel and Eckert (2003), in their comprehensive review of sulfur allotropes, summarized properties of thirty well known allotropes of sulfur, including both high and low pressure structures.

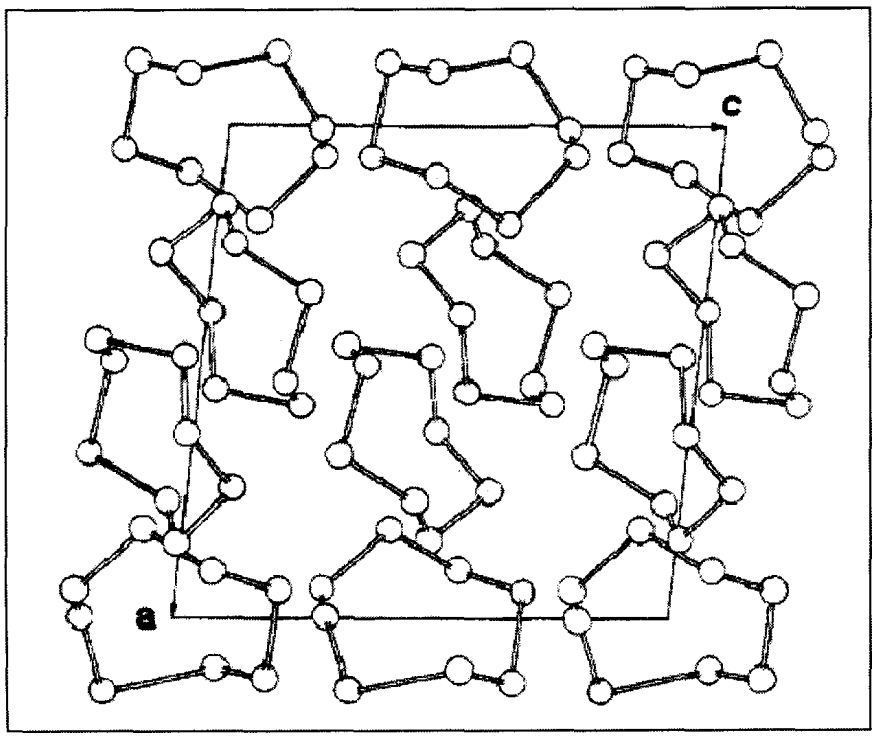

Figure 1.3: The structure of monoclinic sulfur (from Sands, 1965).

Two different types of allotropes can be distinguished: 1) *Intramolecular* allotropes, characterized by distinct chemical bonding of sulfur atoms and resulting in different molecular species; and 2) *Intermolecular* allotropes, which have different lattice structure within crystals.

The nomenclature for most allotropes still lacks a general consensus, however this work adopted the classification from Meyer (1976) as reproduced in Table 1.1. Detailed structural and physical properties, melting points, solubilities and preparation techniques of some of the main sulfur allotropes are reviewed at length by Steudel and Eckert (2003), while extensive spectral studies were conducted by Eckert and Steudel (2003).

Table 1.1: From Meyer (1976)

TABLE I. Guide to Nomenclature

Name	Synonyms	Molecular species	Designation used in this review	Section or ref
α (alpha)	Rhombic, orthorhombic, Muthmann's I	Cycloocta-S	Orthorhombic-α	III.B
β (beta)	Monoclinic I, Muthmann's II, prismatic	Cycloocta-S	Monoclinic-β	III.B
γ (gamma)	Monoclinic II, Muthmann's III, nacreus, mother-of-pearl, Gernez	Cycloocta-S	Monoclinic-γ	III.B
δ (delta)	Monoclinic III, Muthmann's IV, γ-monoclinic	Cycloocta-S	Allotropes of S_8	6, 7
ε (epsilon)	Engel, Aten, rhombohedral, monoclinic Engel	Cyclohexa-S	Rhombohedral	6, 7
ζ (zeta)	5th monoclinic, Korinth	Cycloocta-S	Allotrope of S_8	6, 7
η (eta)	4th monoclinic, Korinth	Cycloocta-S	Allotrope of S_8	6, 7
θ (theta)	Tetragonal, Korinth	Cycloocta-S	Allotrope of S_8	6, 7
ι (iota)	Erämetsä	Cycloocta-S	Allotrope of S_8	6
κ (kappa)	Erämetsä	Cycloocta-S	Allotrope of S_8	6
λ (lambda)		Cycloocta-S	Cycloocta-S_8	6
μ (mu)	(a) Insoluble (b) Polymeric	Catenapoly-S	Solid or liquid Polymeric-S	III.C IV.B
ν (nu)	μ	Mixture	Solid polymeric	III.C
ξ (xi)	Triclinic, Korinth	Cycloocta-S	Allotrope of S_8	6, 7
ο (omicron)	Erämetsä	Cycloocta-S	Allotrope of S_8	6, 7
π (pi)	(a) Aten, Erämetsä (b) Catenaocta-S	Ring mixture	Frozen liquid	IV.A 6
ρ (rho)	Aten, Engel	Cyclohexa-S	Cyclohexa-S	III.B
τ (tau)	Erämetsä	Cycloocta-S	Allotrope of S_8	
φ (phi)	Fibrous	Mixture	Fibrous	III.C, D
φ (phi)	Fibrous, plastic	Polycatena-S	Fibrous	III.C, D
χ (chi)	Plastic	Mixture	Polymeric	III.C
ψ (psi)	Fibrous	Mixture	Fibrous	III.C, D
ω (omega)	Insoluble, white, Das supersublimation	Mixture	Polymeric	III.C
m	Triclinic	Cycloocta-S	Allotrope of S_8	6
n	μ		Solid Polymeric	III.C
Aten	See ε, ρ	Cyclohexa-S	Rhombohedral	III.B
Braun	See μ	Mixture	Solid, Polymeric	6
Engel	See ε, ρ	Cyclohexa-S	Rhombohedral	III.B
Korinth	See ξ, η, θ, ζ	Cycloocta-S		6
Muthmann	See α, β, γ, δ	Cycloocta-S		6
Schmidt	See orthorhombic-S_{12}	Cyclododeca-S		III.B
Amorphous	ω, μ	Mixture	Solid, polymeric	III.C
Cubic	High pressure cubic plastic		High pressure forms	III.D
Fibrous	ψ, φ, phase II	Catenapoly-S	Fibrous	III.C, D
Insoluble	"Crystex," supersublimated	Mixture	Insoluble	III.C
Laminar	Phase I, white, ω, μ, χ	Catenapoly-S	Laminar	III.C, D
Metallic	High pressure metallic	?	High pressure forms	III.D
Photosulfur	Insoluble	?	Photosulfur	VI
Black	(a) Skjerven	?	Quenched liquid	III.E
	(b) Rice, Schenk	Mixture	Trapped vapor	
Brown	Maltsev	Mixture	Trapped vapor	III.E
Green	Rice	Mixture	Trapped vapor	III.E
Orange	Erämetsä			6
Purple	Rice	Mixture	Trapped vapor	III.E
Red	(a) Rice	Mixture	Trapped vapor	III.E
	(b) Erämetsä	Mixture	Trapped vapor	III.E
Violet	Rice	Mixture	Trapped vapor	III.E
E, F, G	Erämetsä's red	Mixture	Allotrope of S_8	6
I, K, L, M	Orange			6

1.2 Liquid Sulfur

Liquid sulfur exhibits unique properties among all other elemental melts (Hosokawa et al., 1994). The high potential for different liquid structures is not an unreasonable expectation given the very large number of solid allotropes. The color of the liquid is pale yellow from its atmospheric melting temperature up to 159°C, after which it changes and acquires a progressively deeper tone of red, attaining almost a dark red color at the boiling point of 445°C (Steudel, 2003). At 159°C there is a sharp increase in viscosity, reaching a maximum at 187°C (Doi, 1963). Following the maximum, viscosity gradually decreases until the boiling point. However, the topic of viscosity will be discussed separately in more detail in the upcoming sections. There is an associated sharp peak in heat capacity at 159°C, hence this point is termed in the literature as the lambda (λ) transition and has been known since Lewis and Randall (1911) reported it. A review of subsequent investigations on the λ-transition is given by Meyer (1976).

Upon heating liquid sulfur, the density at one atmosphere and 120°C changes from 1.802 g/cm^3 to 1.573 g/cm^3 at 440°C, however the λ-transition coincides with the discontinuity in that trend (Figure 1.4). The density at 159°C (432K) is 1.763 g/cm^3 (Patel and Borst, 1971; Zheng and Greer, 1992). Mathematical modeling by Kennedy and Wheeler (1983) utilizing a lattice solution model gave results on density anomaly in liquid sulfur, that are similar to the experimental observations. The color of liquid sulfur was investigated by Meyer et al. (1971), who measured visible absorption of liquid up to 700°C and compared it to the absorption spectra of individual allotropes (Figure 1.5). They concluded that the temperature dependence of the color of liquid sulfur is not caused by thermal broadening of the S_8 spectrum alone, but is also a result of the overlap and

absorption of combined sulfur species contained in the liquid, primarily S_8, polymer, S_3, S_4 and S_6. However, they acknowledged that the molecular and polymeric composition of liquid sulfur has not been completely resolved.

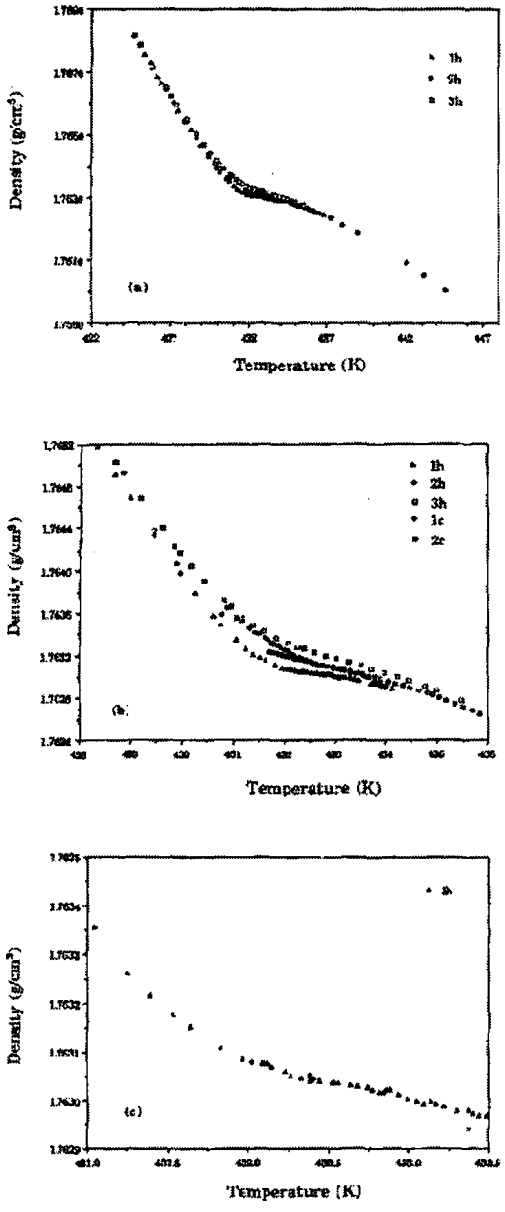

Figure 1.4: Density ρ of liquid sulfur at 1 atm as a function of temperature near the polymerization transition at *Tp* = 432 K. (a) Data from all three heating runs and over the full temperature range. Note the reproducibility far from *Tp*, and the shifts of the density near *Tp*. (b) Data from all three runs, heating and cooling, in the temperature range near *Tp*. Note again the shifts on cycling. Note also the absence of a minimum *in* ρ(T) (c) Data from run 1h, the "best" data set, very near *Tp*. Note again that the slope changes, but there is no minimum (from Zheng and Greer, 1992).

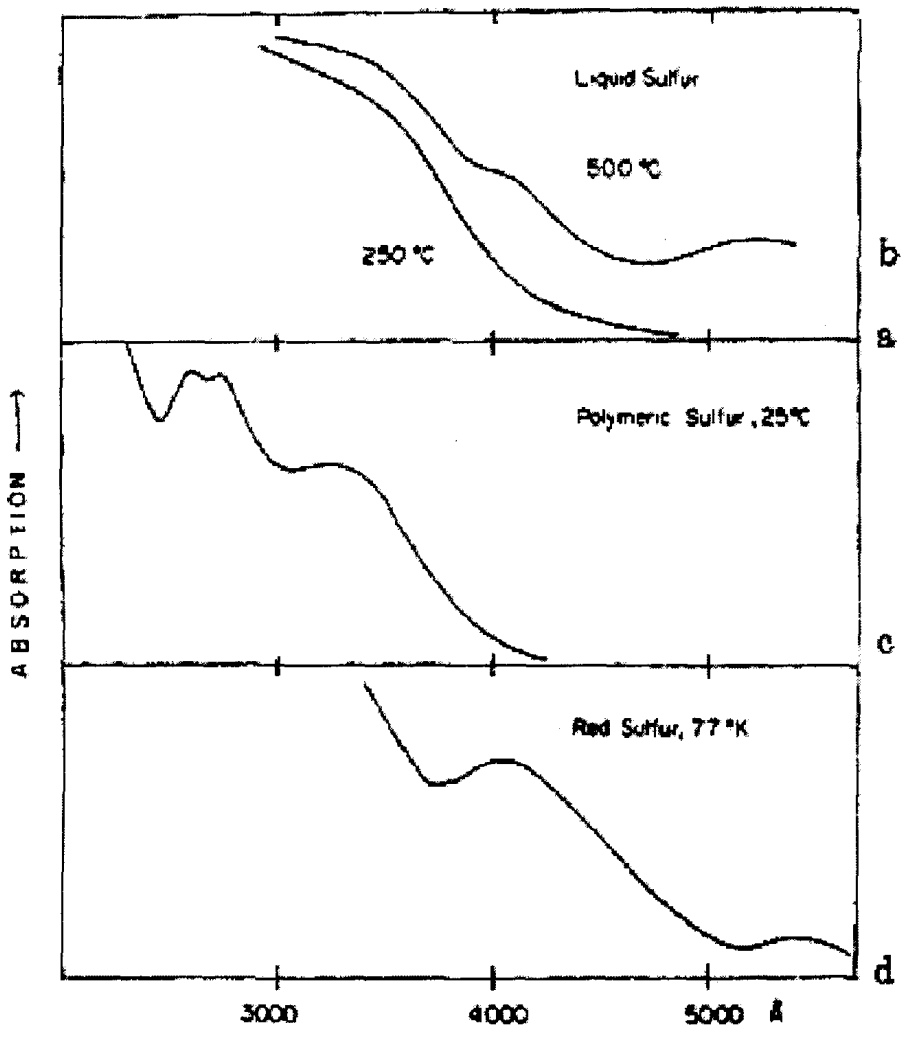

Figure 1.5: Absorption spectra of sulfur samples: (a) liquid sulfur film at 250°C; (b) liquid sulfur film at 500°C; (c) polymeric sulfur at 25°C; and (d) red sulfur glass prepared by quenching boiling liquid to 77°K (from Meyer et al., 1971).

Vezzoli et al. (1976) investigated structural changes in liquid sulfur at 1 atm that were associated with reversible color changes and reported that an increased polymer concentration corresponds with color reddening.

The structure of liquid sulfur has proven challenging to resolve accurately. Initial understanding was that between the melting point of about 119°C and 159°C, liquid

sulfur is composed of S_8 rings (Winter et al., 1988). However, new evidence suggests that a small amount of polymer along with other allotropes (generally termed S_π), is an integral part of the melt from the onset of melting (Steudel, 2003). S_π is defined as a mixture of soluble (in CS_2) sulfur rings other than S_8. Early attempts to quantify S_π (Schenk and Thümmler, 1959) were not accurate enough as they relied on an incorrect cryoscopic constant of equilibrium sulfur melts determined by Beckmann and Platzmann, (1918).

However, subsequent work by West (1959) reported the S_π content at the three phase co-existence point (115.2°C) of 4.8% of the total content. Moreover there is a positive correlation of S_π with temperature (Wiewiorowski et al., 1968). Many authors attempted to resolve the structure and exact nature of S_π (Wiewiorowski and Touro, 1966; MacKnight et al., 1967), however, it was only after Sπ was isolated physically, that Harris (1970) reported the existence of S_6 and S_7 molecules in addition to S_8 rings, and Schmidt and Block (1967) observed the presence of S_{12} rings, that structure of S_π could be unraveled.

Another critical component of liquid sulfur, principally above 159°C is polymeric sulfur or S_μ. While present in small percentages below the λ-transition, the polymer content increases with temperature (Steudel, 2003). However, the consensus on the maximum polymer content before the boiling point has not been reached. Generally accepted amounts of polymer are reported in Table 1.2:

Table 1.1: Compiled from the review by Steudel (2003)

Temperature (C°)	S_μ Polymer content (%)	Author
130	1	(Schenk, 1959)
160	4.5	(Schenk, 1959)
350	37	(Schenk, 1955)

However, the values reported by Koh and Klement (1970) are significantly higher and reach 55 wt% of polymer between 289°C and 295°C. They also noted that duration of heating results in slightly more polymer. Their additional experimental work suggests that for melt equilibrium to be reached, the target temperature must be maintained for at least one hour at atmospheric pressure (Koh and Klemment, 1970). Figure 1.6 illustrates the divergence among reported results. However, there is general consensus that the polymer fraction becomes stable above 300°C.

Often there is confusion in the literature between S_μ and S_∞ (Steudel, 2003) and while technically these terms are the same thing, S_∞ denotes the polymer content in the melt and S_μ refers to insoluble quenched polymeric solid. Such nomenclature will be adopted in the rest of this work. The most reliable way to extract insoluble polymeric structure is in a CS_2 bath, preceded by rapid quench from the liquid state above 159°C as described by Schenk (1955) and Koh and Klement (1970). Due to its low thermal conductivity, quenching liquid sulfur in water or air is not the most optimal way to preserve its true polymer content (Steudel, 2003).

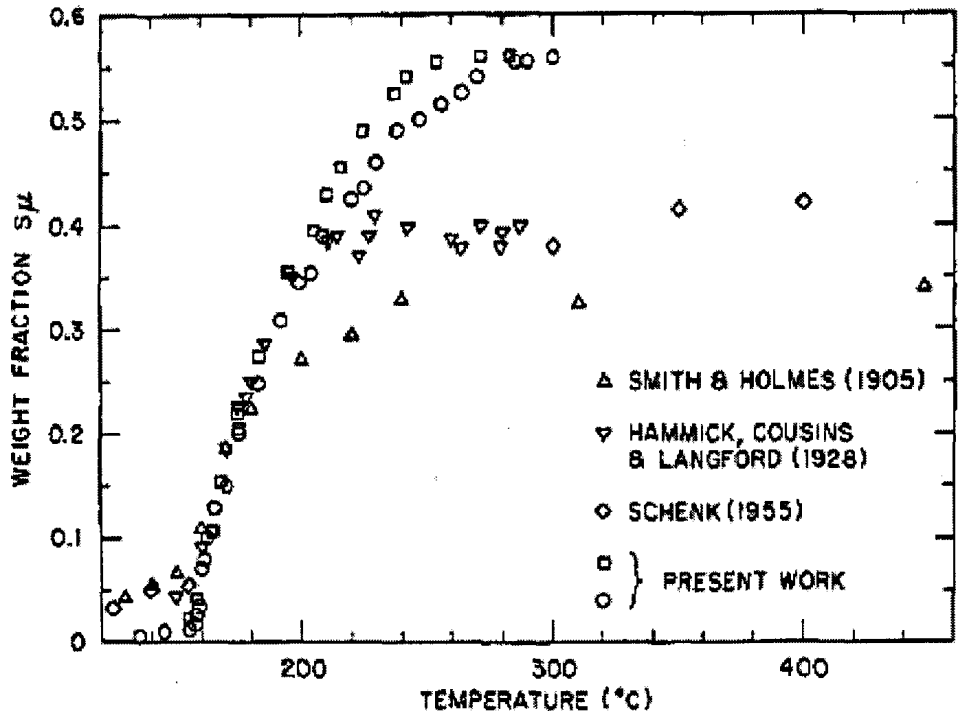

Figure 1.6: Weight fraction of insoluble sulfur (i.e. polymer) vs. temperature from various investigations using different quenching methods. Note the difference between neighbouring circles which represent heating for 15 min. and neighbouring squares which represent heating for 3 hours (from Koh and Klement, 1970).

The best understanding of the polymerization enigma points to free radicals that originate from ring opening of S_6 and S_8 molecules and the accompanying disociation energy, as a main initiator of the polymerization process (Steudel, 2003). Older work such as (Semlyen, 1971) considered polymer structure as primarily composed of extremely large rings, however with the help of electron spin resonance (ESR) it was established that the polymer consists of chain like structures (Koningsberger, 1971).

Additionally, Sakaguchi and Tamura (2007), reported that polymerization can occur well below the polymerization temperature (T_p) of 159°C, which is generally referred to as the λ-transition, just by illuminating liquid sulfur with a pulsed laser, with power above 60 mJ cm^{-2}. Electrical conductivity of liquid sulfur is proportional to temperature with

notable anomalous behavior around 170°C where conductivity is at minimum, coincidently corresponding to the region of the highest viscosity of the melt. A brief review of the electrical conductivity of sulfur is presented by Steudel (2003).

1.2.1 Theories of Polymerization and λ-Transition in Liquid Sulfur

Since the second part of the 20th century, several theoretical works have attempted, with various degrees of success to explain the polymerization of liquid sulfur. The difficulty is that there exists the equilibrium between polymeric and monomeric units throughout the whole temperature range of liquid sulfur and complete polymerization does not occur. In fact, the polymer fraction increases throughout the temperature range, with more pronounced polymer formation around the λ-transition only to be leveled off around 300°C (Koh and Klement, 1970; Biermann et al., 1998).

From a thermodynamic point of view, the nature of polymerization has also been a contentious issue. Early studies on sulfur pointed toward the polymerization as a discontinuous first order phase transition (Ivin, 1974). This, for the reasons that are discussed elsewhere (Greer, 1998), has been an erroneous conclusion, and Wheeler et al. (1980) predicted that polymerization in liquid sulfur is a continuous second order transition. They also reported that their model predicts polymers in the form of long chains, rather than in large loops. Moreover, they showed that the earlier theories, some which will be commented on in more detail further in the text, such as (Scott, 1965; Tobolsky and Eisenberg, 1962), rather than imprecise, are essentially equivalent to the mean field limit of the n→0 limit of the n-vector model of magnetism in a small magnetic

field, where n denotes the dimension of the order parameter of the phase transition. "*...It was thus shown that polymerization transitions could be treated as critical phenomena described by non-classical exponents and the Tobolsky-Eisenberg model is the mean-field limit if the n→0 model*" (Kalampounias et al., 2003a). A full description and mathematical representation of this model is given in Wheeler and Pfeuty (1981). Figure 1.7 compares some of the theoretical models with experimental data.

The development of the equilibrium polymerization theory by Tobolsky and Eisenberg (1959) was a simple, and the best at the time, model treating sulfur polymerization. The highlight of the equilibrium polymerization of sulfur is its successful prediction of the temperature dependence of the degree of polymerization. However, it must be noted that that the success of that treatment is built on the foundations of Gee (1952) and Fairbrother et al. (1955), whose pioneering work resulted in evaluation of the standard enthalpy (H^0) of sulfur at 17 kJ mol^{-1}, based on crude data from older literature and were the first to tackle theoretical aspects of sulfur polymerization. The basic concept of equilibrium polymerization of liquid sulfur considers that a reversible polymerization inception and propagation occurs in the presence of an initiator and directly depends on two equilibrium constants. Those constants are in turn fully dependent on temperature. The full mathematical treatment of the theory can be reviewed in Tobolsky and Eisenberg (1959). While several slightly improved polymerization theories, based on a variety of formalisms such as the spin model of phase transition, kinetic models and chain clustering appeared subsequently over the years, they all have their foundation in the construct of original equilibrium polymerization.

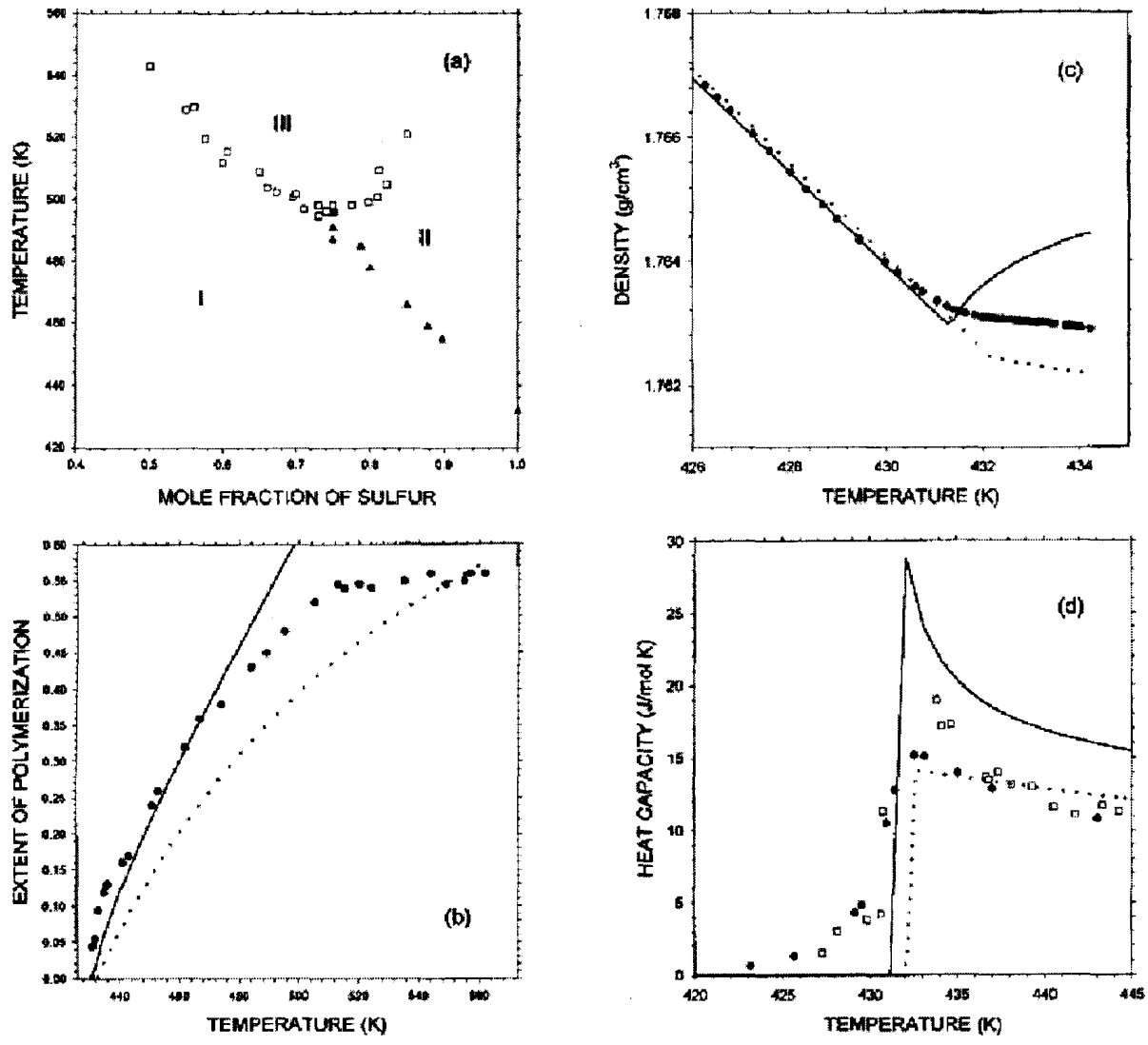

Figure 1.7: Equilibrium polymerization of sulfur: Comparison of experimental data with theoretical models for (a) the phase diagram in a solvent (Larkin et al. 1967; Anderson and Greer, 1988), (b) the extent of polymerization (Koh and Klement, 1970) (c) the mass density (Zheng and Greer, 1992) and (d) the heat capacity (Fehr et al., 1971; West, 1959). For (a) the solid triangles are points on the polymerization line; the open squares are points on the coexistence curve; and the solid square is the experimentally determined liquid-liquid critical point. Region I is a homogeneous mixture of monomeric sulfur in the solvent; region II is a homogeneous mixture of monomeric sulfur in chemical equilibrium with polymeric sulfur, both in the solvent; regions I and II meet at the polymerization line. Region III is a miscibility gap, with two coexisting phases. In (b)-(d), the symbols are the data, the dotted lines represent the mean field model, and the solid lines represent the non-mean field ($n \rightarrow 0$) model (from Greer, 1998).

However, the "living" polymer theory, originally developed by Schwartz (1956) to deal with polymerization of organic molecules, has been further improved and modified through integration of a Flory-Huggins type lattice model which incorporates chain stiffness, variable initiator concentration and polymer-solvent interaction (Dudowicz et al., 1999).

This theoretical treatment of polymerization has the clearest advantage among previous treatments, and when adapted to sulfur, it describes fairly successfully the dynamics of polymer propagation and the λ-transition throughout the whole temperature range of the liquid (Kalampounias et al., 2003b). Nevertheless, this is just a more complex and sophisticated version of equilibrium polymerization and a type of mean field theory. Furthermore, "rounding" refers to smearing of sharp changes observed in the temperature dependence of various physical properties, especially around the λ-transition. The behavior of specific heat in the lattice model of "living polymerization" (Figure 1.8), compelled Kalampounias et al (2003b) to claim that polymerization is not a second order phase transition, contrary to the general consensus in the modern literature. The reason for this behavior is the finite initiator concentration; however, when the initiator presence is sufficiently small, there is a resemblance to a second order phase transition.

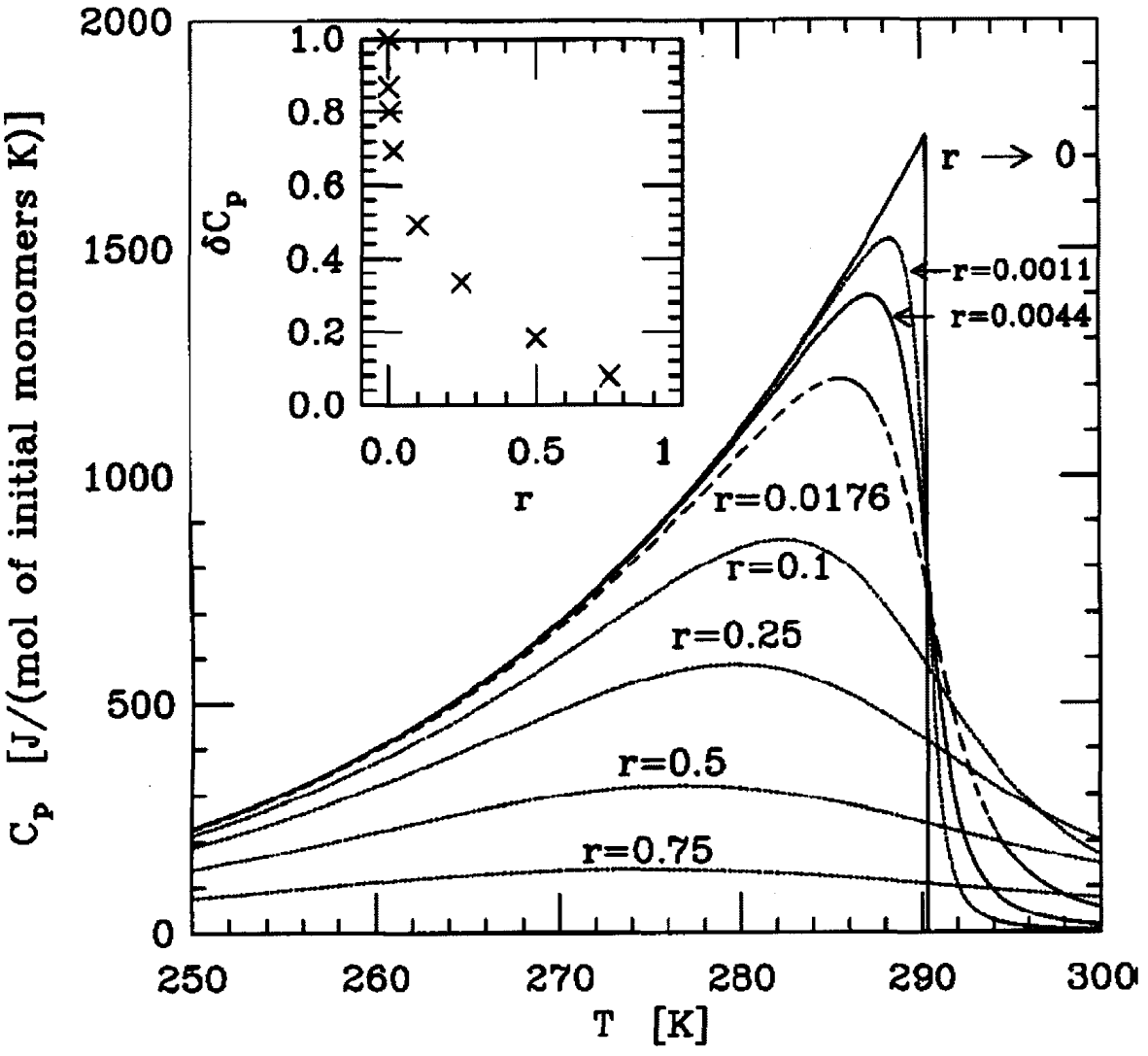

Figure 1.8: Temperature dependence of the specific heat C_P for a living polymer solution over a range of initiator concentrations r and for a fixed initial monomer concentration φ^0_m=0.15. Observe the decrease of the ratio $\delta\ C_P=C_P^*(r)/C_P^*(r\rightarrow 0^+)$ with increasing r. (from Dudowicz et al., 1999).

Kozohevnikov et al. (2004) consequently claim that polymerization is not a second order transition based on the measurement of sound velocity (c) and acoustic absorption of liquid sulfur. From the calculation of sound velocity at zero frequency Anisimov et al. (1987) reported a sharp minimum of c just below T_p; such behavior is expected to be observed experimentally. Based on the deviation of the experimental results from those predicted by the theoretical calculation that assumed a second order transition in liquid

sulfur, Kozhevnikov et al. (2004) embraced the DFD-model (aforementioned lattice model of "living" polymerization by Dudowicz, Freed and Douglas, 1999), dismissing the possibility of a second order phase transition. However, caution should be exercised with such dismissive assumption especially in the case of liquid sulfur, where many physical properties are affected at the onset of λ-transition. Before the dynamics of λ-transition is reviewed in more detail, some recent commendable developments in modeling of sulfur polymerization, aided by ever increasing computational power, are mentioned.

Ballone and Jones (2004), using Monte Carlo simulation with a density functional based force field, investigated equilibrium polymerization of liquid sulfur, reproducing qualitative changes in simulated liquid. They obtained thermodynamic properties in close agreement with experimental data. Along with previous work by the same authors computational models are useful tools in an attempt to unravel liquid sulfur polymerization.

The peculiar behavior of liquid sulfur around the λ-transition, even after almost one hundred and fifty years of investigation, remains somewhat unclear. The origin of the term λ-transition comes from the particular shape of the specific heat curve about 159° C (West, 1959), and not because of the behavior of the viscosity curve, to which many authors erroneously refer. The sharp change in thermodynamic properties (West, 1959), density (Zheng and Greer, 1992) and optical and electrical properties (Vezzoli et al., 1976; Baker and Davey, 1978; Hosokawa et al. 1994), without mentioning an anomalous behavior of viscosity which will be discussed further in the text, have not been explained theoretically to a satisfactory degree. The recent trend in literature is leaning toward

measurement of the acoustical properties by different techniques (Monaco et al., 2005). The prime reason for the focus on the acoustical properties is an inability of neutron scattering to illuminate in more detail, the structure and dynamics of liquid sulfur at and beyond the λ-transition, as exemplified in Descotes et al. (1993). The Raman spectra can only resolve the presence (Kalampounias et al., 2003a,b) and potentially the fraction of the polymer, but it cannot resolve the structural complexities.

Brillouin scattering of liquid sulfur up to 200°C was used in the investigation of the λ-transition by Alvarenga et al. (1996), and while polarized spectra show no significant change near the λ-transition, a depolarized spectrum exhibits a maximum in the same narrow region and coincides with the viscosity anomaly. The importance of the Brillouin scattering lies in the fact that it probes excitations and fluctuations compatible to those of visible light with high frequencies. Additionally, Brillouin experiments can determine the dynamic structure factor, which is essential in evaluation of the sound velocity in the liquid. The aforementioned authors noted some discrepancy between their subsequent calculation of sound velocity and the one experimentally observed, in the available literature. Kozhevnikov et al. (2004) took an ad hoc approach based on the existence of divergence of experimental (Olson et al., 2002) and calculated data for sound velocity, and implied failure in the Maxwell's relations in liquid sulfur around the λ-transition. A second order phase transition based calculation predicts the minima in sound velocity at the λ-transition, while the literature contains reports of experimentally observed velocity dependence on temperature and does not comply with Navier-Stokes hydrodynamics treatment for sound absorption (α) given below.

$$\alpha = [(4\eta/3 + \xi) + \kappa (C_v^{-1} - C_p^{-1})]\, \omega^2/2\rho c^3 \qquad (1.1)$$

where η and ξ are coefficients for the shear and bulk viscosities, respectively, κ is the coefficient of thermal conductivity, C_v and C_p are isochoric and isobaric heat capacities, respectively, and $\omega=2\pi f$ is the angular frequency (Kozhevnikov et al., 2004).

Koshevnikov et al. (2004) thus exploit this contradiction and consequently suggest that absence of propagation of transverse sound waves through liquid sulfur signifies directly that sulfur is not a viscoelastic fluid, while excluding the possibility for the existence of a second order phase transition.

The problem with that approach was addressed by Monaco et al. (2005). They analyzed the data from a powerful inelastic x-ray scattering (IXS) study of the high frequency acoustic dynamics of liquid sulfur across the λ-transition. Measured values of the energy position of the Brillouin peak clearly indicate presence of the viscoelastic liquid, directly opposing reported results by Koshevnikov et al. (2004). This transition lies between the MHz frequency range obtained elsewhere by ultrasound and the THz one provided by Monaco et al. (2005). Additionally, there is an observed non-linear dependence of both high frequency and adiabatic sound velocity on temperature. The results of Monaco et al. (2005) are of critical relevance for the work reported in this thesis and conceivably beyond, as it is imperative to resolve the acoustic absorption with desired resolution, especially about and above the λ-transition, as it can be directly related to kinematic land shear viscosity. Thus, the reader can perhaps appreciate a rather disproportionate review of the above topic. Furthermore, longitudinal sound velocity reported by Monaco et al. (2005) is 40% higher than the values from ultrasonic measurements. Because of the

existence of a rubbery plateau[1] the transverse sound velocity is quite slow (on the order of 10 m/s) which would explain why it has not been detected by Koshevnikov et al. (2004). Consequently, Monaco et al. (2005) propose the existence of an additional low frequency relaxation, thus avoiding failure of the Maxwell's relations in the liquid sulfur system and subsequently giving credence again to Navier-Stokes theory for polymeric solutions, briefly mentioned in the text above. This would also imply that polymeric sulfur contains entangled chains of high molecular weight. The consequent entanglement coupling implies the existence of both slow and fast relaxation process. The proposed low frequency relaxation was indeed confirmed by Scopigno et al. (2007), who reported the evidence of previously unobserved 1-10 kHz frequency range relaxation, utilizing infrared photon correlation spectroscopy (IRPCS). Consequently, on the basis of Maxwell relations, there is definite dependence of viscosity on relaxation time in liquid sulfur, which indeed reconciles a previously contentious issue (Monaco et al., 2005). Figure 1.9 shows the average relaxation time and the chain stretching parameter, both of which correspond closely to structural and viscosity changes in liquid sulfur at the λ-transition. More importantly, this new discovery may be analogous to the behavior generally observed in a dense solution composed of uncross-linked polymers (Scopigno et al., 2007)). The true implication of this revelation for the work presented in this thesis will become apparent much further in the text, especially under high pressure and temperature conditions.

[1] rubbery plateau - a temperature region where the high frequency and low frequency relaxation processes take place (Monaco et al., 2005)

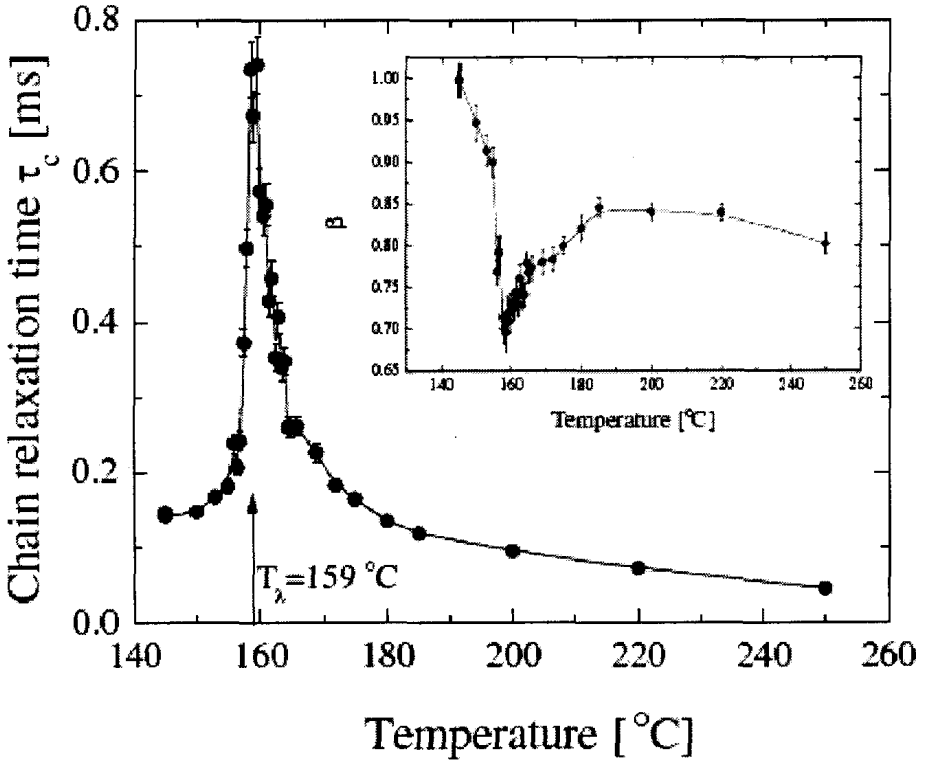

Figure 1.9: Temperature behavior of the chain relaxation, as measured by IRPCS. The line is a guide for the eye. Inset: *T* dependence of the chain stretching parameter (from Scopigno et al., 2007).

1.2.2 High Pressure and Temperature Phase Diagram and Studies of Sulfur

Since the pioneering high pressure experiments on sulfur by Bridgman (1938), high pressure research has advanced greatly and it is a critical investigative tool in material and planetary sciences alongside many other disciplines. A summary of the progress and current advances in high pressure is given by Ito (2007) and Shen et al. (2010).

While sulfur has been studied recently at extremely high pressures using a diamond anvil cell by several authors (Luo et al., 1991; Fujihisa et al., 2004; Degtyareva et al., 2005; Degtyareva et al., 2007), the lower pressure and temperature region, especially from 3-10 GPa, still remains incompletely resolved despite the work by Nagata et al. (1992), Orgzall and Lorenz (1994), Eckert et al. (2000), and Crapanzano et al. (2005). That fact

alone along with an extremely complex and unpredictable behavior of sulfur is illustrated by an absence of consensus on the complete and refined phase diagram of sulfur between 3 and 10 GPa (Figure 1.10). A significant contribution by Brazhkin et al. (1991) and Brazhkin et al. (1999) toward that goal must be duly recognized; however, the resolution of phases and phase transitions remains to be significantly improved (Figure 1.11).

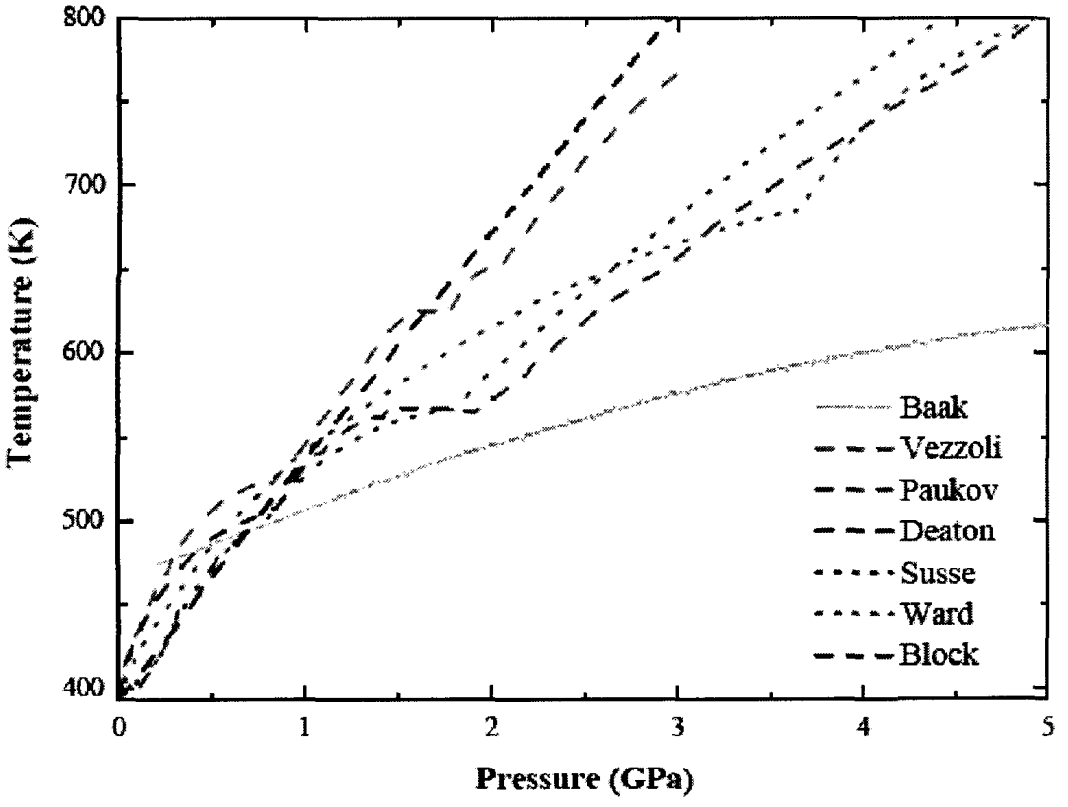

Figure 1.10: Reported melting curves of sulfur. (violet, dot) Susse, Epain and Vodar (1964); (green, dash-dot) Baak (1965); (blue, dash) Deaton and Blum (1965); (dark green, dash) Paukov, Tonkov and Mirinski (1965); (dark green, dot) Ward and Deaton (1967); (orange, dash) Vezzoli, Dachille and Roy (1969c); (red, dash) Block and Piermarini (1973) (from Crapanzano, 2005).

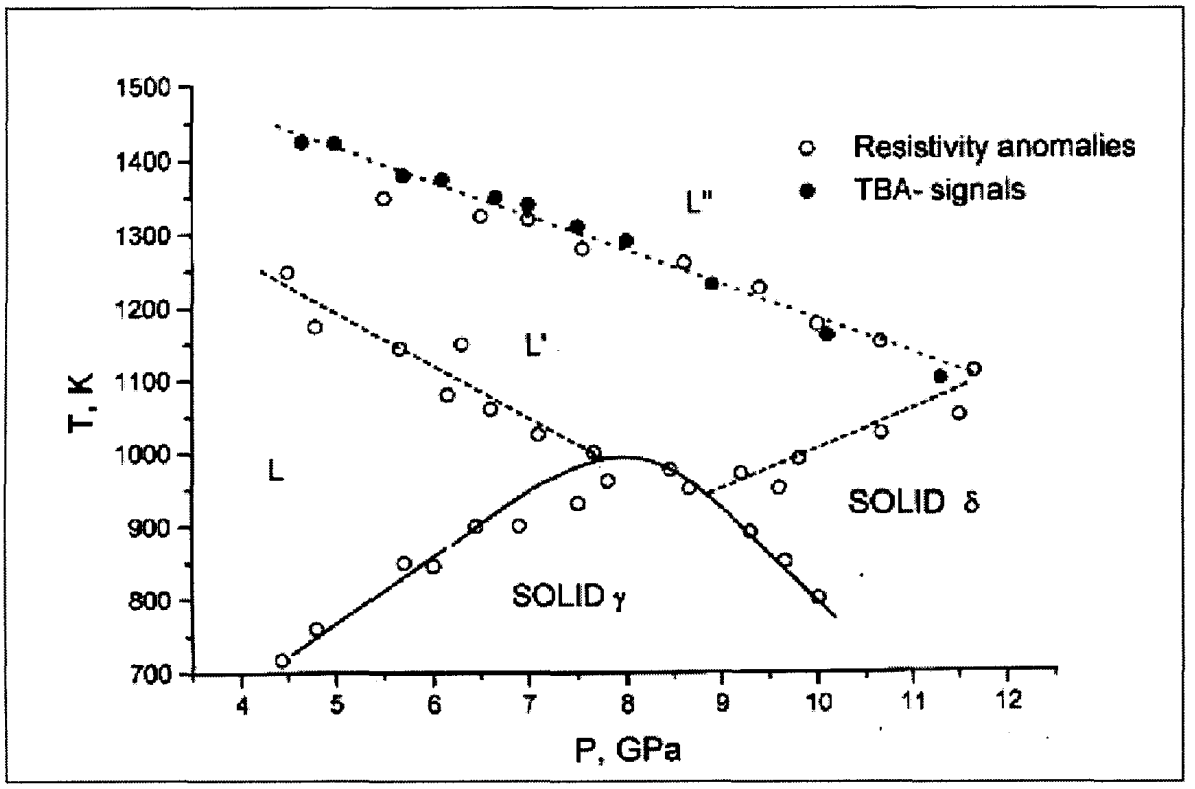

Figure 1.11: *P-T* diagram of solid and liquid S; L, L' and L" denote the liquid phases, γ and δ denote the solid phases. (from Brazhkin et al. 1999)

The primary domain of interest in this thesis lies in the liquid state in the region below 5 GPa, because of access to the L and L' regions at the pressures achievable in the pressure device used. Bridgman (1938) determined the compressibility and bulk modulus of solid sulfur among fifteen other elements. His value of bulk modulus for sulfur has still not been seriously challenged except by Luo and Ruoff (1993), who used a diamond anvil cell, and the value they obtained is rather open to discussion, especially for the pressure region below 5 GPa. However, the discrepancy will be discussed in the method and results section of this thesis. Paukov and Tonkov (1965a) investigated the melting curve of sulfur up to 1 GPa to resolve large discrepancies in the data that existed in literature, even before 1965. They used an instrumental jump in pressure during the heating as an

indicator of the melting point. The curve they obtained is compared with similar investigations in Figure 1.10. Further improvements were sought by Ward and Deaton (1967), utilizing the differential thermal conductivity analysis (DTCA) and piston-cylinder apparatus to investigate the melting curve up to 6 GPa. However, their contribution was most significant in observing phase transition to the fibrous phase at 3.7 GPa and just below the melting curve, at 410°C. Additionally their melting appears to be one of the most accurate ones ever produced. In solid sulfur up to 6.5 GPa, Geller (1967) found an additional phase before the fibrous sulfur transition. However, only after extensive efforts by Vezzoli et al. (1969c) where they conducted over 700 runs, had the full complexity of sulfur become obvious. Their work confirmed that sulfur not only has the most complex phase diagram of all known elements, but also the highest number of allotropes (Figure 1.12). More importantly, they also discovered evidence for five different phases in the liquid below 3 GPa.

However, the melting curve produced by the same team (Vezzoli et al., 1969a) had appeared to be rather optimistic in temperature range with respect to other investigations of the same phenomenon. The same investigators had published critical work on the possibility of polymerization under pressure (Vezzoli et al., 1969b). Notably, they recognized that while "*sulfur is a valuable system for the study of pressure effect on polymerization*", the absence of the investigations covering the topic of polymerization under high pressure is principally due to experimental difficulties that accompany such undertaking. The authors reported four distinct liquid phases below 3 GPa and also reported polymer content in phase D and E up to 1.7 GPa and up to 400°C (Figure 1.13). However, no quantifiable amount of polymer was reported, and no determination was

made regarding the increasing or decreasing polymer content with pressure. Additionally that is the only paper known to the author of this thesis that reports evidence of polymeric liquid sulfur ***under high pressure***.

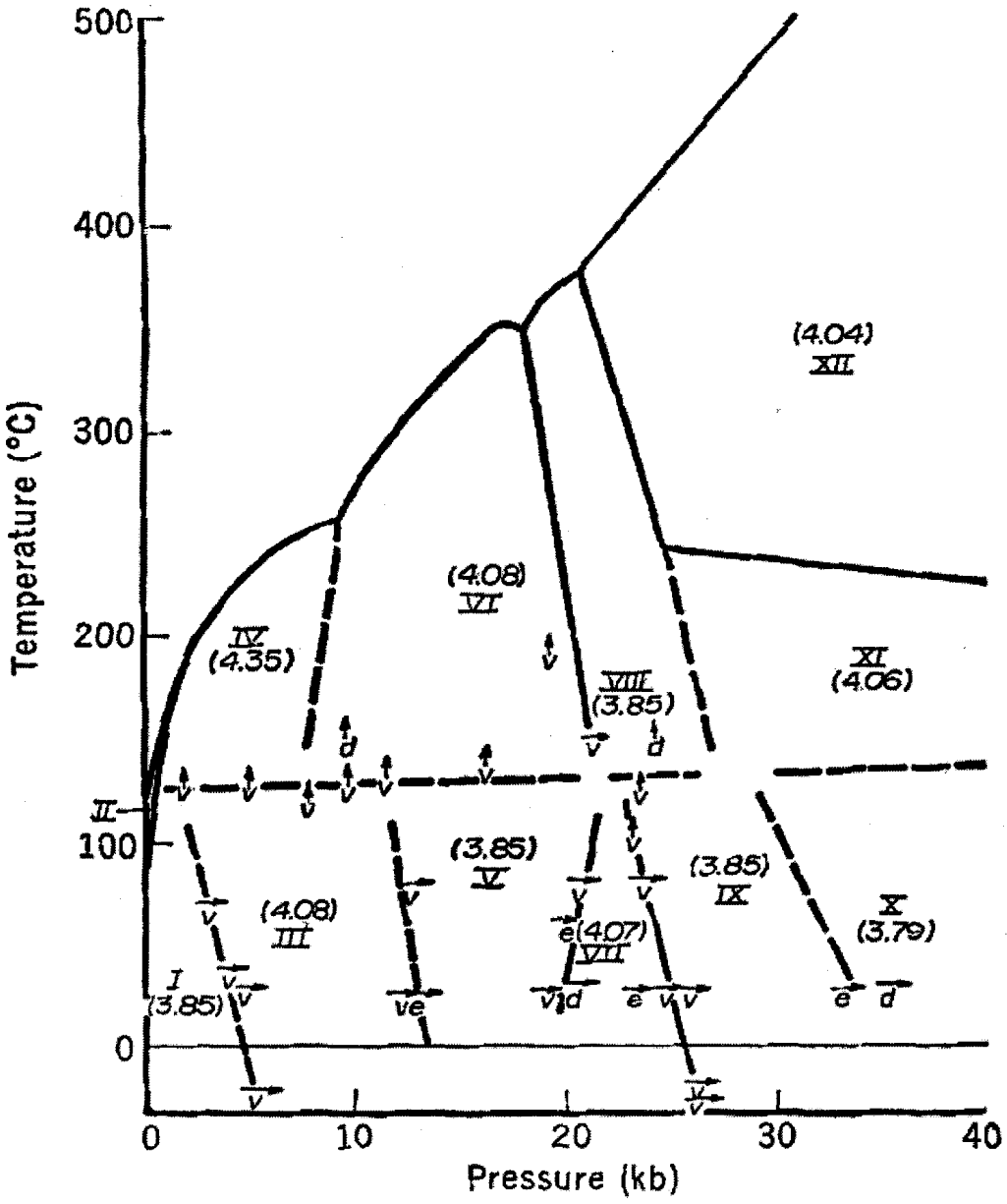

Figure 1.12: Phase diagram of sulfur up to 4 GPa and 500°C with 12 crystalline phases. The numbers in parentheses refer to the bond length (from Vezzoli et al., 1969c).

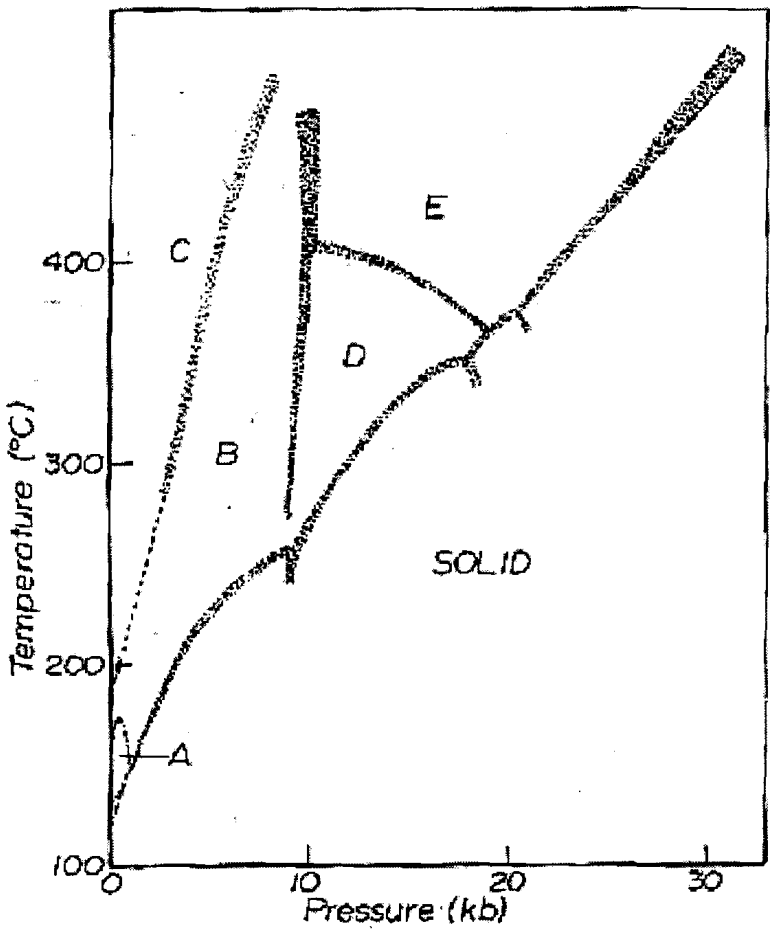

Figure 1.13: Melting curve and liquid phases of sulfur from atomospheric pressure up to 31 kbar or 3.1 GPa (Vezzoli et al., 1969a)

Fibrous sulfur (generally termed as sulfur XII) was investigated more rigorously by Vezzoli and Zeto (1970) at 3.5 GPa and 415°C, with a particular focus on structural properties. The highest intensity x-ray diffraction peak for *d* spacing of this high pressure allotrope is 4.04 Å, confirming the previous finding by Baak (1965), while other peaks corresponding to smaller d spacing are not as prominent. This structure exhibits great long term stability. A helical chain structure was determined in sulfur XII, which is characterized by high density. Notably sulfur XII has much higher negative thermal coefficient of electrical resistance than orthorhombic structure of sulfur I, which is a sign

of moderate semiconducting behavior. The comparison of quenched liquid samples at 3.5 GPa and 555°C, by x-ray diffraction indicates the same properties as the quenched liquid E (polymeric in nature, inferred to contain helical chains), shown in Figure 1.13. Moreover, this signifies that structural continuity extends from solid to liquid, and this important observation is suggested by the authors themselves. Nagata et al. (1992) studied sulfur at pressures below 10 GPa by the Raman spectroscopy and X-ray diffraction. They found a reversible phase transition at 5.2 GPa and room temperature, however they acknowledged the ambiguity and difficulty to confirm previously reported transitions below 8.3 GPa. However, Luo and Ruoff (1993) determined the glass transition of sulfur at 24 GPa and observed a clear transition from orthorhombic to monoclinic at 5.3 GPa and room temperature, using a diamond anvil cell and x-ray diffraction. That result closely corresponded to Nagata et al. (1992) finding just a year earlier. Notably Orgazall and Lorrenz (1994) observed a transition to the S_6 molecular structure at pressures above 9 GPa. Results that match fairly well the ones obtained in previous studies were obtained by Yoshioka and Nagata (1995), where a high pressure phase was reported at 5.2 GPa and the S_6 transition onset at about 10 GPa. The reviews of these studies illustrate the complexities in attempting to resolve, with desired resolution, the phase diagram of solid and liquid sulfur below 10 GPa mentioned during the introduction to the topic. The same sentiment is summarized by Crapanzano et al. (2005) where they stated "*...on reading recent literature on its* (sulfur) *high-pressure phases, a confused picture emerges where different techniques obtain different results*". These authors used x-ray diffraction and investigated the region between 6 and 11 GPa and the temperature range between 300 K and 1000 K to refine the phase diagram of sulfur. The

results were summarized in Figure 1.14 and the existence of a possible triple point must be emphasized as it points to the fact that the S_6 molecular phase can only be observed at high temperature.

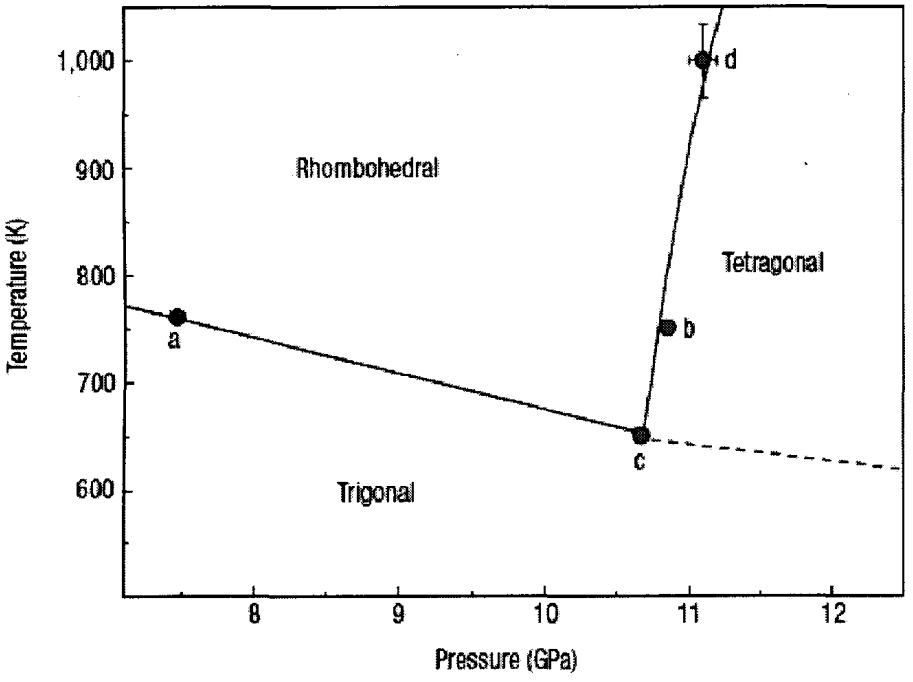

Figure 1.14: Schematic phase diagram of sulfur between 7 and 12 GPa (after Crapanzano et al., 2005)

Before discussing viscosity as the last section in the introduction of this thesis and the focal point of the research conducted here, it is only appropriate that a concluding paragraph of this subtopic ends with notes about an important and relevant recent paper that envelops the pressure and temperature region in the proximity where experiments of this thesis have been performed. Crichton et al. (2001) revisited sulfur XII (Figure 1.12) to investigate the structure of fibrous ψ-sulfur. After refining the data obtained in situ by synchrotron X-ray diffraction, and under 3 GPa and 400°C, they reported a two-chain

helical form of sulfur with nine atoms per unit cell. Notably, two helices are not the same in topology and bond lengths. Details of the structure are presented in their paper (Crichton et al., 2001), however, the relevance of this is that the work by Vezzoli et al. (1969b) has been confirmed, and more importantly, the structures across the solid-liquid boundary are structurally related. The extent of short or long range structural relations between solid and liquid will be discussed in further chapters of this thesis.

1.2.3 Viscosity of Liquid Sulfur

For nearly the past three hundred years, viscosity has been used to gain an insight in structural properties of the liquid. Sulfur in particular, because of its unusual properties in the liquid state, has been studied extensively in the second part of the past century, however almost all of those viscosity studies were conducted at atmospheric conditions, and only one at a high pressure. Above melting, viscosity decreases gradually and reaches a minimum of 0.007 Pa·s at 157°C, only to increase sharply at 159°C and reaches a maximum of 93.2 Pa·s at 187°C. Above 187°C, viscosity gradually decreases until the boiling point, where it reaches a value of 0.1 Pa·s (Steudel, 2003 and references therein). Intrigued by such peculiar behavior of liquid sulfur, Bacon and Fanelli (1943) conducted a pioneering study to obtain viscosity results throughout the temperature range shown in Figure 1.15 with more resolution than was previously available at that time. They also pioneered the method of purifying sulfur by boiling, as impurities have been known to affect results drastically. Indeed, they obtained results that are still valid today and shown in Figure 1.15.

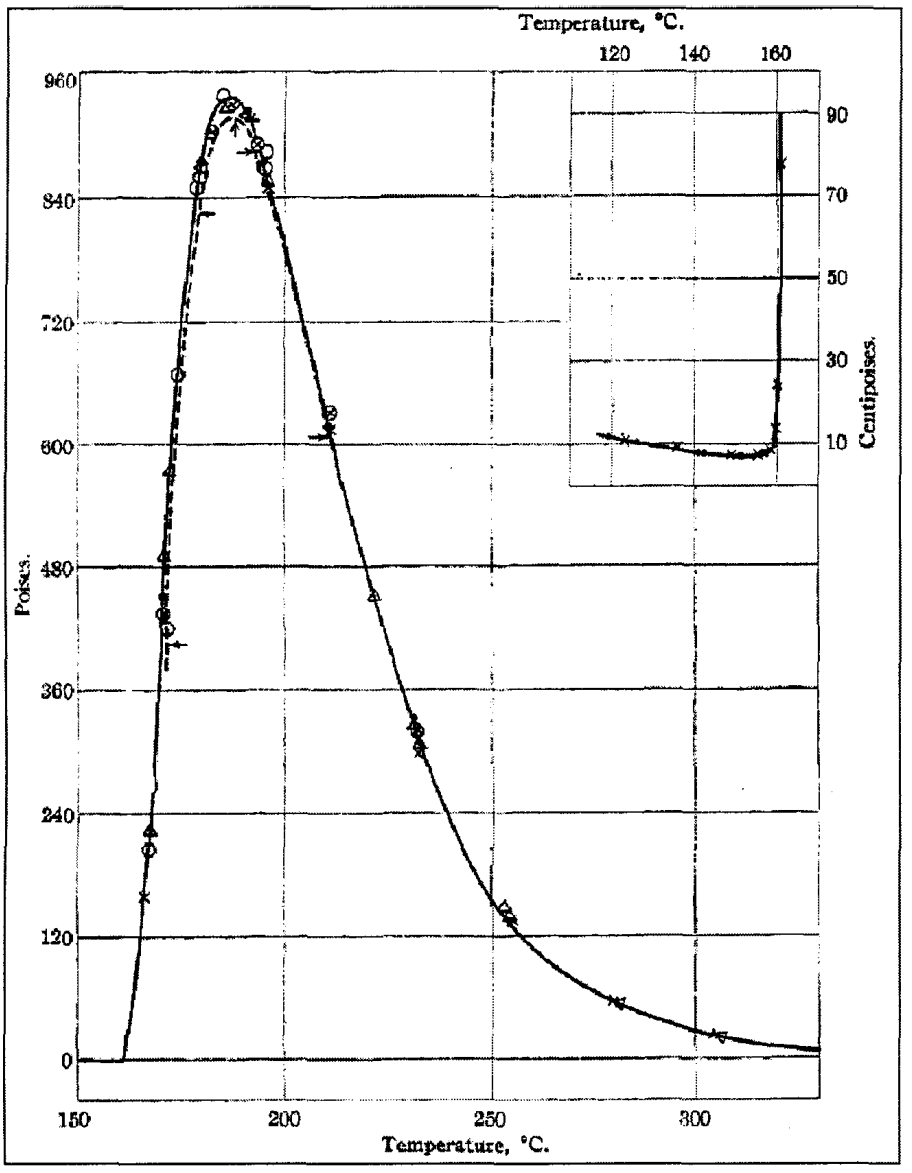

Figure 1.15: Plot of viscosity vs. temperature as obtained by Bacon and Fanelli (1943).

Matsushima (1959) investigated effects of small quantities of selenium and arsenic on the viscosity of liquid sulfur. Arsenic increases the viscosity of sulfur above 159°C, and depresses the minimum in viscosity to a lower temperature. Pressure effects on viscosity of liquid sulfur up to 100 atm had been investigated by Doi (1963) by means of combined rolling ball viscometry and theoretical treatment. The reported results contradict the calculation by Powell and Eyring (1943) who predicted viscosity decrease with pressure.

Theoretical treatment of viscosity of liquid sulfur was conducted by Touro and Wiewiorowski (1966). They treated S_8 as a pseudo-solvent and the polymer as a pseudo-solute, and devised a mathematical formulation based on that simple supposition. However, they correctly interpreted the chain length and viscosity relationship, particularly beyond 159°C. Noteworthy is the attempt by Eisenberg (1968) to treat viscosity in terms of the degree of polymerization and the monomer concentration, based on the assumption that viscosity is a function of molecular flow alone. However, calculated values were significantly lower than experimentally obtained values and consequently the proposed theory was found unsuitable for implementation at higher temperatures. A more complex approach to explain viscosity of liquid sulfur was formulated by Cates (1987). The model was underlined by the "reptation" theory of continually reversible breaking of polymer chains, which was combined with earlier classical equilibrium polymerization theory. Remarkably, while it was possible to adjust parameters to fit the viscosity curve produced by Bacon and Fanelli (1943), this approach remained just a fairly good approximation because of some fundamental limitations of the underpinning "reptation" theory. Ruiz-Garcia et al. (1989), while investigating the shear viscosity of liquid S between 118°C and 163°C, noted an intense influence of impurities on viscosity, most pronounced in the proximity of the λ-transition. They acknowledged the need to seek more refinement on the obtained data and noted that choice of experimental vessel is critical in order to avoid reaction with molten sulfur. Furthermore, they discovered that an illuminating source of light could affect viscosity of the molten sulfur, and effects were quantified based on the intensity of the light source. However it was not until very recently, that Terasaki et al. (2004) investigated the

viscosity behavior of sulfur at pressures up to 9.7 GPa and in the region immediately above the melting curve, with maximum temperature at the pressure limit, of 1067 K. The results are consistent and show a negative correlation of pressure and viscosity as it has been predicted by Powell and Eyring (1943). They also reported that ..."*the polymerization temperature was found to decrease with increasing pressure... and* (polymerization temperature) *intersects the melting curve at 0.13 GPa*" based on the work by previous investigators cited in the (Terasaki et al., 2004). Thus, according to them, the effect of the λ-transition on the viscosity of liquid sulfur at pressures higher than 0.13 GPa is neglected. However, this particular issue will be discussed later in this thesis and consideration will be given to an alternate scenario. Remarkably, the viscosities they obtained range from 0.45 Pa·s to 0.105 Pa·s which closely match the viscosity of liquid sulfur at the boiling point.

1.3 The Aim of This Thesis

The primary objective of the work conducted here is to investigate potential viscosity change across the liquid-liquid phase transition, as reported by Brazhkin et al. (1999), at a fixed pressure of 4.5GPa.

The secondary objectives of this thesis are as follows. The first is to investigate a possible polymerization under high pressure as hinted by Vezzoli et al. (1969b) and to quantify it.

The existence of a possible local liquid-liquid phase transition has been theorized and experimentally observed at lower pressures (by Vezzoli et al., 1969b). Consequently, the

possibility or nature of such phenomenon shall be probed using thermodynamic relation to the viscosity.

Finally, recent research, both theoretical and experimental (Katayama et al., 2004), points to separate phase equilibrium and coexistence, and will be explored further in liquid sulfur.

2. Experimental Methods, Procedure and Calculations

2.1 Experimental Methods

Viscosity is one of the basic transport properties of liquids and it is indicative of structural dynamics of the specific substance. The term viscosity refers to internal friction of a fluid and governs the rate at which liquid can flow. Generally, the literature may refer to two forms of viscosity, dynamic and kinematic. Dynamic viscosity can be understood in terms of the ratio of the shear stress and strain in the liquid (LeBlanc et al., 1999). However, kinematic viscosity, preferentially used in fluid dynamics, requires the knowledge of the fluid density and it is expressed as a ratio between dynamic viscosity and system density. The aim in this work is to evaluate the dynamic viscosity of liquid sulfur at high pressure and over a range of temperatures.

The viscosity behavior of liquids varies greatly between different classes of fluids, such as Newtonian and non-Newtonian liquids (LeBlanc et al, 1999), which have distinctly different characteristics of viscosity in terms of shear stress and strain.

Methods of measuring viscosity have been continuously refined for the past three hundred years and currently a number of reliable, purpose and material dependent, methods exist and are being used in a wide range of industries and applications. An excellent review of most relevant viscosity measurement techniques and methods that apply to molten alloys is given by Brooks et al (2004). However, a complete and comprehensive treatment of viscosity, from a historical review to a full assessment of methodology and theoretical treatments is given in Viswanath et al. (2007).

One of the simplest ways of measuring viscosity is the falling sphere method reviewed by Ryan and Blevins (1987) and Leblanc et al. (1999). For melts with very low viscosity, a high pressure setup at a synchrotron radiation facility is the best choice for the experimental method (Uchida et al., 2002; Ohtani et al., 2005). Due to long wait times for those facilities and significant financial commitment, the decision was made to use the currently available high pressure cubic anvil press and to utilize the quench method of falling sphere to evaluate viscosity of liquid sulfur at 4.5 GPa and the instrumental target temperatures of 726°C and 1100°C.

2.1.1 High Pressure and Temperature Instruments and Materials

All experiments were performed in a 1000 ton cubic anvil press (Figure 2.1) with the inverted ram type operation, in the High Pressure and High Temperature Lab, at the University of Western Ontario. The six anvils simultaneously compressing the cube, which acts as a pressure transmitting medium, (Figure 2.2) attempt to produce a hydrostatic pressure environment. The rams are hydraulically driven and are constrained to move in synchronization by means of guide pins that interconnect them. The pressure calibration based on Bi, Tl, and Ba standards was performed previously according to Secco (1994). The maximum error in pressure is estimated to be 5% at 4.5 GPa pressure.

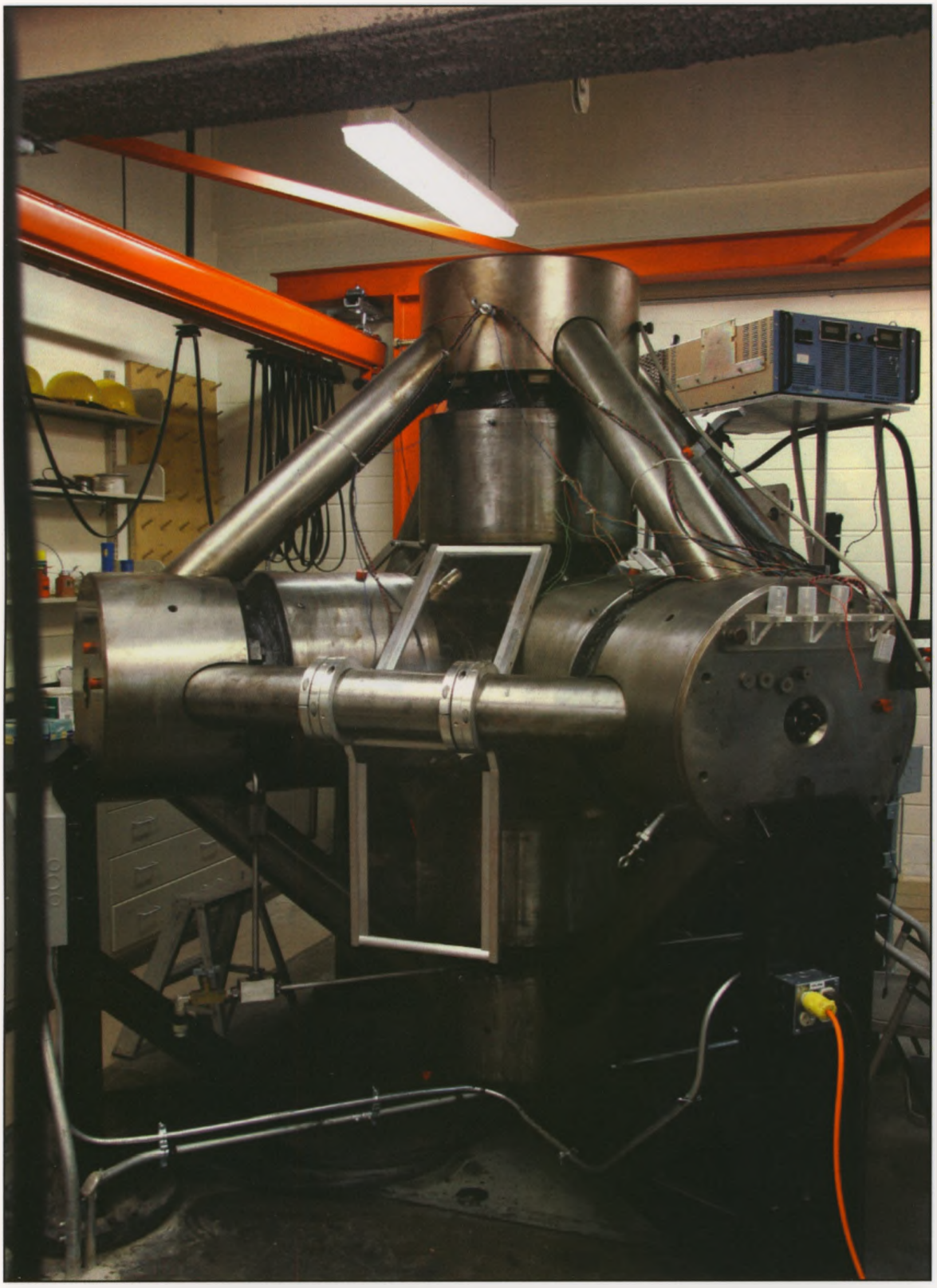

Figure 2. 1: The 1000 ton cubic anvil press, the High Pressure and High Temperature Lab at the University of Western Ontario

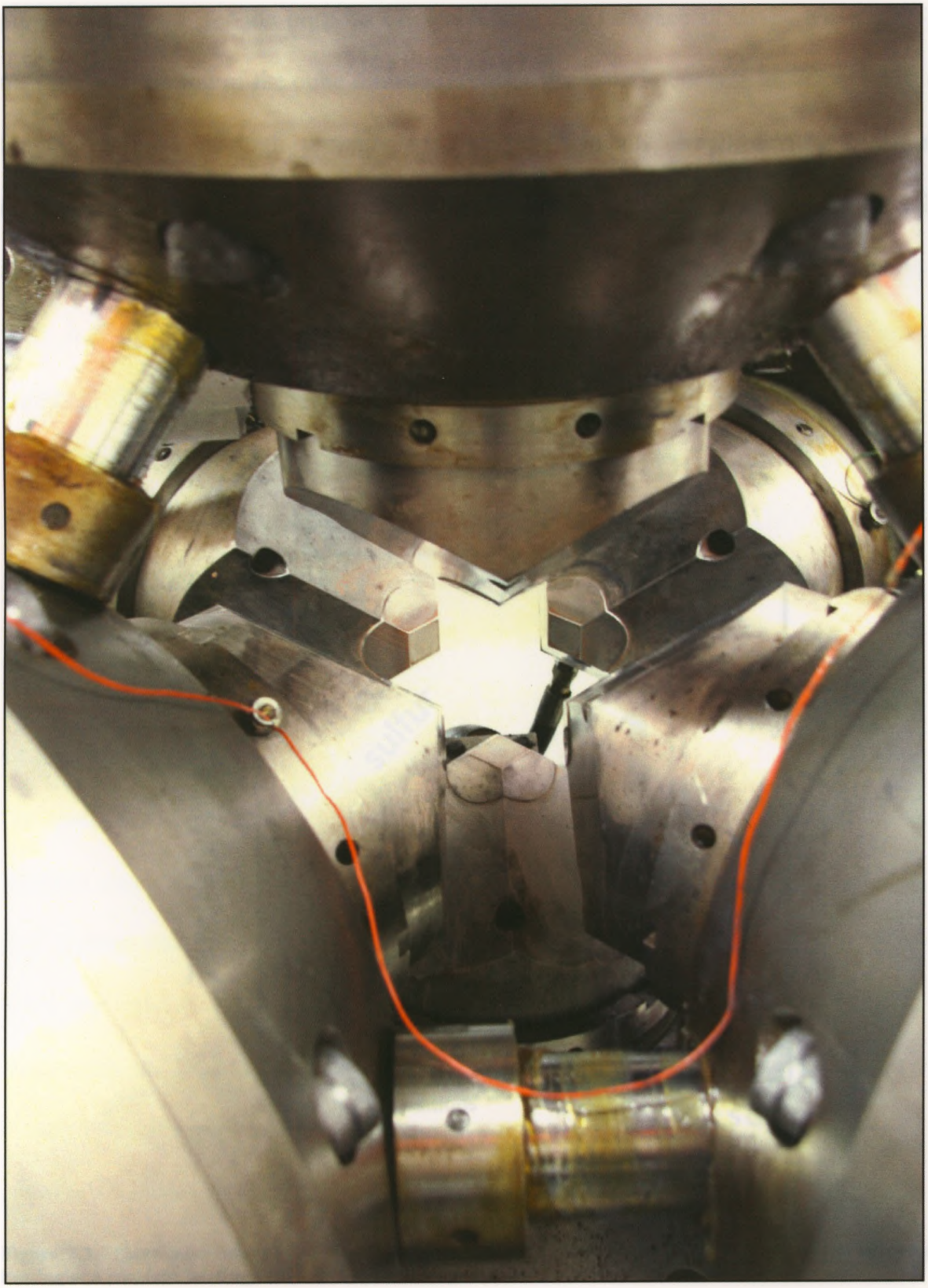

Figure 2.2: The arrangement of six cubic anvils in the 1000 ton press

One experiment was carried using a blank pyrophylite cube, which acted as a solid pressure medium, for the purpose of establishing the presence of deviatoric strain. The maximum deviation of the cube dimensions after the experiment was less than 1.3%, and for the purpose of high pressure viscosity experiments, small deviatoric stress is negligible due to the particular thermodynamic path maintained for all runs (Figure 2.3), and because liquids do not support shear stress.

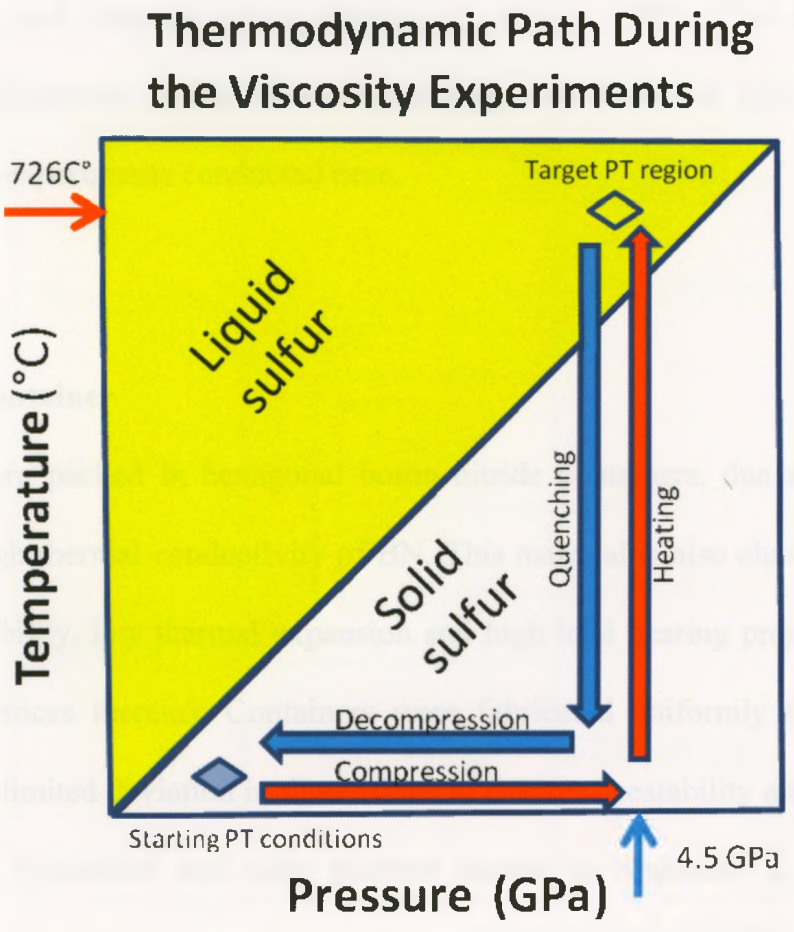

Figure 2.3: Thermodynamic path during the experiments. The compression was applied first following by, heating at a constant heating rate.

2.1.2 Pressure Medium

Pyrophylite, a hydrated aluminous phyllosilicate, $Al_2Si_4O_{10}(OH)_2$, was used as a quasi-hydrostatic pressure medium, because of the weak van der Waals bonds holding the adjacent tetrahedral layers together (Hicks and Secco, 1997, and references therein), and consequently, because of its ability to flow at high pressures and form gaskets. Physical properties, such as machinability, low thermal conductivity and high electrical resistivity, make it suitable for the application in high pressure experiments. The only concern regarding this material stems from the fact that it undergoes temperature dependent dehydroxylation and decomposition (Hicks and Secco, 1997). This aspect will be revisited later. However, the potential contribution of liberated H_2O is considered negligible in the experiments conducted here.

2.1.3 Sample Container

The samples were packed in hexagonal boron nitride containers, due to the chemical inertness and high thermal conductivity of BN. This material is also characterized by its high thermal stability, low thermal expansion and high load bearing properties (Eichler, 2010, and references therein). Containers were fabricated uniformly to maintain the consistency and limited deviation in dimensions to ensure repeatability and confidence in obtained results (container and cube pictures shown in Appendix 1, Figure A1.1). Initially, the first ten experiments were trial and error in an attempt to determine the optimal size for the sample containers. The final values for dimensions of the sample container that were used for later experiments are listed in Table 2.1:

Table 2.1: Dimensions* of the sample containers

Height with lid	*External diameter*	*Cap thickness*	*Side walls thickness*	*Internal diameter*	*Bottom thickness*
13.5 mm	*8 mm*	*1.5mm*	*1.5mm*	*5 mm*	*3 mm*

** all dimensions: ± 0.1 mm*

The cross section of the pyrophyllite cube and the components therein are shown in Figure 2.4. The sequence of initial to post-experimental pyrophyllite cubes is given in Figure 2.5. A representative sample of tools used in packing and empty sample cup is shown in Figure 2.6.

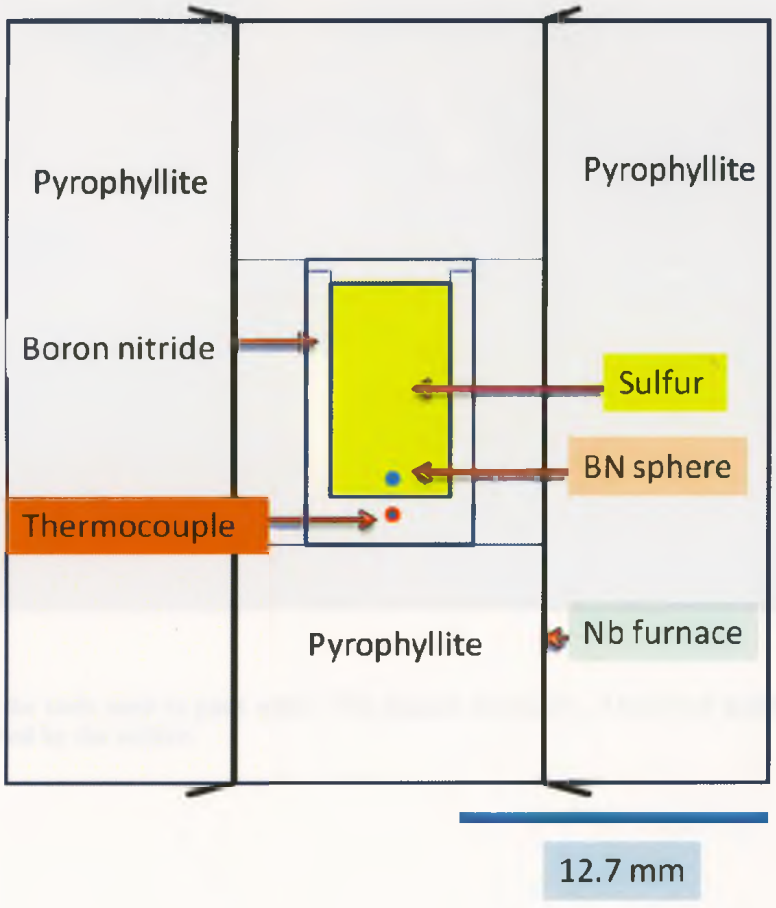

Figure 2.4: The cross section of the pyrophyllite cubic pressure cell

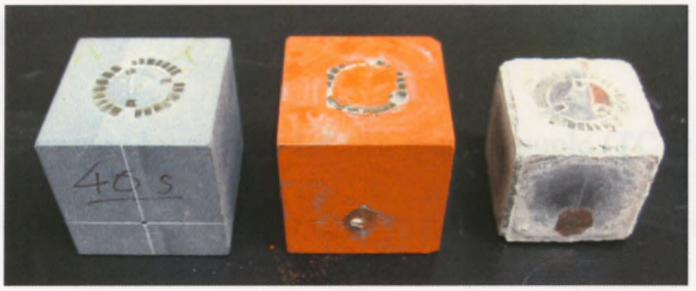

Figure 2.5: Assembled cubes shown in stages (left to right: (i) pre-experiment assembled cube, (ii) cube coated with iron oxide just before emplacement into the press, and (iii) post-experiment, just removed from the press)

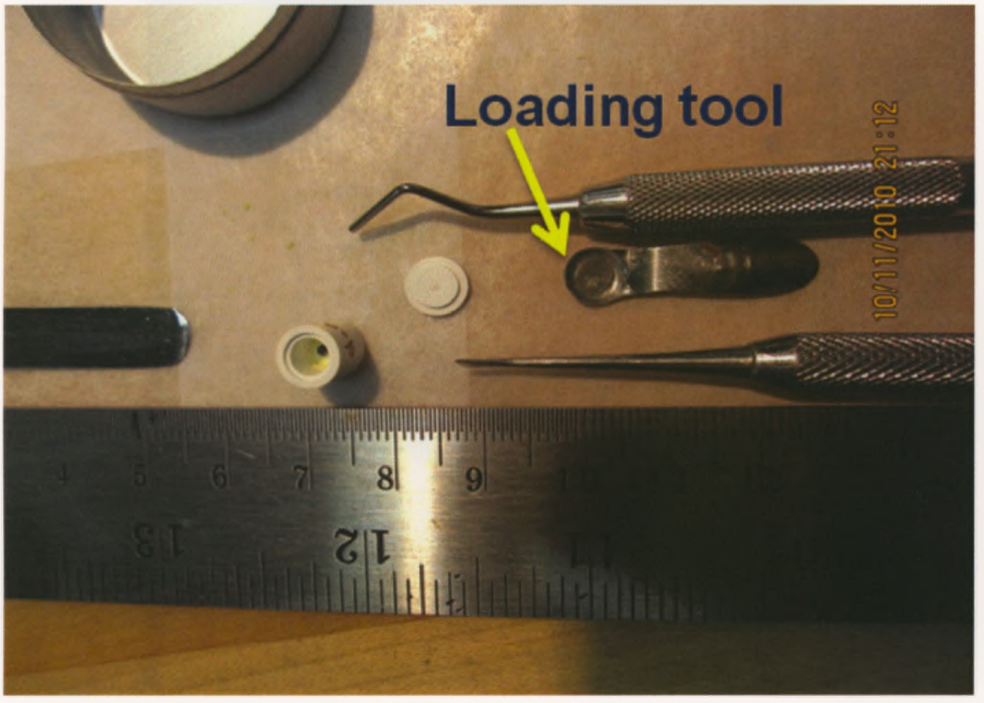

Figure 2.6: Some of the tools used to pack sulfur into sample containers. The arrow points to the loading tool designed and fabricated by the author.

2.1.4 Thermocouple

Temperature was determined by a Pt/Pt-10%Rh thermocouple (TC) placed at the bottom of the sample container (Figure 2.7). The temperature measurements were instrumentally corrected for the effects of pressure on the TC emf (Bundy, 1961; Getting and Kennedy, 1970). The uncertainty in temperature measurement, including instrumental uncertainty (Rempe and Wilkins, 2005), after the correction, is taken to be no more than 0.25% (or 2.75°C at 1100°C) in the experimental temperature range.

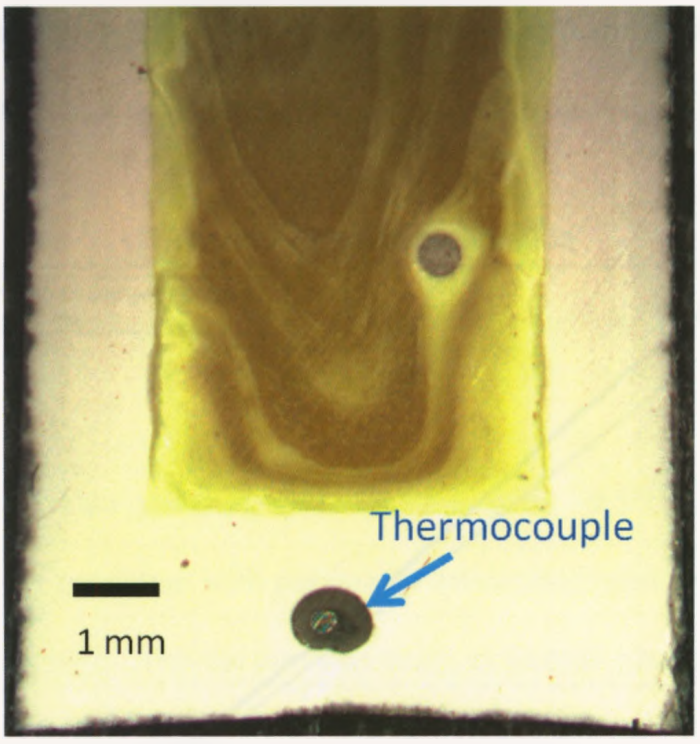

Figure 2.7: Photograph showing preferred location for the thermocouple through the base of the sample container, axially aligned. Yellow material is quenched sulfur and the graphite sphere is clearly visible in the upper right.

The choice for placement of the thermocouple in the bottom of the container, lined up axially, was made to maintain the maximum accuracy and reproducibility in the

temperature measurement resulting from the thermal gradient in a sample container (Schloessin and Lenson, 1989). The placement of TC in the noted location, coupled with the reinforced bottom of the sample cup container was given preference over other designs in order to ensure structural integrity of the assembly during the compression.

2.1.5 Thermal Gradient

The thermal gradient was determined by placing one thermocouple in the middle of the sample container and one at the bottom. Consequently, the thermal gradient was defined throughout the experimental temperature range (Figure 2.8 and Figure 2.9).

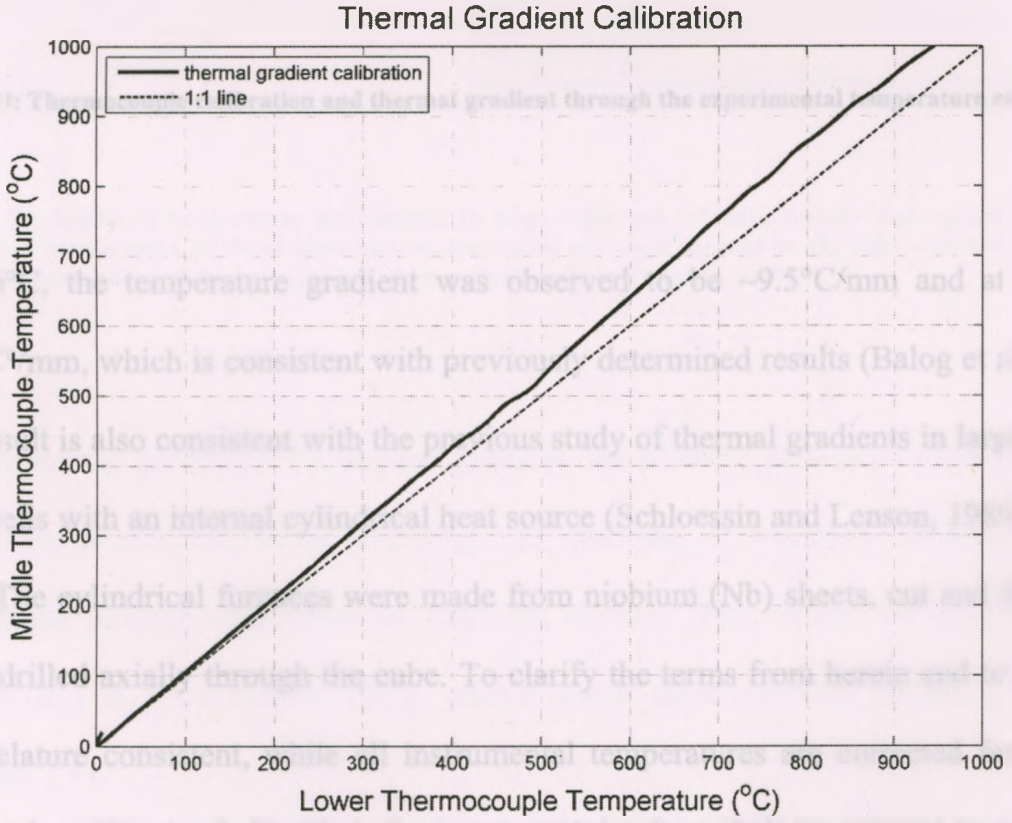

Figure 2.8: Thermal gradient calibration. The dashed line represents an ideal scenario with no thermal gradient present.

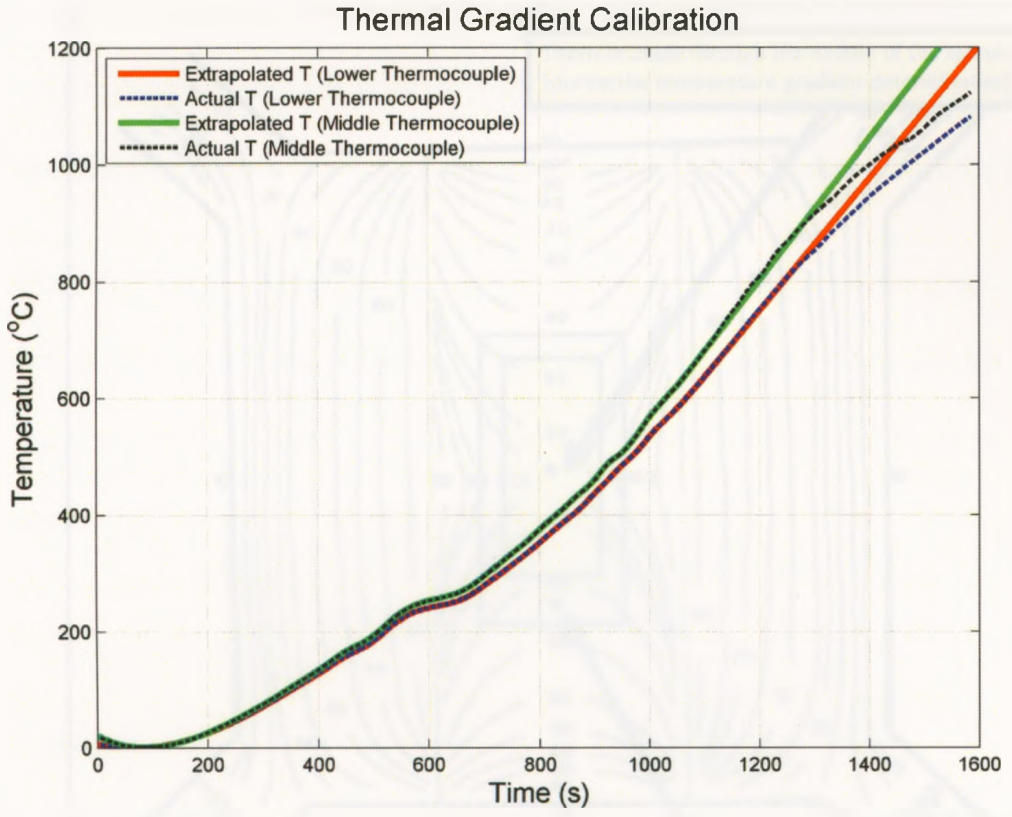

Figure 2.9: Thermocouple calibration and thermal gradient through the experimental temperature range.

At 726°C, the temperature gradient was observed to be ~9.5°C/mm and at 1100°C, ~14.3C°/mm, which is consistent with previously determined results (Balog et al., 2001). This result is also consistent with the previous study of thermal gradients in large volume cubic cells with an internal cylindrical heat source (Schloessin and Lenson, 1989) (Figure 2.10). The cylindrical furnaces were made from niobium (Nb) sheets, cut and fitted in a sleeve drilled axially through the cube. To clarify the terms from herein and to keep the nomenclature consistent, while all instrumental temperatures are corrected for thermal gradient (see Chapter 3, Results), the instrumental values shall be referred to in the text unless stated otherwise.

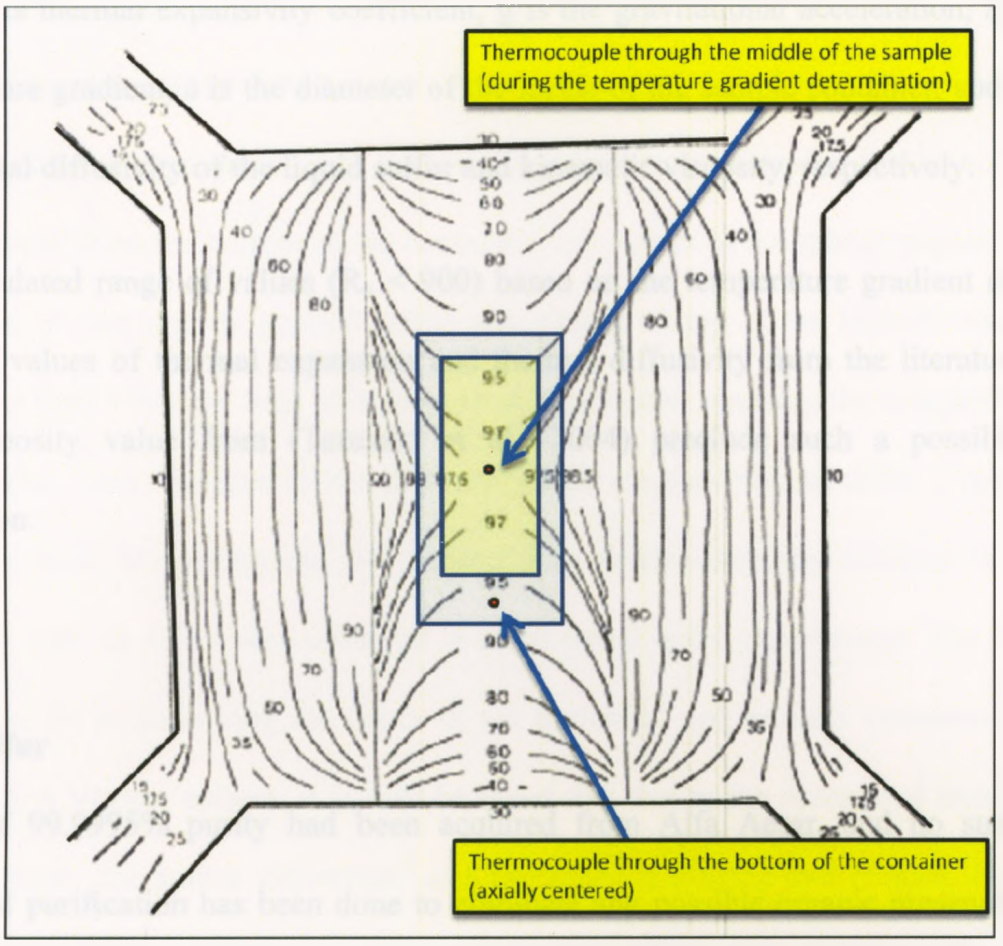

Figure 2.10: Model of temperature distribution in large cubic cell (1" edge length) with cylindrical heater. Contours of temperature (in % of maximum temperature) are superimposed on the cube with already formed gaskets, and placement of thermocouples is shown (Schloessin and Lenson, 1989).

Considering the presence of a thermal gradient, the possible presence of the convective regime, as a possible factor affecting the outcome of viscosity evaluations, was investigated through calculation of Rayleigh number. The critical value of Rayleigh number (R_n) is 1708 (Faber, 1995), above which the convective regime is possible (equation 2.1).

$$R_n=\alpha g \Delta T a^3/\kappa \nu, \qquad (2.1)$$

where α is thermal expansivity coefficient, g is the gravitational acceleration, ΔT is the temperature gradient, a is the diameter of the inside of the sample container, and κ and ν are thermal diffusivity of the liquid sulfur and kinematic viscosity, respectively.

The calculated range of values ($R_n < 900$) based on the temperature gradient and wide range of values of thermal expansion and thermal diffusivity from the literature along with viscosity value from (Terasaki et al., 2004) preclude such a possibility for convection.

2.1.6 Sulfur

Sulfur of 99.9995% purity had been acquired from Alfa Aesar, and no subsequent additional purification has been done to eliminate any possible organic presence as was done by Bacon and Fanneli (1942). Small chunks (Figure 2.11) were ground to powder and packed to the same consistency into the BN containers. That was achieved by listening for the very particular sound that compacted sulfur emits while compressing any voids; it resembles the sound produced by walking on a dry snow on a very cold day. The consistency of packing was such that the samples were packed to bulk density of ~1.8 g/cm^3. While that indicates the presence of porous spaces within the bulk sample relative to the published density of orthorhombic sulfur of 2.07 g/cm^3 (Meyer, 1976), the density achieved here is almost the same as that of liquid sulfur at the melting temperature at atmospheric pressure. Packing was done by hand, and great care was given to the prevention of any possible contamination of the sulfur sample, by thoroughly cleaning tools with commercial grade alcohol in addition to maintaining the working area in the

exceptionally clean state. BN containers were cleaned from any dust and contamination by forced air. A predetermined amount of sulfur (controlled by the amount in the loading tool) would have been loaded into the sample container consistently, first to achieve the desired depth from the bottom of the container, subsequent to the sphere emplacement. A new layer of just slightly pressed sulfur was placed on top of the initially compressed layer, and then a narrow hole was formed in the middle, reaching the originally placed bottom layer. This was then followed by the sphere emplacement in sulfur (Figure 2.12). This was done to prevent the BN sphere from electro-statically sticking to the BN container wall, as it has been observed in some initial failed experiments. The error was minimized by re-measuring the depth of the preloaded and initially compressed sulfur layer with a Vernier caliper. It should be noted that due to the absence of required task specific tools, the author improvised and fabricated a loading tool (Figure 2.6), while modifying others to achieve the efficiency and precision in preparation of parts and assembly stages.

Figure 2.11: Sulfur sample in a crystalline form (mortar ~ 7 cm diamtere)

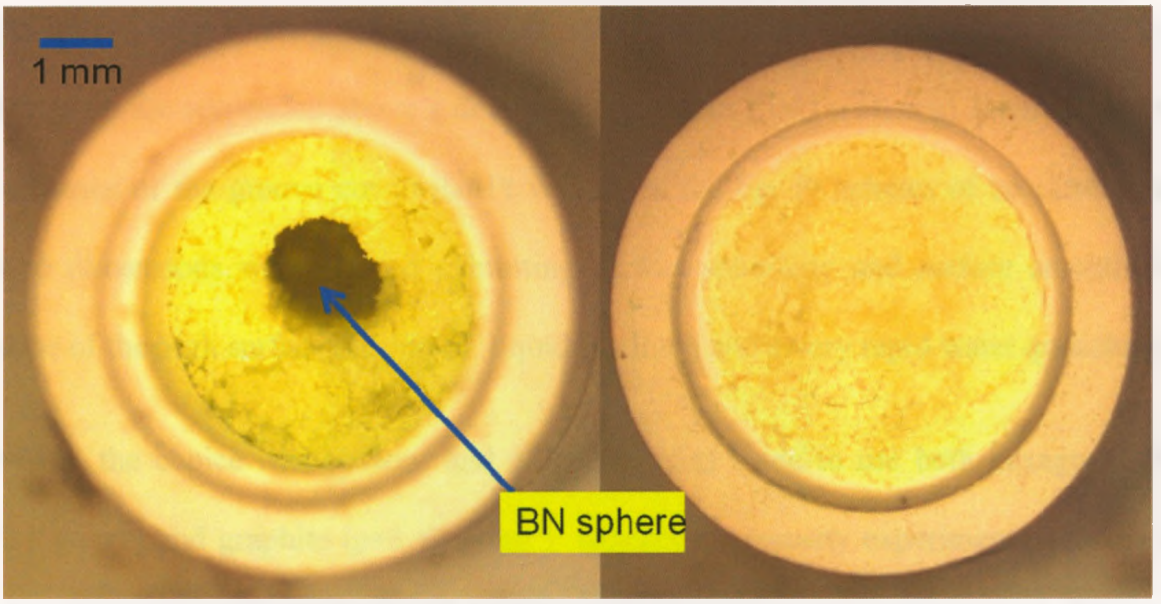

Figure 2.12: Left: sample container being loaded with the BN sphere at a pre-determined distance from the bottom; Right: fully loaded and packed sulfur in the sample container

2.1.7 Spheres

During the preliminary runs and motivated by the results obtained by Terasaki et al. (2004), attempts were made to determine not only the appropriate container size, but also to select the appropriate material for the spheres and to fabricate them to the most optimal size. The major obstacle was the expected low viscosity and liquid sulfur reactivity with a wide range of materials. Both platinum and chromium-steel, along with graphite and BN spheres were used in preliminary stages. There was no appreciable visible reaction with any of the above mentioned materials.

A reliable way to make perfectly spherical Pt spheres of a uniform size was developed. That was achieved by taking a Pt wire of desired diameter (in this case 0.254 mm) and based on the volume of the desired sphere, the wire was sharply grooved at the distance from the tip which provides the correct volume of the wire cylinder to make desired size

of the sphere. Any welding apparatus with enough power can be used, where both flame and wire tip are suspended above a deep glass container filled with cold water. Based on the distance of the groove cut in the Pt wire from the tip, Pt spheres of consistent and desired dimensions were formed exhibiting perfect sphericity and surface smoothness because of the high surface tension of liquid platinum and a very rapid water quenching.

However, the choice was obvious and a decision was made to use both hexagonal BN (ρ=2.1 g/cm^3) and graphite (ρ=1.63 g/cm^3)[2] spheres in viscosity experiments because of the low density contrast with liquid sulfur at given pressure and temperatures. Platinum and chromium steel were both rejected, because of the high density contrast and inability to heat or quench the sample rapidly enough to determine the actual velocity of the sphere. Thus, it was possible to constrain the velocity of spheres and subsequently measure viscosity of liquid sulfur at high pressure and temperatures. The spheres were fabricated using a modified and simplified method reported by Crandall (1970), where an air driven sphere grinder lined up internally with a low grit sanding material. The inability to gauge or control sphere sizes, meant that machined cylinders of either boron nitride or graphite had to be watched for hours at the time and continuously measured until a desired and uniform size had been achieved. The results are shown in Figure 2.13 and Figure 2.14 (also see Appendix 1, Figure A1.2).

[2] Graphite density was measured in-house by using a standard experimental procedure of repeatedly measuring the mass and volume of accurately machined (± 0.0025 mm) graphite cylinders of different sizes and averaging all measurements. The final value of 1.63 g/cm^3 corresponds to the value obtained from the manufacturer.

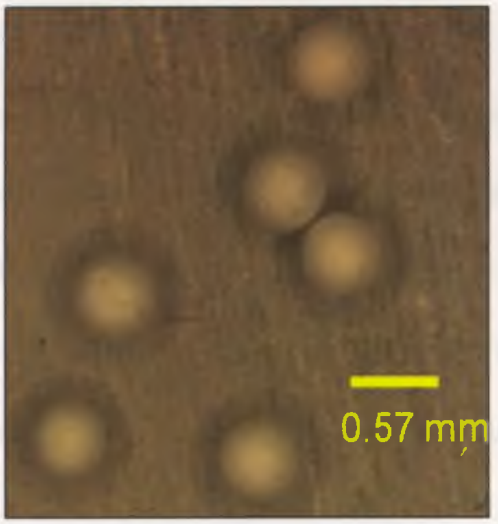

Figure 2.13: Example of BN spheres and the consistency in sizes.

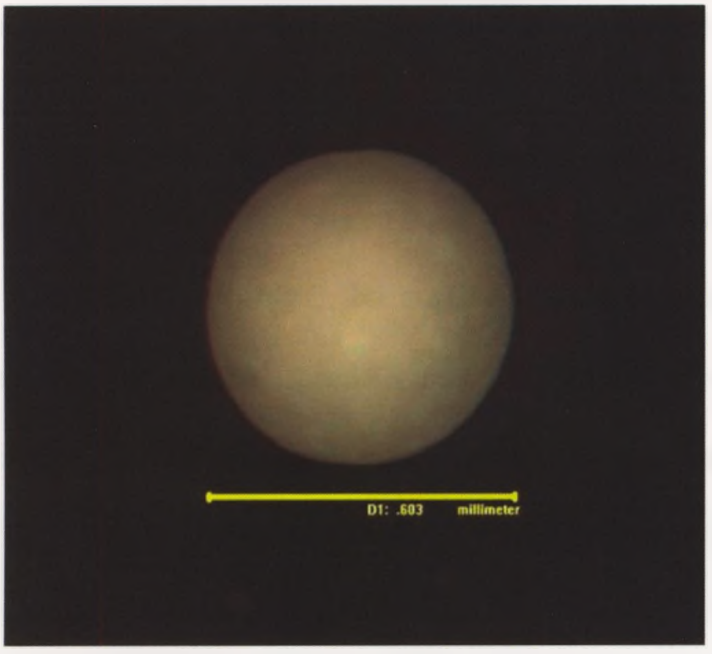

Figure 2.14: An example of sphericity of a BN sphere used in experiments.

2.2 Experimental Procedure

Finished and assembled cubes were painted with alcohol dissolved iron oxide to aid in gasket formation during the compression stage. Once completely dry and after the press had been thoroughly cleaned and lubricated (standard procedure before every experiment), the cube was loaded in the press. Pressure was then raised to 4.5GPa, and subsequently corrected three times until no further relaxation and no drop in pressure was observed. Heating was then achieved through the computer controlled power supply that sent power through the opposite vertical anvils to the electrical resistance heated niobium furnace. The computer control also enabled a constant heating rate, which is critical in observation of any phase change using latent heat effect in the TC as an indication. For the L region (target instrumental temperature of 726°C), the feedback control on the computer was engaged to stabilize temperature as close as possible to 726°C and to prevent large temperature oscillations.

For the L' region, the feedback function was engaged at 900°C (almost 200°C before the target temperature) to stabilize at 1100°C, because of the high heating rate. After the heating at the target temperature for a predetermined amount of time (generally from seconds to 10's of seconds), the experiment was quenched by shutting off the power to the furnace, and followed by a slow decompression in order to prevent catastrophic fracturing of the tungsten-carbide (WC) anvils. During the experiments conducted in this thesis, generally twelve hours were allowed for a full decompression.

After the cube was removed from the press (Figure 2.15), a very careful sectioning by grinding was conducted to locate the sphere embedded in the quenched sulfur. The measurement of the distance the sphere traveled in a given time interval was done under a

Nikon microscope (up to 50X magnification) using Elements software with a scale calibrated relative to the specific magnification, and subsequently the velocity was calculated as a function of distance and time. The experimental difficulty expressed by many authors, especially when measuring viscosity in the regions far above the melting curve, is in the fact that sphere is already moving, and possibly so at the terminal velocity prior to reaching the target temperature. It was not possible to reconstruct the full motion of the sphere from the melting point of the sample to the desired temperature as a function of time, with the desired degree of precision. However, what was done instead was to use the target temperature, and a recovered location of the sphere as function of time, as the initial position reference point, following quenching immediately upon reaching that predetermined temperature. Then the location where the sphere arrived, between melting point of sulfur and the target temperature, in a given time and at a constant heating rate is taken as the reference point from which further measurements noted above are conducted. The picture (Figure 2.16) taken in the initial stages during preliminary investigations and refining of the measuring method illustrate the above point well. It should be noted that use of zirconia as a thermal insulator was avoided to enable more accelerated quenching.

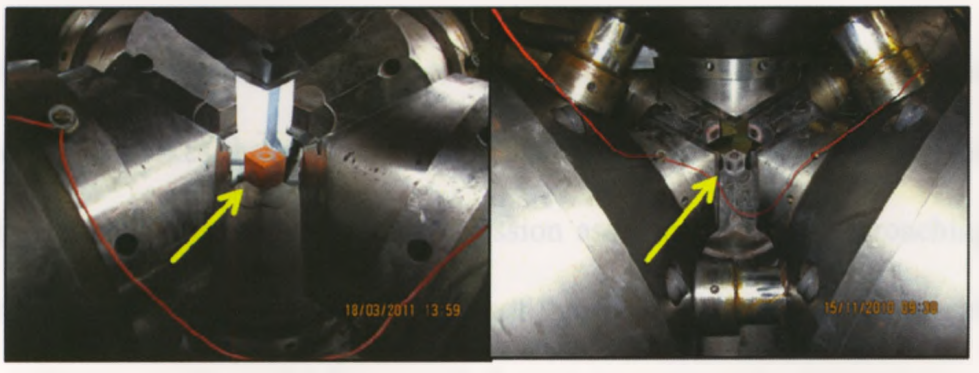

Figure 2.15: 1" cube in the press prior to the experiment (left) and after the experiment (right).

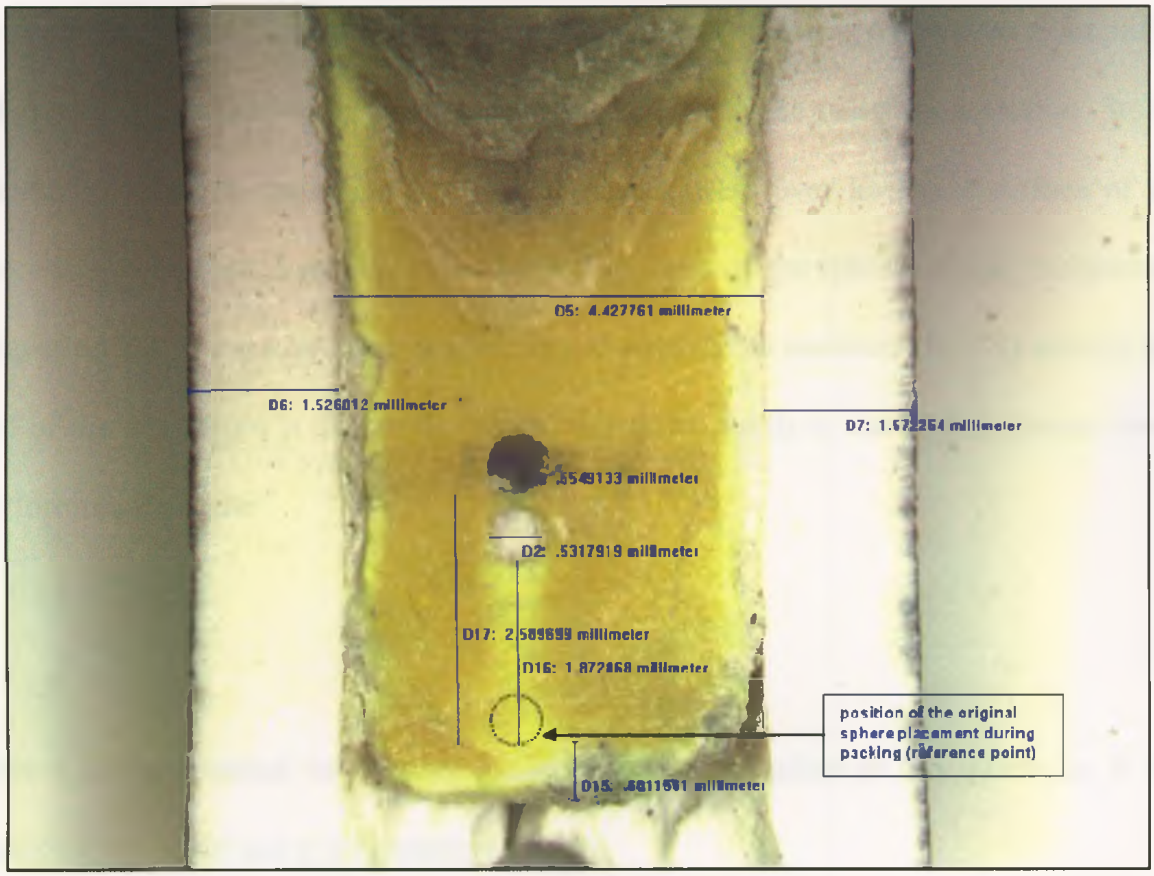

Figure 2.16: Picture of the C and BN sphere locations in a sectioned sample container, after the predetermined time at or above the target temperature during preliminary and testing stages of investigation of sphere types and sizes. Travel distances are accurately measured by the Nikon microscope and Elements software with a measuring magnification-calibrated scale. Note that the distance from the bottom of the sample container is precisely known and it is shown in the picture.

2.3 Calculation and Thermodynamic and Elastic Parameters

The theoretical basis for the calculation of the viscosity using the falling sphere method is underlined in the Stokes theory and his derivation of an expression for the viscous drag force acting on a falling sphere. This expression assumes that the approaching flow is very slow and consequently the acceleration of the fluid, as it passes around sphere, can be ignored. The method is valid for a small Reynolds number ($R_e \leq 1$) and a steady state

environment. The full derivation is beyond the scope of this thesis; however, a simplified mathematical formulation is given further in the text in the calculation section. Stokes essentially added up pressures and viscous shear stress over an entire surface of the sphere to obtain what is known as the total drag force on the sphere, which is expressed in equation 2.3. It must be noted that at very low Reynolds numbers ($R_e \leq 1$) exactly one third of the drag force is due to the pressure and two-thirds is due to the viscous force. The formula for R_e is:

$$R_e = \frac{vr\rho_L}{\eta} \qquad (2.2)$$

where v is the terminal velocity of the sphere, r is the radius of the sphere, ρ_L is the density of the liquid and η is dynamic viscosity.

The diagram of forces acting on the BN sphere in experiments in this thesis is given in Figure 2.17, which can be expressed mathematically as

$$F_W = -mg = -\rho_S V g \qquad (2.3)$$

$$F_D = -(6\pi\eta v r) \qquad (2.4)$$

$$F_B = \rho_L V g \qquad (2.5)$$

Where F_W is the weight of the sphere, F_D is the viscous drag on the sphere, F_B is the buoyancy force, m is mass, g is gravitational acceleration, ρ_S is the density of the sphere V is the volume of the sphere, η is dynamic viscosity, v is the terminal velocity of the sphere, r_S is the radius of the sphere and ρ_L is the density of the liquid.

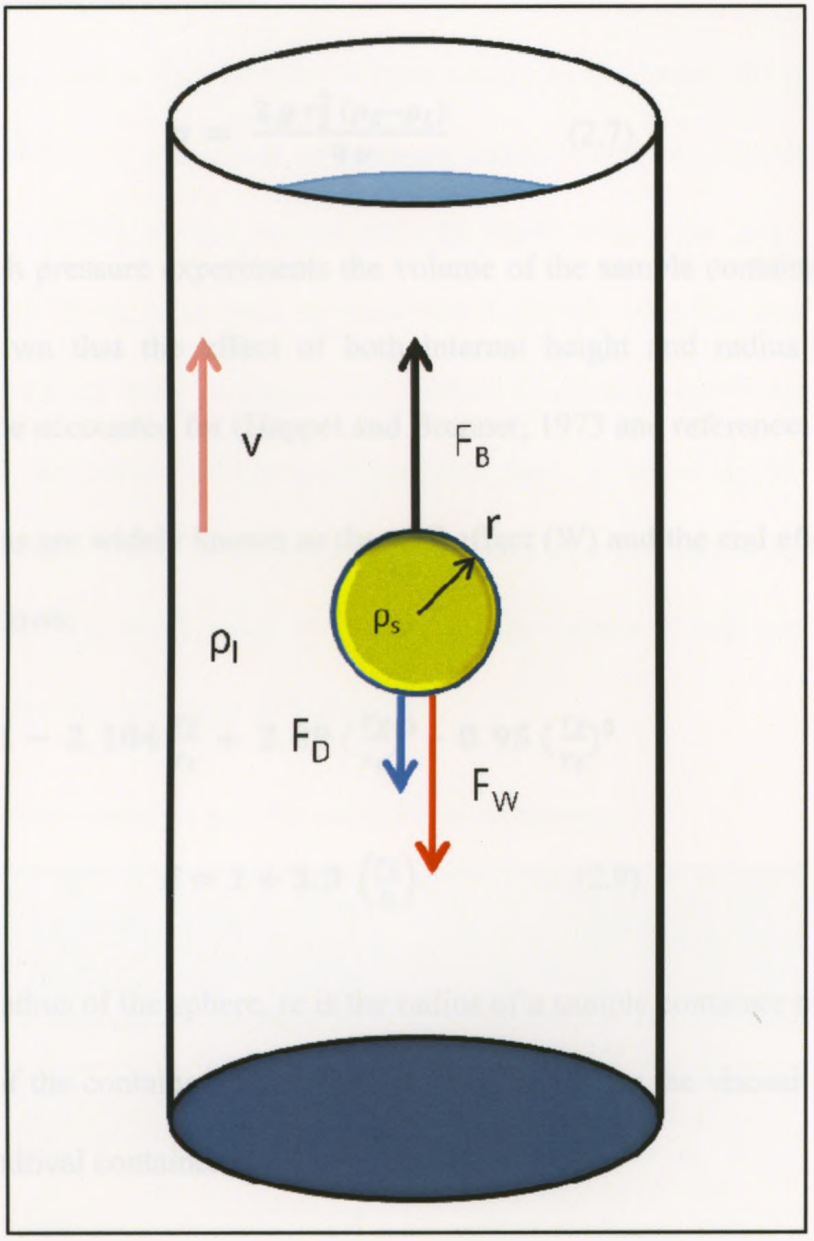

Figure 2.17: Graphical representation of a sphere descending in a viscous liquid and forces acting on it. It reaches the terminal speed when the sum of the forces acting on it is zero.

Setting up an expression as follows:

$$F_W + F_D + F_B = 0 \qquad (2.6)$$

Keeping in mind that $\mathbf{V = 4/3\ \pi\ r^3}$, and solving for viscosity (η), the Stokes equation for falling sphere viscosity is obtained:

$$\eta = \frac{2\, g\, r_S^2\, (\rho_S - \rho_L)}{9\, v} \qquad (2.7)$$

However, in high pressure experiments the volume of the sample container is finite, and it has been shown that the effect of both internal height and radius of the sample container must be accounted for (Happel and Brenner, 1973 and references therein).

Those corrections are widely known as the wall effect (W) and the end effect (E) and are expressed as follows:

$$W = 1 - 2.104\, \frac{r_S}{r_C} + 2.09\, (\frac{r_S}{r_C})^3 - 0.95\, (\frac{r_S}{r_C})^5 \qquad (2.8)$$

$$E = 1 + 3.3\, \left(\frac{r_S}{h}\right) \qquad (2.9)$$

where r_S is the radius of the sphere, rc is the radius of a sample container respectively and h is the height of the container. Thus, the final expression for the viscosity of the falling sphere in a cylindrical container is

$$\eta = \frac{2\, g\, r_S^2\, W\, (\rho_S - \rho_L)}{9\, E\, v} \qquad (2.10)$$

Hence, to calculate viscosity it is necessary to know the terminal (maximum) velocity of the sphere.

2.3.1 Bulk Modulus and Thermal Expansion Coefficient for Sulfur, hexagonal BN and Hexagonal Graphite

To obtain accurate values for viscosity it is necessary to determine the densities of both the liquid and spheres as a function of pressure and temperature. The Birch-Murnaghan equation of state (EOS) of the second and the third order were used in the density calculations in this work. The main obstacle has definitely been the lack of appropriate and reliable values for bulk modulus and thermal expansion coefficient, not only for sulfur but also for boron nitride and graphite used in experiments here. A large divergence of values found in literature is troubling and the following Table 2.2 and Table 2.3 illustrate that point rather dramatically. The values of bulk modulus for sulfur are not as abundant and are given in Table 2.4.

Table 2.2: Values of bulk modulus for graphite compiled from the literature

Graphite Bulk Modulus (B_0) and Bulk Modulus Pressure Derivative (B')		
B_0 (GPa)	B'	Source
12	--	Rydberg et al., 2003
23*	--	Boey and Bacon, 1986
26.8	13.22	Janotti et al., 2001
29	--	Lynch and Drickamer, 1966
31	--	Zhao and Spain, 1989
33*	--	Boey and Bacon, 1986
33.8	8.9	Hanfland et al., 1989
34.5	8.9	Solozhenko and Solozhenko, 2000
35.8	--	Blasklee et al., 1970
38	9	Lowitzer et al., 2006
41*	--	Kim and Chen, 2004
43.6	--	Kim and Chen, 2004
28.98 - 33.8	--	Ooi et al., 2006
29.5 (t)	9.4	Solozhenko and Solozhenko, 2000
7.3 - 10.7	--	Boey and Bacon, 1986

** authors stated values obtained by other studies*

(t) turbostratic

Table 2.3: Values of bulk modulus for hexagonal BN compiled from literature. The value of bulk modulus used in the calculations here is from Solozhenko et al. (1995)

h-BN Bulk Modulus (B_0) and Bulk Modulus Pressure Derivative (B')		
B_0 (GPa)	B'	Source
2.13	9.6	Janotti et al., 2001
11	--	Rydberg et al., 2003
17.2 (t)	--	Solozhenko and Solozhenko, 1999
17.6	19.5	Zhao et al., 1997
21	16	Fuchizaki et al., 2008
26	--	Lelonis et al., 2003
26.7	10.72	Janotti et al., 2001
27.6	10.5	Godec et al., 2000
28	--	Boudiombo et al., 1997
29.9	**9.3**	**Solozhenko et al., 1995**
30.1	10.1	Albe, 1997
32	--	Kim and Chen, 2004
36.5	5.6	Solozhenko and Peun, 1997
36.7	5.6	Solozhenko et al., 1995
37	--	Kern et al., 1999

(t) turbostratic

Table 2.4: Values of bulk modulus for sulfur, along with thermal expansion coefficient, compiled from the literature. The value of bulk modulus used in the calculations here is from Yu et al. (2009), while thermal expansion coefficient comes from Thermal Properties of Metals (ASM IMPDC, 2002).

Sulfur Bulk Modulus (B_0), Bulk Modulus Pressure Derivative (B') and Thermal Expansion Coefficient (α)			
B_0 (GPa)	B'	α (K^{-1})	Source
7.74	--	$103 \cdot 10^{-4}$	Saunders et al., 1986
7.93 at 50°C	--	--	Bridgman, 1945
7.57	--	--	Sumer, 1955
--	--	$2.53 \cdot 10^{-4}$	Wallis et al., 1986
7.94	--	--	**Yu et al., 2009**
--	--	**$0.64 \cdot 10^{-4}$**	**ASM IMPDC, 2002**
--	--	$4.3 \cdot 10^{-4}$	Zheng and Greer, 1992
--	--	$5.58 \cdot 10^{-4}$	Espeau and Céolin, 2007
--	--	$5.5 \cdot 10^{-4}$	Kennedy and Wheeler, 1983
10.5	--	--	Wang et al., 1987
7.2	--	--	Hafner et al., 1990
14.5	7	--	Luo and Ruoff, 1994
9.37	5.43	--	Vaidya and Kennedy, 1971

2.3.2 Density Calculation at 4.5 GPa and up to 1100°C

The densities of liquid sulfur and both boron nitride and graphite spheres were calculated using the second and third order Birch-Murnaghan equation of state, respectively.

$$P = \frac{3B_0}{2}\left[\left(\frac{\rho}{\rho_0}\right)^{7/3} - \left(\frac{\rho}{\rho_0}\right)^{5/3}\right] \qquad (2.11)$$

$$P = \frac{3B_0}{2}\left[\left(\frac{\rho}{\rho_0}\right)^{7/3} - \left(\frac{\rho}{\rho_0}\right)^{5/3}\right]\left\{1 + \frac{3}{4}(B' - 4)\left[\left(\frac{\rho}{\rho_0}\right)^{25/3} - 1\right]\right\} \qquad (2.12)$$

Thermal expansion coefficient correction of density at high temperature was calculated from the classic expression for α,

$$\rho = \rho_0 (1 - \alpha \Delta T) \qquad (2.13)$$

where α is the thermal expansion coefficient, ρ is density at high temperature and pressure, ρ_0 is density at high pressure and room temperature and ΔT is the temperature difference.

2.4 Micro XRD, Raman and CS_2 Dissolution

Micro X-ray diffraction (μ-XRD) measurements on the pure powdered crystalline sulfur were completed in order to investigate the presence of possible impurities and to obtain a reference data for future investigations. The advantage of (μ-XRD) is in fact that is non-destructive, thus allowing the preservation of the sample. Moreover, it offers a reliable analysis of the specific parts of the sample (Flemming et al., 2005). The instrument used in this study is a Bruker D8 micro diffractometer (Figure 2.18) at the University of

Western Ontario, Department of Earth Sciences. The operational parameters for the diffractometer were set at 40 kV and 40 mA respectively, to maintain Cu$K\alpha$ radiation. $K\alpha$ beam was gauged at 500 μm. $K\beta$ radiation was filtered by Goebel mirror parallel optics system. The samples were mounted on XYZ stage and handled according to the procedure described by Flemming et al. (2005). Samples remained stationary during the scan as a result of θ-θ geometry of the diffractometer. The Omega scan mode was used for the analysis, where the amount of time spent per scanned spot was estimated at a little over one hour. Subsequent analysis that followed involved the use of GADDS 2D detector to analyze diffracted X-rays, while GADDS software was used to process the signal and to produce one dimensional plot of intensity vs. 2θ. EVA software was used to identify the individual allotropes of sulfur.

Figure 2.18: Bruker D8 and micro XRD apparatus at the University of Western Ontario

The Raman effect results from the interaction of the electromagnetic (visible) radiation and of the lattice vibrations and such interaction causes Raman diffusion. The Raman spectroscopy is based on inelastic scattering of monochromatic light changes that occur when beam interacts with a sample. Photons of the laser beam interact with vibration modes of the molecules or with lattice phonons and get reemitted at different frequency relative to photons in the incident monochromatic light. Comparison of a detected shift in frequency is consequently defined as the Raman effect. The Raman spectroscopic method enables insight in vibrational and rotational dynamics of molecules. For the measurements of the Raman spectra, a custom-built micro-Raman system, courtesy of Dr. Shieh and his students, was used, with the monochromatic 514.5 nm wavelength argon ion laser as the excitation source. To collect the Raman signal, 180 degree geometry along with 0.5-m spectrometer and a liquid nitrogen cooled CCD detector were used to collect the Raman signal (Shieh, 2011). Each Raman spectrum was collected for about 1800 seconds and Raman data were analyzed with the Peak Fit (Sigma Plot) program.

A CS_2 bath is a relatively simple method to determine the weight percent of polymer in quenched sulfur above the λ-transition as described by Koh and Klement (1970). CS_2 dissolves all allotropic species of sulfur except polymer, and while it is a practical tool to establish the presence of the polymeric material, the quantitative results obtained may strongly depend on the quenching rate (Steudel, 2003). A general practice is to use liquid nitrogen to cool polymer containing liquid sulfur to obtain the highest accuracy in the polymer content, however, here, in situ quenching had to be utilized due to experimental constraints of the high pressure and temperature apparatus. A standard chemistry practice of repeating CS_2 runs three times for half hour each, in conjunction with the pre-

experimental and post-experimental high precision sample weight measurements was followed, courtesy of Dr. Wisner and Dr. Hudson.

2.5 Calculation of Errors

The error margins for the critical parameters are reported in Table 2.5, and those values are used in error calculations in this work.

Table 2.5: Instrumental uncertainties used in calculation of error propagation

Uncertainties	
Container height (mm)	0.1
Container inner diameter (mm)	0.1
Sphere diameter (mm)	0.01
Sphere travel distance (mm)	0.01
Pressure (%)	5
Temperature (°C)	3
Time (s)	0.1

The standard approach in error analysis used here is based on the extensive treatment of uncertainties in falling ball viscometers found in Brizard et al. (2005) and Feng et al. (2006), in addition to corrections applied for high pressure and temperature conditions under which the viscosity experiments were conducted. The uncertainties are reported along with results in the next section.

The error in viscosity was calculated using a standard approach for error propagation (equations 2.14 and 2.15), also implemented by other workers in falling-sphere measurements of viscosity (Tinker et al, 2004).

$$\Delta f(x_i) = \sqrt{\sum \left(\frac{\partial f}{\partial x_i}\right)^2 (\Delta x_i)^2} \qquad (2.14)$$

Here, Δf is the uncertainty in the computed quantity, f is the function that depends on one or more variables x_i, $\partial f/\partial x_i$ is a partial derivative of the function f with respect to $x_{i,,}$ x_i is the directly measured quantity and Δx_i is the error in the directly measured quantity.

3. Results

3.1 Viscosity

Carefully sectioned cubes are shown in Figure 3.1 and Figure 3.2 for the L region and the L' region, respectively.

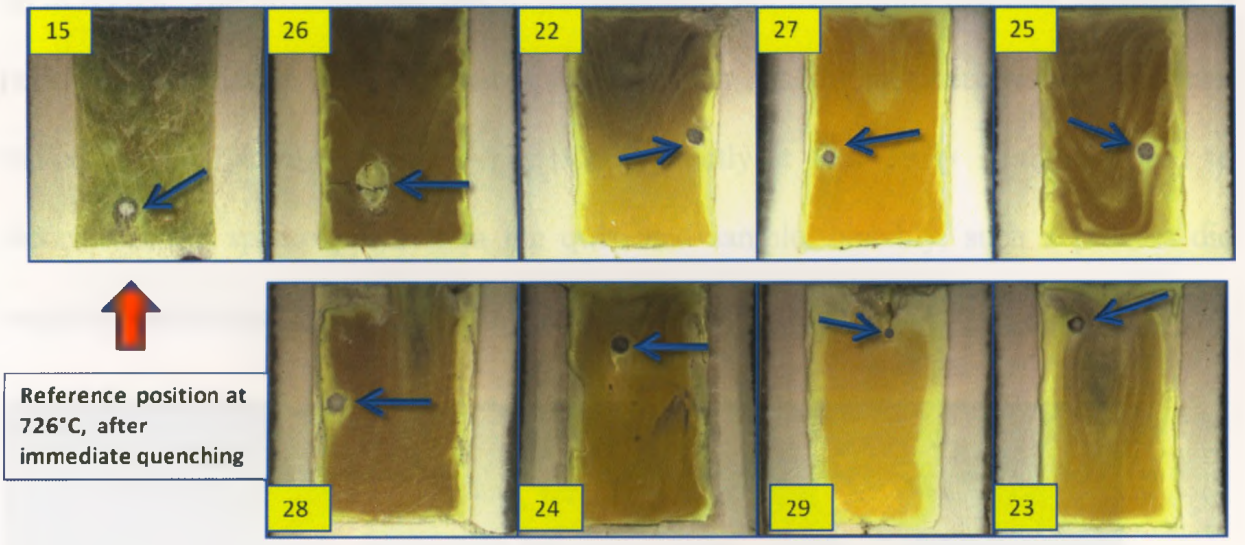

Figure 3.1: Sectioned and ground cubes showing sphere positions for experiments performed in the L region (4.5 GPa, 726°C). Numbers correspond to experiment numbers.

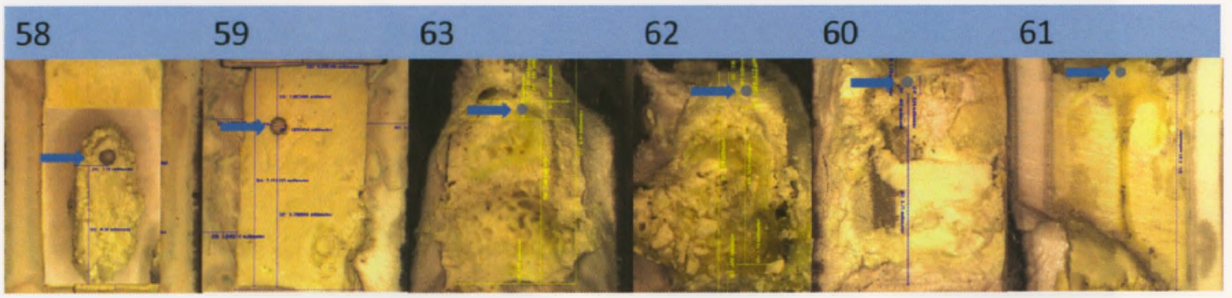

Figure 3.2: Sectioned and ground cubes showing sphere positions for experiments performed in the L' region (4.5 GPa, 1100°C). Numbers correspond to experiment numbers.

While it was relatively easy to recover the spheres in their quenched position in the L region, with the presence of only limited blooming and polymer expansion, the force of the polymer pressure in the L' region was such that it would explode the sample container along with the surrounding parts of the cube immediately on opening (Figure 3.3, Figure A1.10). Coincidentally, only one paper (Cataldo, 1996) mentions the blooming phenomenon that was observed in fibrous sulfur (S_{XII}) below the melting and up to 6 GPa. The difficult part was to painstakingly put everything together. However, a peculiar phenomenon was observed in the L' region, where the sphere would have been trailed by the polymer (Figure 3.4). Consequently it was fairly straightforward to reconstruct the sphere position in the quenched sample. Notably, such a process did require an enormous amount of time (generally hours per sample).

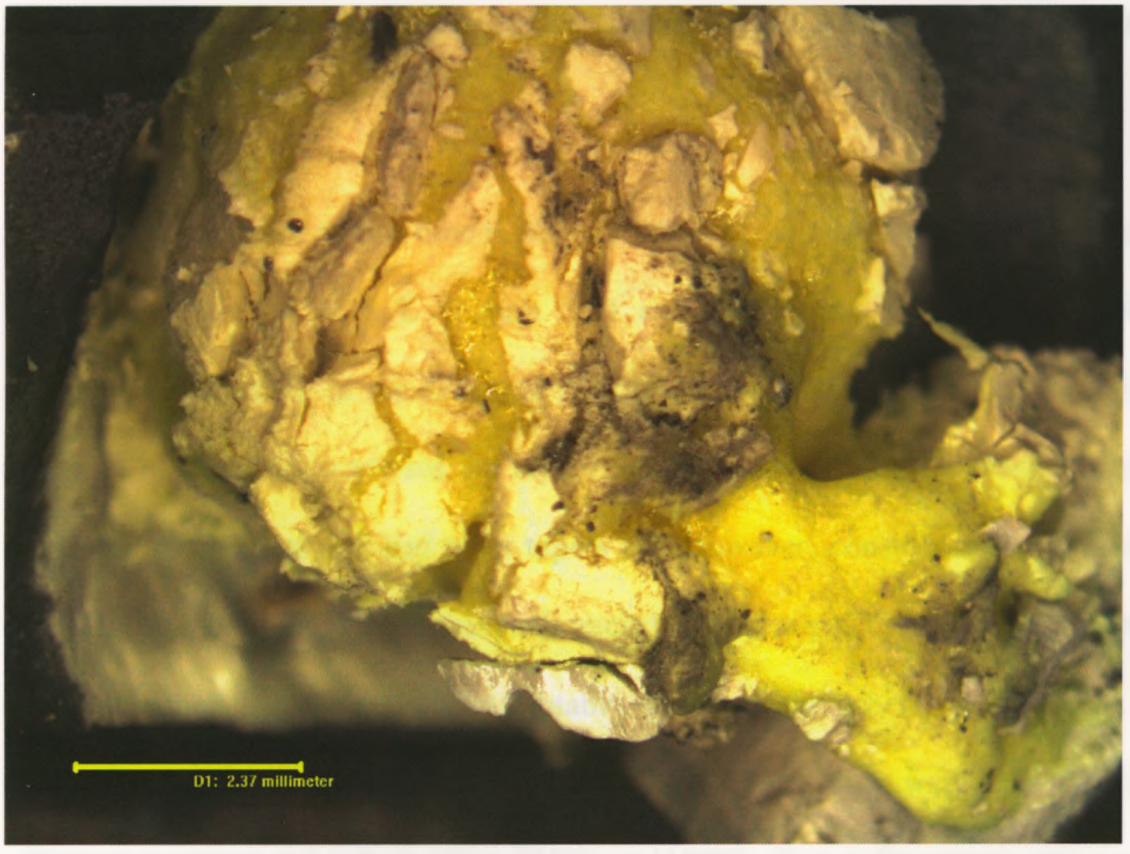

Figure 3.3: The sample exploded out of the container. The scale in the lower left corner is 2.37 mm.

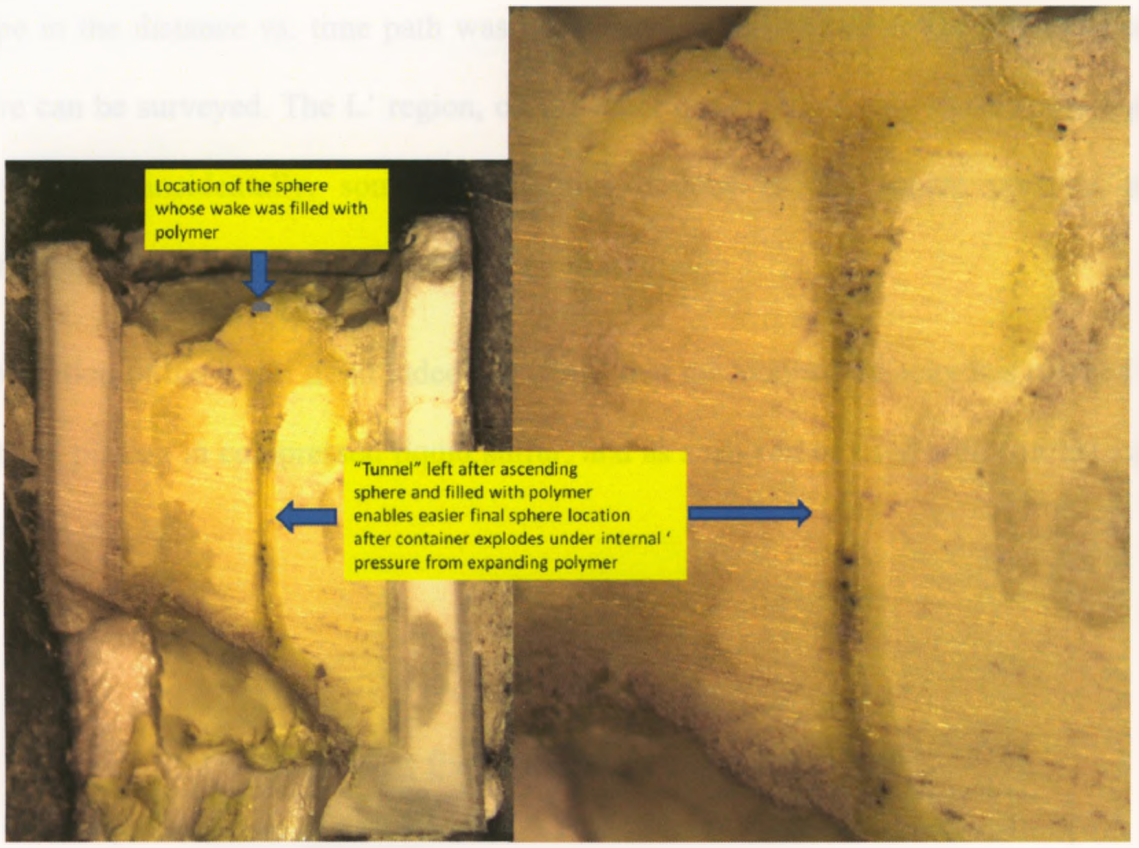

Figure 3.4: The cross section of the sample container, where the upward moving sphere left a tunnel filled with polymer.

Sphere travel distance versus time is plotted in Figure 3.5 and Figure 3.6. There is a clear linear trend for the both L (Figure 3.5) and L' (Figure 3.6) regions, with more pronounced scattering in the L region possibly due to the wall drag effect. Moreover, positions of the spheres toward the top of the container exhibit the possible end effect, illustrated by the fact that last point tapers off. However, considering the scatter in the data prior to that, it is possible that such quenched sphere positions may be interpreted as a scatter, rather than the end effect. Notably, however, the spheres in the both L and L' regions had reached their terminal velocity long before they were quenched in their reference positions at t = 0, at either 726°C or 1100°C. This is the reason why a typical S

shape in the distance vs. time path was not observed, as only the upper region of such curve can be surveyed. The L' region, on the other hand, shows only slight scattering in the data. Coincidentally, some irregularities noticed in the sphere position may correspond to the wall effect, as can be seen from Figure 3.1.

Observation of the linear trend indeed confirms that the attained velocity has reached the terminal plateau in compressed liquid sulfur, and as such can be used with confidence to calculate viscosity.

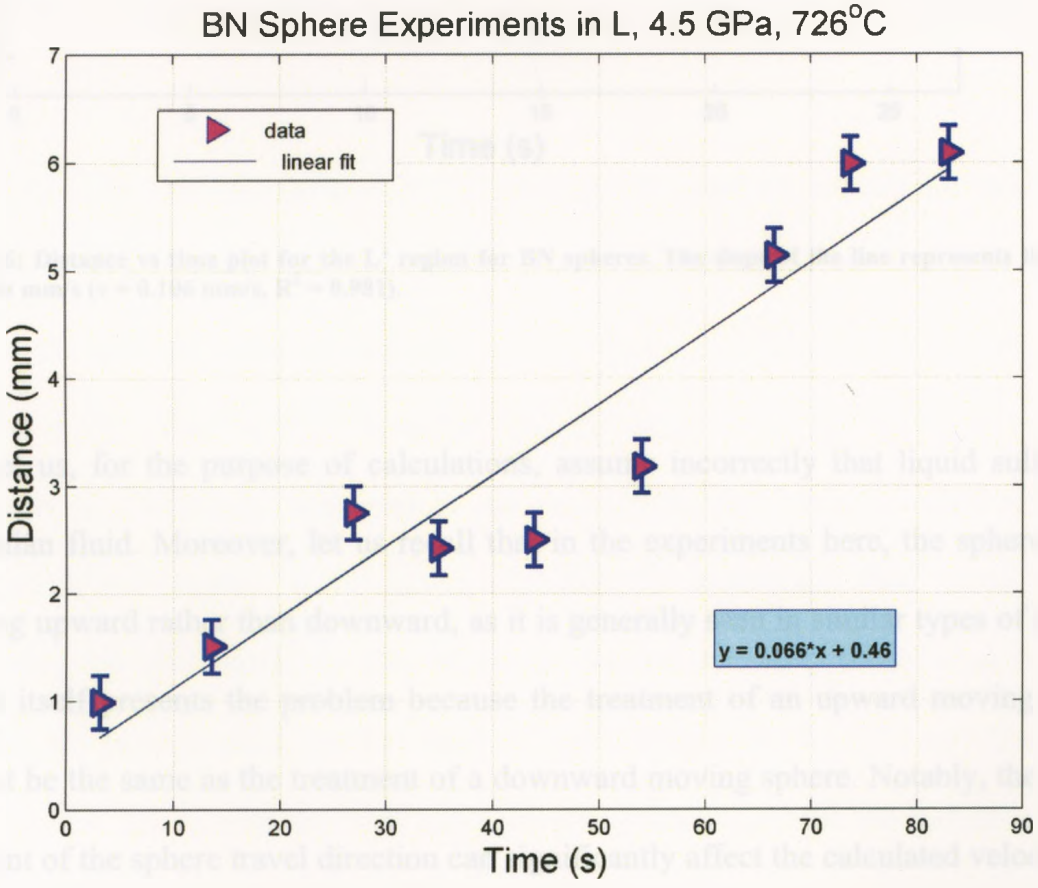

Figure 3.5: Distance vs time plot for the L region for BN spheres. The slope of the line represents the sphere velocity in mm/s (v = 0.066 mm/s, R^2 = 0.912).

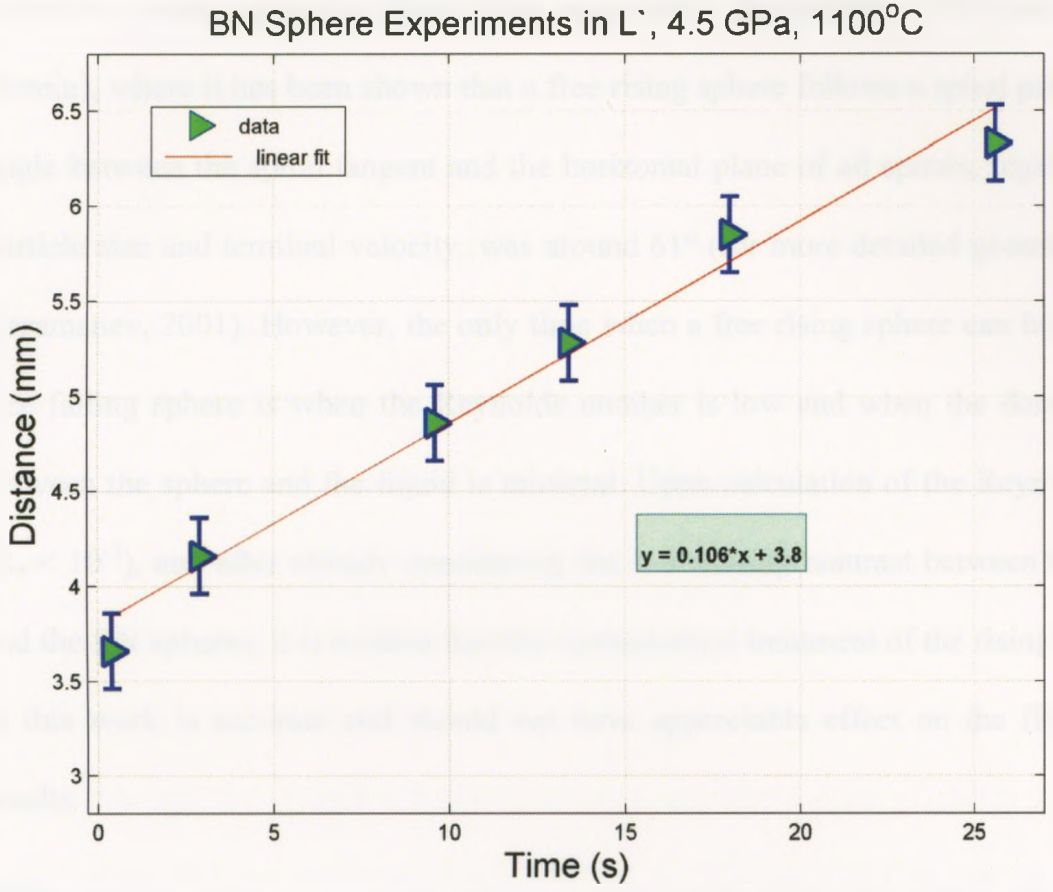

Figure 3.6: Distance vs time plot for the L' region for BN spheres. The slope of the line represents the sphere velocity in mm/s (v = 0.106 mm/s, R^2 = 0.981).

First, let us, for the purpose of calculations, assume incorrectly that liquid sulfur is a Newtonian fluid. Moreover, let us recall that in the experiments here, the spheres were traveling upward rather than downward, as it is generally seen in similar types of studies. This in itself presents the problem because the treatment of an upward moving sphere may not be the same as the treatment of a downward moving sphere. Notably, the proper treatment of the sphere travel direction can significantly affect the calculated velocity and consequently the viscosity results. Galileo was the first one to study the free rise of a buoyant sphere in a liquid and concluded that it should be treated the same as the free falling sphere. For more than four centuries such approach has been assumed correct.

However, recent research dispels that assumption (Karamanev, 2001 and references therein), where it has been shown that a free rising sphere follows a spiral path where the angle between the spiral tangent and the horizontal plane of all spirals, regardless of the particle size and terminal velocity, was around 61° (for more detailed geometry, refer to Karamanev, 2001). However, the only time when a free rising sphere can be treated as a free falling sphere is when the Reynolds number is low and when the density contrast between the sphere and the liquid is minimal. Upon calculation of the Reynolds number ($R_e < 10^{-3}$), and after already considering the low density contrast between liquid sulfur and the BN spheres, it is evident that the mathematical treatment of the rising BN spheres in this work is accurate and should not have appreciable effect on the final viscosity results.

Difficulties have been encountered when selecting the value for sulfur bulk modulus. A limited number of values are reported in literature as seen in the previous chapter, however, the great deviation among those values made it challenging to know which one to select. If the values of bulk modulus (B_0) and its pressure derivative (B') used in Terasaki et al. (2004) are employed in the calculations here, then it would seem that sulfur has lower density at the given experimental conditions, than boron nitride. Considering the observations in this work are contrary to that (i.e. BN rises in liquid sulfur), it can be concluded that the value of bulk modulus of 14.5 GPa and its pressure derivative of 7, are excessively high and cannot accurately describe the density of liquid sulfur at 4.5 GPa and at either 726°C or 1100°C instrumental temperature; where instrumental refers to the instrumentally recorded value without any thermal gradient correction. It should be noted however, that such error was not a serious contribution to

their final results because the density contrast of the platinum sphere they used is many times greater than the density contrast of the BN spheres used in the experiments here. Therefore, the impact and propagation of such error in evaluation of sulfur density and consequently viscosity, is to a great extent suppressed by the use of dense platinum spheres. Those values for B_0 and B' have been originally reported by Luo and Ruoff (1993), and the possible explanation for such high bulk modulus may be found in the fact that they used a diamond anvil cell (DAC) and subsequent XRD measurement to obtain those numbers. The problem of using DAC at lower and medium pressures to obtain the values is principally the dominance of the uniaxial pressure vector and the absence of the hydrostatic or quasi hydrostatic conditions. It appears that values obtained by Bridgman (1945) can still be considered experimentally relevant values of sulfur B_0 under the compression. His reported value for sulfur bulk modulus of 7.93 GPa corresponds well to the value of 7.94 GPa chosen for the calculation in this work. This value was obtained by a rapid compression of sulfur to an amorphous state (Yu et al., 2009) at pressures that are relatively close to the experimental ones applied in this work. Further confidence in the chosen value comes after referring to older work by Abowitz (1977) where he compared compressibility of sulfur, selenium and tellurium. Boron nitride is a great deal different from sulfur, where, after the three distinct values for bulk modulus and its pressure derivative have been selected and compared (Fuchizaki et al. 2008, Solozhenko et al. 1995; Solozhenko and Peun, 1997), the subsequent calculated densities yield less than one percent deviation in the obtained values. Thus the B_0 of 29.9 GPa from Solozhenko et al. (1995) is the generally accepted experimental value in the literature. It should be noted that anomalous values sometimes observed in the literature (Zhao et al., 1999) are

due to turbostratic effects, a term generally describing a crystalline structure where the basal planes have slipped sideways relative to each other as a result of manufacturing and machining stresses. The values for thermal expansion coefficients for sulfur and boron nitride are taken from ASM IMPDC (2002) and Solozhenko et al. (1995), respectively.

The density calculations and thermal expansion corrections at experimental temperatures have been subsequently determined for sulfur and BN, and derived viscosities for L and L' region of liquid sulfur and are given in Table 3.1 along with corresponding densities respectively. A reasonable treatment of the uncertainties, assuming the relatively accurate value of sulfur bulk modulus and consequent density, yields a margin of error in the calculated viscosity to be in the range of 16% in the L region and 12% in the L' region. That is significantly higher than the error reported by Terasaki et al. (2004); however, it is very reasonable relative to the experimental method. Moreover, the contributions of wall (W) and end effects (E) are up to a maximum of 0.75 and 1.19, respectively.

Table 3.1: Viscosity in the L and L' regions at 4.5 GPa and 726°C and 1100°C, respectively.

BN Parameters				Sulfur Parameters						
ρ_{BN} (kg/m^3)	Corrected ρ_{BN} (kg/m^3)	B_{0T} (GPa)	B_T'	ρ_S (kg/m^3)	Corrected ρ_S (kg/m^3)	B_{0T} (GPa)	B_T'	Velocity (mm/s)	Region	Viscosity (Pa·s)
2315	2256	29.9	9.3	2450	2360	7.94	--	0.066	L	**0.140 ± 0.023**
2315	2225	29.9	9.3	2450	2302	7.94	--	0.106	L'	**0.050 ± 0.006**

L region: Pressure = 4.5 GPa, Temperature ~ 726 °C, Temperature corrected for thermal gradient ~777 °C

L' region: Pressure = 4.5 GPa, Temperature ~ 1100 °C, Temperature corrected for thermal gradient ~1180 °C

For comparison purposes, other values obtained from the different bulk modulus parameters for sulfur are given in Table 3.2 (L region) and in Table 3.3 (L' region) to illustrate the unreasonable deviation of such values of sulfur reported in literature.

Table 3.2: Viscosity in the L region obtained using different values of bulk modulus

BN Parameters				Sulfur Parameters					L Region	
ρ_{BN} (kg/m^3)	Corrected ρ_{BN} (kg/m^3)	B_{0T} (GPa)	B_T'	ρ_S (kg/m^3)	Corrected ρ_S (kg/m^3)	B_{0T} (GPa)	B_T'	$\rho_S - \rho_{BN}$	Sphere Terminal Velocity (mm/s)	Viscosity (Pa·s)
2315	2256	29.9	9.3	2496	2376	7.2	--	120	0.066	**0.221 ± 0.037**
2315	2256	29.9	9.3	2462	2342	7.74	--	86	0.066	**0.160 ± 0.027**
2315	2256	29.9	9.3	2450	2332	7.93	--	76	0.066	**0.140 ± 0.023**
2315	2256	29.9	9.3	2365	2251	7.94	5.43	-5	0.066	**0.010 ± 0.002**
2315	2256	29.9	9.3	2307	2196	7.94	7	-60	0.066	**0.112 ± 0.019**
2315	2256	29.9	9.3	2306	2195	9.37	5.43	-61	0.066	**0.114 ± 0.019**
2315	2256	29.9	9.3	2142	2039	14.5	7	-217	0.066	**0.402 ± 0.067**

L region: P = 4.5 GPa, corrected T ~ 777 °C

Highlighted rows: negative values for ($\rho_S - \rho_{BN}$) indicate that the sphere should sink (not observed)

Table 3.3: Viscosity on the L' region obtained using different values of bulk modulus

BN Parameters				Sulfur Parameters					L' Region	
ρ_{BN} (kg/m^3)	Corrected ρ_{BN} (kg/m^3)	B_{0T} (GPa)	B_T'	ρ_S (kg/m^3)	Corrected ρ_S (kg/m^3)	B_{0T} (GPa)	B_T'	$\rho_S - \rho_{BN}$	Sphere Terminal Velocity (mm/s)	Viscosity (Pa·s)
2315	2225	29.9	9.3	2496	2305	7.2	--	80	0.106	**0.108 ± 0.012**
2315	2225	29.9	9.3	2462	2272	7.74	--	48	0.106	**0.065 ± 0.007**
2315	2225	29.9	9.3	2450	2262	7.93	--	37	0.106	**0.050 ± 0.006**
2315	2225	29.9	9.3	2365	2183	7.94	5.43	-41	0.106	**0.056 ± 0.006**
2315	2225	29.9	9.3	2307	2130	7.94	7	-95	0.106	**0.128 ± 0.015**
2315	2225	29.9	9.3	2306	2129	9.37	5.43	-96	0.106	**0.130 ± 0.015**
2315	2225	29.9	9.3	2142	1978	14.5	7	-247	0.106	**0.334 ± 0.038**

L' region: P = 4.5 GPa, corrected T ~ 1180 °C

Highlighted rows: negative values for ($\rho_S - \rho_{BN}$) indicate that the sphere should sink (not observed)

The viscosity results derived in this work correspond well with the values reported by Terasaki et al. (2004); viscosity seems to decrease with increasing temperature (Schmeiser at al., 2005 and references therein). Moreover, sulfur exhibits an anomalous behavior, where viscosity decreases with pressure as evident from the table below (Table 3.4), which is contrary to what Doi (1963) showed under small pressure increases up to

100 atmospheres. That type of behavior has been observed in silicates (McMillan and Wilding, 2009 and references therein) and aluminosilicates (Kushiro, 1980), and coincidently, both of these are polymers under high pressure. However, the topic of polymerization under pressure will be revisited later. For comparison, a table of different viscosity values from Terasaki et al. (2004) are shown in Table 3.4.

Table 3.4: The viscosity values for different pressures and temperatures of liquid sulfur as reported by Terasaki et al. (2004)

Run No	P (GPa)	T^a (K)	Sphere diameter (μm)	v (mm s^{-1})	η (Pa s)
S560-1	3.2(3)	788(22)	93	0.14	0.45(2)
S560-2	3.2(3)	793(11)	112	0.12	0.69(8)
S564	5.14(7)	866(10)	122	0.27	0.36(4)
S562	7.8(3)	962(8)	118	0.45	0.19(2)
S660	9.1(2)	991(6)	101	0.45	0.147(6)
S652	9.7(5)	1067(1)	94	0.53	0.105(4)

[a] The temperature error represents a change of temperature during the falling of the sphere.

It is evident that viscosity of liquid sulfur is less than one half of the viscosity of L liquid region, and while such behavior might be attributable to the higher temperature, it is not clear immediately if the transition to the L' has any contribution to the observed value. Coincidently, the viscosity results for liquid Se under high pressure and along the melting curve show a sharp decrease of viscosity across the boundary of the two liquids (Brazhkin et al., 2007). A partial phase diagram of sulfur with plotted viscosity results from Terasaki et al. (2004) and this work are given in Figure 3.7.

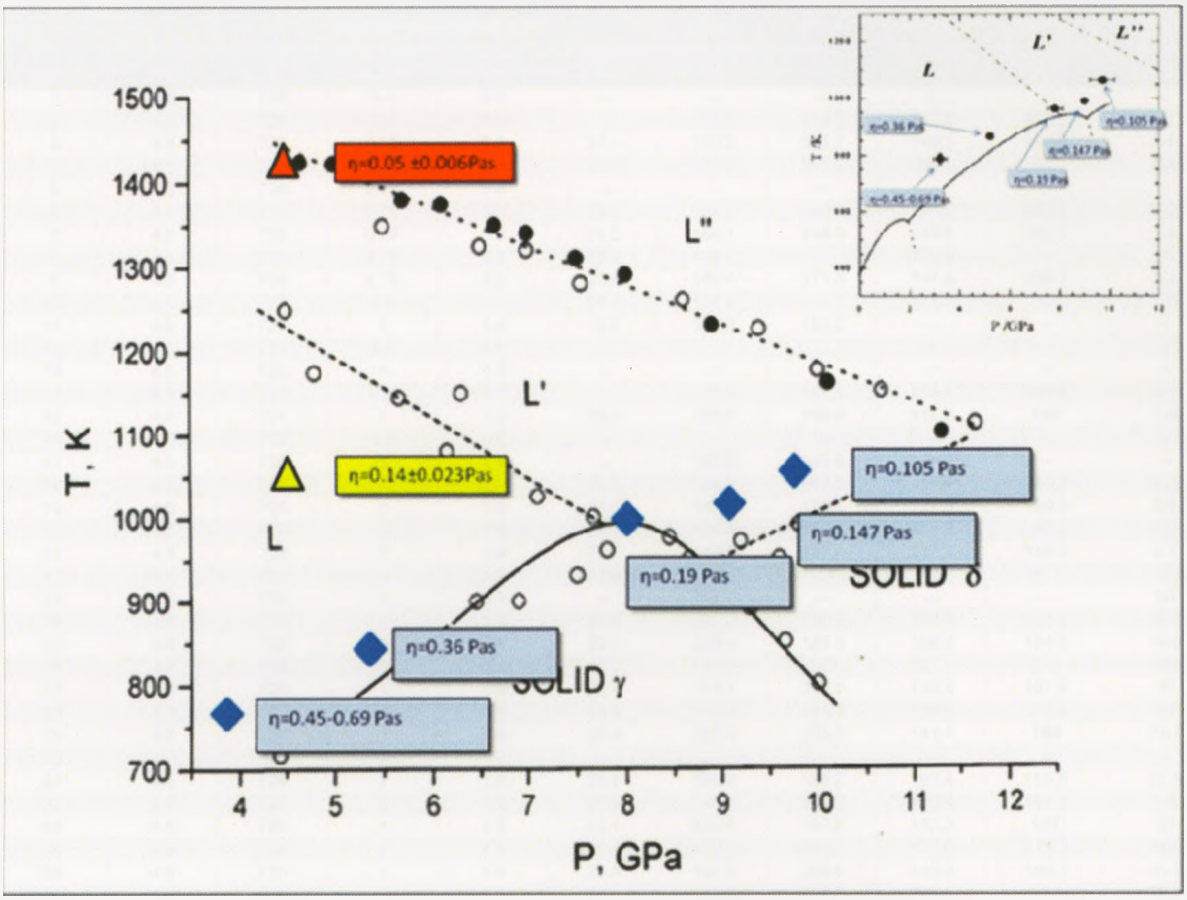

Figure 3.7: Main figure: Phase diagram from Brazhkin et al. (1999) showing phase diagram of sulfur from 3.5 – 12.5 GPa as well as three liquids denoted as L, L' and L". Open circles denote resistivity anomalies and black circles denote thermobaric analyses. The results from Terasaki et al. (2004) are posted in blue diamonds, while yellow and red triangles represent measurements in this work. Small inset: the original plot from Terasaki et al. (2004) paper with their viscosity values superimposed (also shown in the large diagram).

The behavior of the velocity of C spheres was anomalous during the experiments. The critical relevance of such phenomenon, its interpretation and significance are discussed later in the text.

Below, four tables with summaries and all relevant parameters are given.

Table 3.5: All runs with their respective parameters.

Run #	Pressure (GPa)	Temperature (°C)	Heating Rate (Computer Input)	Heating Rate (actual) (°C/s)	Cooling Rate (°C/s)	Time above theoretical melting point, 500°C (s)	Time above actual melting point (s)	Time between 500° -726°C (s)	Time between actual melting point and 726° C (s)	Time above 726°C (s)
1	4.5	726	0.5	0.6	--	--	--	--	--	--
2	4.5	726	0.5	0.6	--	207.9	504.2	195.8	482.7	1.7
3	4.5	726	0.75	1.0	24.1	160.2	301.7	149.1	284.8	2.3
4	4.5	726	0.75	1.0	24.5	179.9	311.1	166.1	291.1	5.1
5	4.5	726	0.75	1.0	--	--	--	--	--	--
6	4.5	726	0.75	1.0	23.6	159.2	266.4	147.5	250.5	2.2
7	4.5	726	0.75	1.0	24.2	160.1	245.9	148.8	231.3	1.0
8	4.5	726	0.75	1.0	23.1	188.4	--	176.9	--	1.1
9	4.5	726	0.75	1.0	23.6	159.4	271.6	147.8	255.7	2.2
10	4.5	726	0.9	--	23.4	185.9	--	173.5	--	3.0
11	4.5	726	1	1.9	19.0	129.2	182.2	--	--	--
12	4.5	726	0.5	0.6	--	--	--	--	--	--
13	4.5	726	1	1.9	--	--	--	--	--	--
14	4.5	726	1	1.9		124.9	168.1	114.1	155.9	2.2
15	4.5	726	1	1.9	25.8	128.3	203.9	117.8	190	1.0
16	4.5	726	0.5	0.6	--	--	--	--	--	--
17	4.5	726	1	1.9	--	165.5	245.9	--	--	--
18	4.5	726	1	1.9	25.8	129.3	267.2	116.9	248.3	4.3
19	4.5	726	1	1.9	24.0	141.9	175.1	127.5	159.9	5.6
20	4.5	726	1	1.9	24.9	161.4	158.4	149.9	146.9	2.9
21	4.5	726	1	1.9	23.7	149.2	157.4	137.2	145.3	3.1
22	4.5	726	1	1.9	23.8	204.3	127	169	95.1	27
23	4.5	726	1	1.9	--	--	--	--	--	83
24	4.5	726	1	1.9	24.5	237.2	198.6	162.7	125.5	66.5
25	4.5	726	1	1.9	23.5	220.4	185.5	168.2	134.5	43.9
26	4.5	726	1	1.9	25.2	149.7	283	127.7	254	13.6
27	4.5	726	1	1.9	23.4	176.1	233.2	132.8	187.9	35
28	4.5	726	1	1.9	24.0	201.9	244.4	139.6	180.8	54
29	4.5	726	1	1.9	23.4	223.3	272.3	141.4	189	73.7
30	--	--	--	--	--	--	--	--	--	--
31	4.5	726	1	1.9	23.2	194.4	186.2	163.4	155.3	22.6
32	4.5	726	1	1.9	23.0	141.5	200.1	130.4	187.1	1.4
33	4.5	726	1	1.9	23.1	223.5	197.8	192.2	167	23
34	4.5	726	1	1.9	25.4	170.6	261.7	127.6	215.3	34.9
35	4.5	726	1	1.9	23.9	197.9	253.6	145.3	199.1	44.3
36	4.5	726	1	1.9	24.0	210.3	267.9	128.4	184	73.7
37	4.5	726	1	1.9	23.2	296.1	267.5	173.4	145.6	114.4
38	4.5	726	1	1.9	25.0	346.9	309.8	184.6	148.7	154.1
39	4.5	726	1	1.9	26.2	191.6	170.5	180.6	160.2	0.8
40	4.5	726	9.9	12.7	24.2	34	--	--	--	4
41	4.5	726	1	1.9	26.9	142.5	302.6	131.8	283.5	2.4
42	4.5	726	1	1.9	24.6	143.2	207.3	132.1	194.3	2.3
43	4.5	726	1	1.9	--	--	--	--	--	--
44	4.5	726	1	1.9	--	--	--	--	--	3
45	4.0	800	0.5	0.6	24.4	280.0	469.8	201.4	387.6	70.8
46	4.5	726	1	1.9	26.6	184.4	168.6	163.4	148	12.5
47	4.5	800	1	1.9	25.3	309.5	538.1	227.6	450.5	74.3
48		726	1	1.9	24.7	170.3	203.7	127.6	160.4	35.2
49	3.5	800	1	1.9	--	--	--	--	--	--
50	3.5	800	0.5	0.6	24.4	308.4	491.5	227.7	407.7	72.9
51	4.5	--	--	--	--	--		--		--
52	4.5	726	1	1.9	25.7	243.5	374.8	131	255.4	104.5
53	4.5	726	1	1.9	--	374.8		134		303
54	4.5	726	1	1.9	25.9	288.7	456.7	126.9	287.4	154.1
55	4.5	726	1	1.9	25.4	292.6	391.3	130.2	225.3	154.6
56	4.5	726	1	1.9	24.3	334.4	374.4	142.1	182	184.9
57	4.5	726	1	1.9	24.1	384.9	446.4	133.5	193.3	242.5
58	4.5	1100	5	5.7	28.4	--	--	--	--	0.4*
59	4.5	1100	5	5.7	30.9	--	--	--	--	2.9*
60	4.5	1100	5	5.7	32.3	--	--	--	--	18*
61	4.5	1100	5	5.7	31.2	--	--	--	--	25.6*
62	4.5	1100	5	5.7	30.4	--	--	--	--	13.4*
63	4.5	1100	5	5.7	30.2	--	--	--	--	9.6*
64	4.5	726	1	1.9	24.6	--	--	--	--	--
65	4.5	726	1	1.9	25.8	167	302.5	126.1	256.1	33.2

Errors: Pressure = 5%, Time = ±0.1 s, Temperature = ±3 C

* Time above 1100° C

Table 3.6: All runs with temperature parameters pertaining to the melting and maximum attained temperatures.

Run #	Melting Temperature (°C)	Temperature Correction for Thermal Gradient (°C)	Corrected Melting Temperature (°C)	Maximum Temperature Attained (°C)	Temperature Correction for Thermal Gradient (°C)	Corrected Max Temperature Attained (°C)	Temperature Difference Between Melting Point and First Inferred Phase Change (°C)
1	470.0	25.7	495.7	–	–	–	–
2	–	–	–	727.5	51.0	778.4	–
3	363.5	23.1	386.7	760.4	53.4	813.8	146.8
4	–	–	–	731.8	51.3	783.1	–
5	–	–	–	739.7	51.9	791.6	–
6	398.8	25.5	424.3	727.6	51.0	778.6	102.2
7	420.1	24.7	444.9	727.3	51.0	778.2	163.8
8	–		–	726.8	51.0	777.7	–
9	394.0	24.7	418.7	727.2	51.0	778.1	102.2
10	–	–		731.8	51.3	783.1	–
11	440.2	23.8	464.0	726.0	50.9	776.9	84.1
12	–	–	–	–	–	–	–
13	–	–	–	–	–	–	–
14	463.9	27.4	491.3	728.9	51.1	780.0	62.5
15	415.9	25.5	441.3	727.4	51.0	778.4	78.9
16	–	–	–	–	–	–	–
17	–	–	–	726.0	50.9	776.9	–
18	348.1	22.0	370.1	736.4	51.6	788.0	149.8
19	480.0	22.7	502.7	738.7	51.8	790.5	109.6
20	501.1	25.6	526.7	733.7	51.5	785.1	72.3
21	497.3	24.2	521.5	731.4	51.2	782.6	98.4
22	590.5	39.4	629.9	758.8	53.3	812.1	46.8
23	506.5	27.9	534.4			0.0	140.3
24	536.5	33.4	569.8	777.5	54.6	832.1	49.0
25	531.2	32.8	564.0	761.1	53.4	814.5	71.3
26	344.9	21.6	366.4	741.3	52.0	793.3	144.3
27	450.3	26.6	476.9	761.7	53.5	815.2	63.3
28	466.1	26.9	493.1	762.1	53.5	815.5	43.4
29	464.4	27.4	491.9	773.4	54.2	827.6	117.4
30	–	–	–	–	–	–	–
31	504.0	26.7	530.7	747.1	52.4	799.5	92.5
32	451.3	26.9	478.2	727.4	51.0	778.3	55.7
33	512.6	29.7	542.3	745.3	52.3	797.6	49.8
34	419.0	24.9	444.0	772.8	54.2	827.1	110.4
35	454.3	27.6	481.9	761.4	53.4	814.8	57.9
36	450.2	26.6	476.8	761.3	53.4	814.7	135.9
37	520.9	31.4	552.3	766.3	53.8	820.1	23.4
38	532.0	32.9	564.8	776.3	54.5	830.7	32.8
39	518.5	31.1	549.6	726.4	50.9	777.3	53.3
40	–	–	–	754.4	52.9	807.3	–
41	313.5	19.5	332.9	733.7	51.5	785.2	240.7
42	451.1	26.9	477.9	728.0	51.0	779.0	70.6
43	–	–	–				–
44	–	–	–	727.0	51.0	778.0	–
45	416.9	25.3	442.2	805.0	56.6	861.6	81.4
46	512.9	29.7	542.6	727.2	51.0	778.1	82.2
47	375.2	22.9	398.1	800.9	56.3	857.2	166.8
48	482.6	22.2	504.8	767.3	53.8	821.2	64.3
49	–	–	–	–	–	–	–
50	426.2	23.7	449.9	800.8	56.3	857.0	120.8
51	–	–	–	856.8	60.3	917.1	–
52	349.7	22.2	371.9	780.4	54.8	835.1	194.4
53	409.8	26.2	436.0	768.1	53.9	822.1	121.0
54	328.2	19.9	348.1	770.3	54.0	824.3	182.9
55	411.7	26.0	437.8	774.9	54.4	829.3	91.5
56	475.9	23.8	499.6	769.5	54.0	823.4	109.7
57	453.6	27.6	481.2	771.2	54.1	825.3	92.8
58	–	–	–	1100.3	77.7	1178.0	–
59	–	–	–	1110.2	78.4	1188.7	–
60	–	–	–	1129.9	79.9	1209.8	–
61	–	–	–	1132.0	80.0	1212.1	–
62	–	–	–	1128.5	79.8	1208.3	–
63	–	–	–	1124.2	79.5	1203.7	–
64	–	–	–	750.4	52.6	803.0	–
65	368.4	23.1	391.5	764.8	53.7	818.4	164.6

Table 3.7: Phase change information for all runs.

Run #	First Inferred Phase Change (°C)	Temperature Correction for Thermal Gradient (°C)	Corrected First Inferred Phase Change (°C)	Second Infered Phase Change (°C)	Temperature Correction for Thermal Gradient (°C)	Corrected Second Inferred Phase Change (°C)
1	–	–		–	–	–
2	526.6	32.3	558.9	633.3	44.1	677.5
3	506.0	27.5	533.5	625.2	43.2	668.3
4	–			–	–	–
5	–	–		–	–	–
6	501.0	25.6	526.6	589.4	39.2	628.6
7	571.0	37.6	608.6	608.2	40.9	649.1
8	–			–	–	–
9	496.8	24.2	520.9	627.4	43.5	670.9
10	–	–		–	–	–
11	517.5	30.7	548.1	620.4	42.5	662.9
12	–	–	–	–	–	–
13	–	–	–	–	–	–
14	522.2	31.6	553.8	604.8	40.6	645.4
15	496.3	23.9	520.2	595.2	39.7	634.9
16	–	–	–	–	–	–
17	–	–	–	–	–	–
18	496.0	23.9	519.9	609.7	41.1	650.9
19	574.3	37.9	612.2	606.4	40.7	647.1
20	562.4	36.6	599.0	610.2	41.1	651.3
21	581.4	38.5	619.9	633.8	44.2	678.0
22	632.6	44.1	676.8	649.2	45.4	694.6
23	630.7	43.9	674.7	–	–	–
24	580.4	38.5	618.8	628.4	43.6	672.0
25	595.5	39.8	635.3	625.4	43.2	668.6
26	488.5	22.2	510.8	599.2	40.0	639.2
27	511.1	29.2	540.2	595.6	39.8	635.4
28	508.3	28.2	536.5	581.2	38.5	619.7
29	571.5	37.7	609.2	638.4	44.6	683.0
30	–	–	–	–	–	–
31	584.4	38.8	623.2	634.1	44.2	678.3
32	506.3	27.5	533.8	571.5	37.7	609.2
33	556.2	35.9	592.1	596.5	39.8	636.2
34	522.7	31.7	554.4	626.8	43.5	670.2
35	510.7	29.2	539.8	624.0	43.0	667.0
36	574.7	38.0	612.7	609.1	41.0	650.2
37	541.6	34.1	575.7	625.2	43.2	668.4
38	561.1	36.5	597.6	611.2	41.3	652.5
39	565.7	37.1	602.8	628.6	43.7	672.3
40	–	–		–	–	–
41	539.8	33.8	573.7	625.1	43.2	668.3
42	517.6	30.9	548.5	612.9	41.5	654.5
43	–	–		–	–	–
44	–	–		–	–	–
45	498.8	24.9	523.7	584.8	38.9	623.7
46	585.8	39.0	624.8	629.0	43.7	672.7
47	532.0	32.9	564.9	592.8	39.5	632.4
48	535.7	33.4	569.1	614.0	41.7	655.7
49	–	–	–	–	–	–
50	537.2	33.5	570.6	638.5	44.6	683.0
51	–	–		–	–	–
52	533.2	33.0	566.2	614.3	41.7	655.9
53	525.1	32.0	557.1	592.2	39.5	631.7
54	504.3	26.7	531.0	522.8	31.7	554.5
55	502.9	26.4	529.3	594.1	39.6	633.7
56	571.6	37.7	609.3	601.8	40.3	642.1
57	540.1	33.8	573.9	594.3	39.6	633.9
58	–	–	–	–	–	–
59	–	–	–	–	–	–
60	–	–	–	–	–	–
61	–	–	–	–	–	–
62	–	–	–	–	–	–
63	–	–	–	–	–	–
64	–	–	–	–	–	–
65	524.2	31.9	556.1	598.7	40.0	638.7

Table 3.8: Experimental data for all runs.

Run #	Sphere diameter (mm)	Sphere Type/ Composition	Distance of the Sphere from the Bottom (mm)	Distance sphere moved (mm)	Polimer percentage (visually estimated)	Visible Presence of Microflow	Notes
1	--	Pt	--	--	--	--	failed
2	--	Pt	0.0	--	--	Y	thermocouple calibration, melting T inconclusive
3	--	chromium steel	0.0	--	--	--	
4	--	C	0.0	--	--	Y	inconclusive
5	--	--	--	--	--	--	thermocouple calibration
6	1.19	C	0.0	--	--	Y	
7	1.19	C	0.0	--	--	Y	
8	1.22	C	0.0	--	--	Y	Inconclusive
9	1.26	C	0.0	--	--	Y	
10	0.81	BN	0.0	--	--	Y	Inconclusive
11	0.6, 0.6	C, BN	0.0	2.32	< 20%	Y	C sphere placed on the bottom of the cup
12	--	--	--	--	--	--	no confidence in results, incorrect wiring
13	0.5	BN	0.5	--	--	--	computer error, data lost
14	0.55	BN	0.5	0.49	< 20%	Y	sphere got stuck to the container wall
15	0.56	BN	0.5	0.95	> 20%	Y	--
16	--	--	--	--	--	--	thermocouple calibration
17	0.53,0.57	C, BN	0.5	2.590 / 1.873	< 20%	Y	-
18	0.53,0.56	C, BN	0.5	--	< 20%	Y	spheres got stuck to the container wall
19	0.57	BN	0.5	1.75	> 20%	Y	--
20	0.55	C	0.5	4.12	< 20%	Y	--
21	0.56	BN	0.5	0.99	< 20%	Y	--
22	0.55	BN	0.5	2.75	> 20%	Y	--
23	0.57	Bn	0.5	6.09	< 20%	Y	--
24	0.55	BN	0.5	5.14	< 20%	Y	--
25	0.55	BN	0.5	2.50	> 20%	Y	--
26	0.56	BN	0.5	1.51	> 20%	Y	--
27	0.57	BN	0.5	2.42	< 20%	Y	--
28	0.58	BN	0.5	3.18	> 20%	Y	--
29	0.56	BN	0.5	5.99	< 20%	Y	--
30	0.56	BN	0.5	--			
31	0.56	BN	0.5	--	> 20%	Y	sphere got stuck
32	0.57	BN	0.5	--	> 20%	Y	--
33	0.57	BN	0.5	--	> 20%	Y	--
34	0.55	BN	0.5	--	> 20%	Y	--
35	0.58	BN	0.5	--	> 20%	Y	--
36	0.56	BN	0.5	--	> 20%	Y	--
37	0.58	BN	0.5	--	> 20%	Y	--
38	0.57	BN	0.5	--	> 20%	Y	--
39	1.13	chromium steel	0.5	--	> 20%	Y	chromium steel sphere
40	1.13	chromium steel	0.5	--	> 20%	Y	chromium steel sphere
41	0.48	C	2.0	3.92	> 20%	Y	
42	0.48	C	2.0	3.62	> 20%	Y	
43	--	--	2.0	--	--	Y	
44	0.52	C	2.0	3.23	> 20%	Y	
45	--	--	--	--	> 20%	Y	polymerization and melting curve investigation
46	0.56	C	2.0	3.00	> 20%	Y	
47	--		--	--	> 20%	Y	polymerization and melting curve investigation
48	0.46	C	2.0	2.94	> 20%	Y	
49	--	--	--	--	> 20%	Y	polymerization and melting curve investigation
50	--	--	--	--	> 20%	Y	polymerization and melting curve investigation
51	--	--	--	--	--	--	failed due to faulty and leaking valve on the press
52	0.50	C	2.0	1.82	> 20%	Y	
53	0.47	C	2.0	6.80	> 20%	Y	
54	0.60	BN	2.0	3.22	> 20%	Y	
55	0.57	C	2.0	3.40	> 20%	Y	
56	0.45	C	2.0	0.70	> 20%	Y	
57	0.52	C	2.0	2.70	> 20%	Y	
58	0.61	BN	**	3.66	> 20%	--	
59	0.62	BN	**	4.16	> 20%	--	
60	0.59	BN	**	5.85	> 20%	--	
61	0.62	BN	**	6.33	> 20%	--	
62	0.63	BN	**	5.28	> 20%	--	
63	0.62	BN	**	4.86	> 20%	--	
64	--	--	--	--	> 20%	Y	polymer inverstigation
65	--	--	--	--	> 20%	Y	polymer inverstigation

** Measured for each run

3.2 Polymerization at 4.5 GPa and around 726°C

When quenched from temperatures above 726°C and subsequently sectioned, the sulfur samples exhibited rather peculiar characteristics. A partially translucent and flexible deep red material was recovered having almost the same properties as sulfur quenched above 159°C, or the λ-transition, as described by Steudel (2003) and Meyer (1976). Additionally, the exact shape, color and spatial arrangement within the sample container of the dark red material was found to be a direct function of time. This particular phenomenon will be revisited further in the text. Moreover, a bright yellow material that blooms and expands after depressurization from a sample container was observed along with a brittle whitish-yellowish crystalline material. Before the more detailed discussion focused on discoveries in this thesis takes place, some further background on the subject at hand is warranted.

A color change from the yellow liquid to dark red, seen in recovered samples, has been also described by Vezzoli et al. (1976) and was directly attributed to the increasing polymer concentration. Moreover, it was suggested by Eisenberg (1963) that the polymer component is an integral part of the liquid at high pressure and that the λ-transition temperature is inversely proportional to the pressure. Eisenberg (1963) calculated using the method of equilibrium polymerization, that the λ-transition coincides with the melting curve at 0.085 GPa. This remains unclear as it has not been directly investigated and a great deal of confusion surrounds such prediction (Crapanzano, 2005). It is possible to find statements in the older literature declaring that polymerization ceases after that pressure, while only recently Crapanzano (2005) stated that Vezzoli, in personal communication with her, stated that above 0.085 GPa solid sulfur melts directly into

polymeric form. It should be noted that the neither claim is substantiated to a satisfactory degree, as no specific research has investigated this topic much further except Vezzoli et al. (1969b) using the DTA and quenching method up to 3.1 GPa and 500°C. They discovered that "de-polymerization" temperature shifts from 187°C to 206°C. However, now it can be clearly recognized that such a statement is based on the behavior of viscosity (slowly decreases with increasing temperature above 187°C where actual degree of polymerization increases all the way to the boiling point of liquid sulfur (Koh and Klement, 1970). However, that is not to say that one should dismiss their work based on such a misinterpretation. What they discovered is critical as it strongly relates to the observations made in this work. The phase diagram (Figure 3.8) showing five different liquid phases is important so that the reader can track the discussion about specific phases Vezzoli et al. (1969b) discovered and the properties of aforementioned, with the intention of connecting them to the discoveries and observations made in this thesis.

First, Vezzoli et al. (1969b) extrapolated the "polymerization curve" to coincide with the melting curve at 0.07 GPa. This should indicate that sulfur quenched above that pressure must be polymeric. However, they reported that a sample quenched from the B field (from 0.07 up to about 1 GPa), while showing some limited flexibility, was fully soluble in CS_2 and consequently polymer free. Similarly, samples quenched from the C field (higher temperature region) were brittle and were shown to be S_8 crystallites, with no polymer present. However, samples quenched from the D field were reddish in color, highly stretchable and somewhat insoluble in CS_2, clearly indicating that they contain polymer.

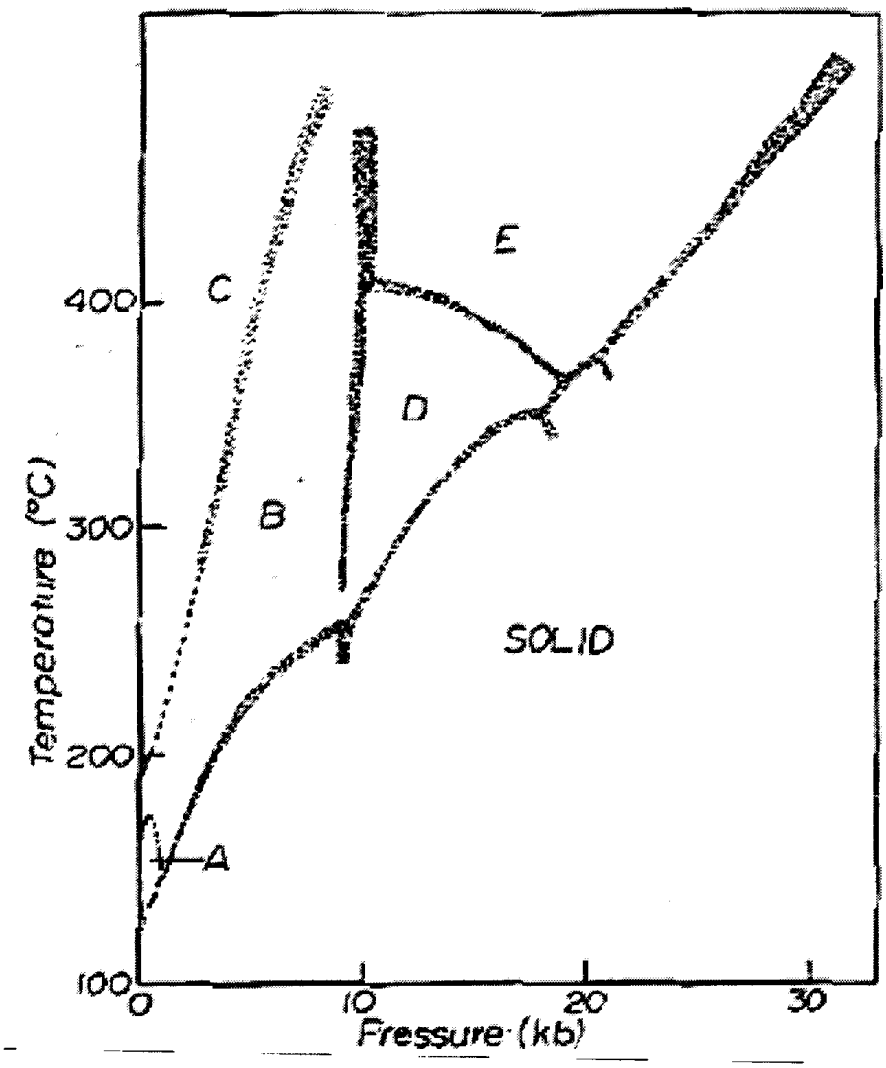

Figure 3.8: Melting curve and liquid phases of sulfur from atmospheric pressure to 31 kbar (Vezzoli et al., 1969b).

Figure 3.8 shows that the D region extends from 1 GPa to 2 GPa at ~350°C. Properties of liquid in the region E closely correspond to the D-liquid and exhibit very 'high' but not quantified polymer content. More importantly, they showed that products quenched from those metastable phase boundaries contain a minimum of two products that exist in equilibrium at those pressure and temperature conditions.

If one recalls that Chrichton et al. (2001) showed that the region of solid sulfur at 3 GPa and around 400°C, with trigonal geometry, exhibits the long helical chain structure, then it should be no surprise that such a solid structure melts directly into the liquid containing polymeric chains (Figure 3.9).

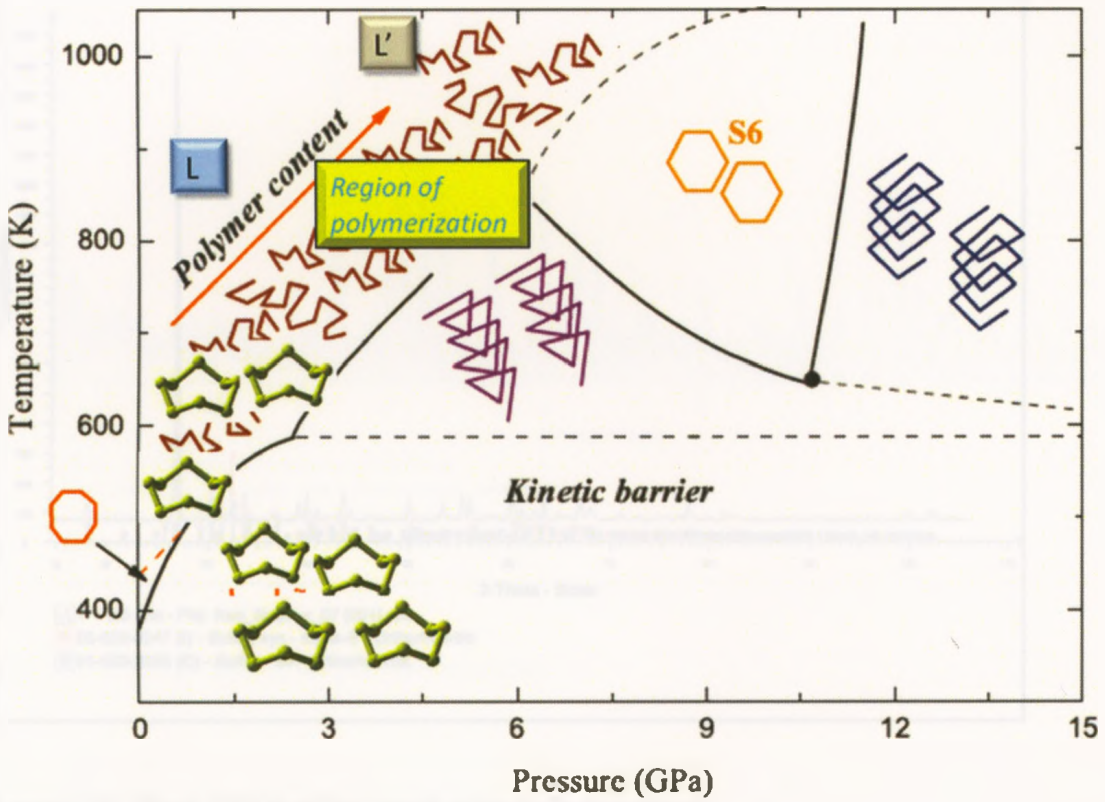

Figure 3.9: Phase diagram of sulfur showing high pressure and temperature phases, including the expected polymeric phase in a liquid above 3 GPa as a result of helical structures in solid below the melting curve (adopted from Crapanzano, 2005).

Thus, such observations as indicated at the beginning of the chapter were conducive to investigate the polymerization phenomenon at high pressure in more detail and to quantify it for the first time.

Micro x-ray diffraction (μXRD) was used to investigate the starting powdered sulfur sample (Figure 3.10), and subsequently to investigate the sample with a clear dark red region and the regions where bright yellow sulfur was expanded and bloomed beyond its original volume (Figure 3.11). Subsequently, a comparison was made to the original orthorhombic powdered sample.

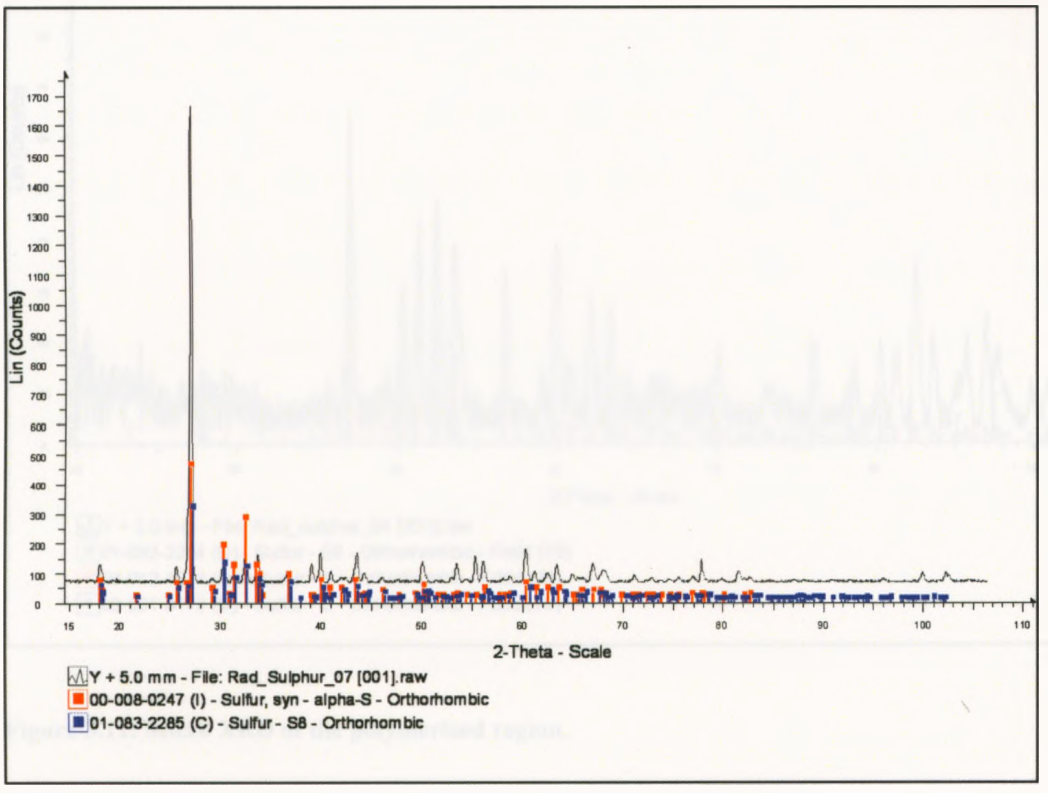

Figure 3.10: Micro XRD of sulfur sample prior to the experiment.

The μXRD pattern of the fresh powdered sulfur showed only the presence of S_8 with high intensity peak (Figure 3.10). The μXRD of the polymeric sample still shows S_8 predominantly (Figure 3.11), however the peak intensities are significantly smaller. Moreover, Vezzoli et al. (1969b) observed the same pattern, where they stated: "…(quenched polymer sulfur)…*gave an x-ray pattern on 'annealing' similar to that of*

orthorhombic sulfur, except for relative intensities and the presence of a new strong reflection at 4.52 Å".

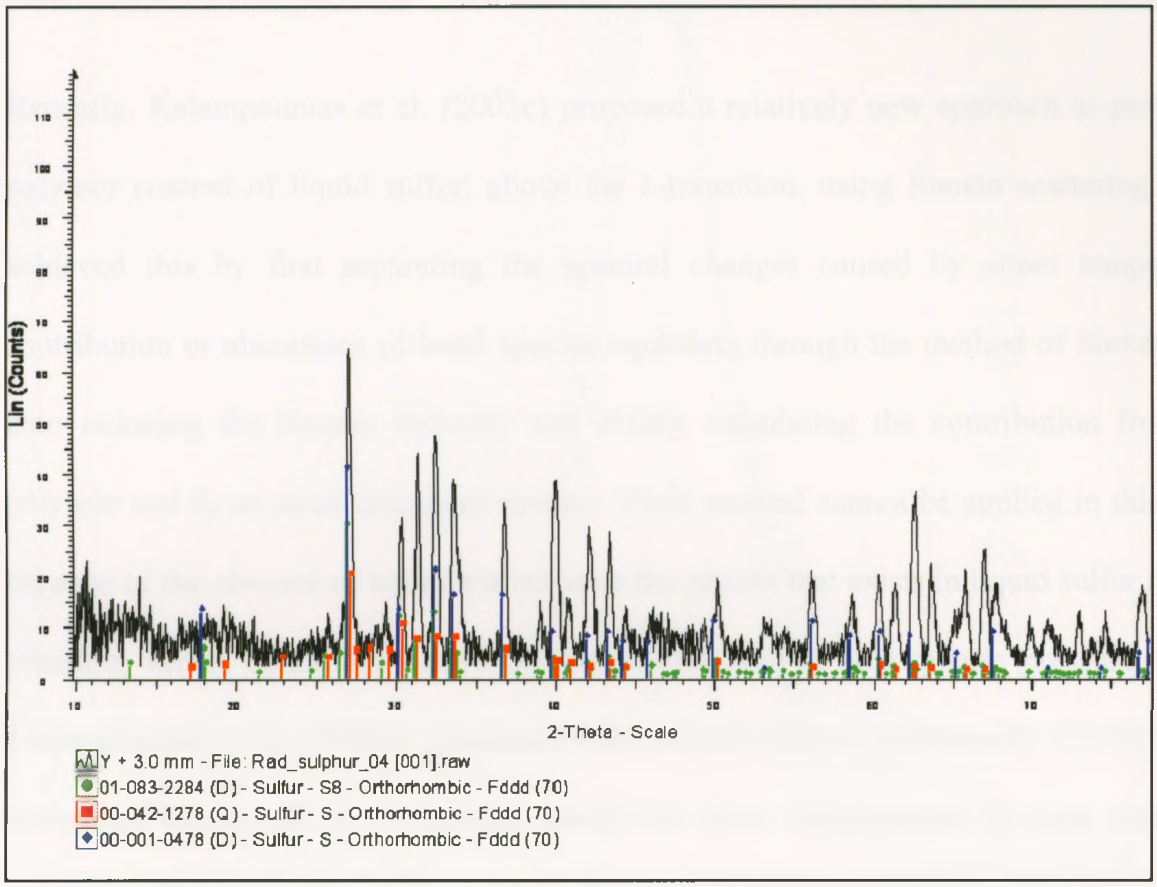

Figure 3.11: Micro XRD of the polymerized region.

While the results from μXRD are in part inconclusive, the Raman spectroscopy was less ambiguous, and demonstrated a clear presence of S_μ in all quenched samples, particularly at 461 cm^{-1}. In comparison to all other sulfur allotropes, the Raman spectra of polymeric sulfur are some of the simplest. The primary reason is that regardless of the way the polymer species have been prepared, the peak in the Raman spectra will be the same for all polymers. Hence, for high pressure and temperature quenched sulfur, the Raman spectra will be the same as for the phase quenched at atmospheric pressure and in turn,

this will be the same as the gas phase or even the spectra for the melt above the λ-transition (Eckert and Steudel, 2003). The dominant band is at about 460 cm^{-1} and the weak band is at about 425 cm^{-1}, and both have been detected using the Peak Fit software.

Recently, Kalampounias et al. (2003c) proposed a relatively new approach to probe the polymer content of liquid sulfur, above the λ-transition, using Raman scattering. They achieved this by first separating the spectral changes caused by either temperature contribution or alterations of local species equilibria through the method of Stokes-side, then reducing the Raman intensity and finally calculating the contribution from the polymer and S_8 as other dominant species. Their method cannot be applied in this work because of the absence of equilibria between the phases that exists in liquid sulfur at high pressure, versus conditions above the λ-transition and at atmospheric pressure, where Kalampounias et al. (2003c) conducted their measurements. Additionally, experimental setup and constraints in this thesis would not allow employment of such analytical technique. However, the relevance of the Kalampounias et al. (2003c) work for this thesis is in the fact that they showed changes in the Raman spectra of liquid sulfur with increasing temperature and polymer content. What is noticeable immediately is the peak shifting around 472 cm^{-1} due to increase in polymer. There is also a gradual increase in intensity of the band around 460 cm^{-1}, which clearly defines the polymer (Figure 3.12). Similar changes are observed in the plots of the Raman spectra, obtained in this work.

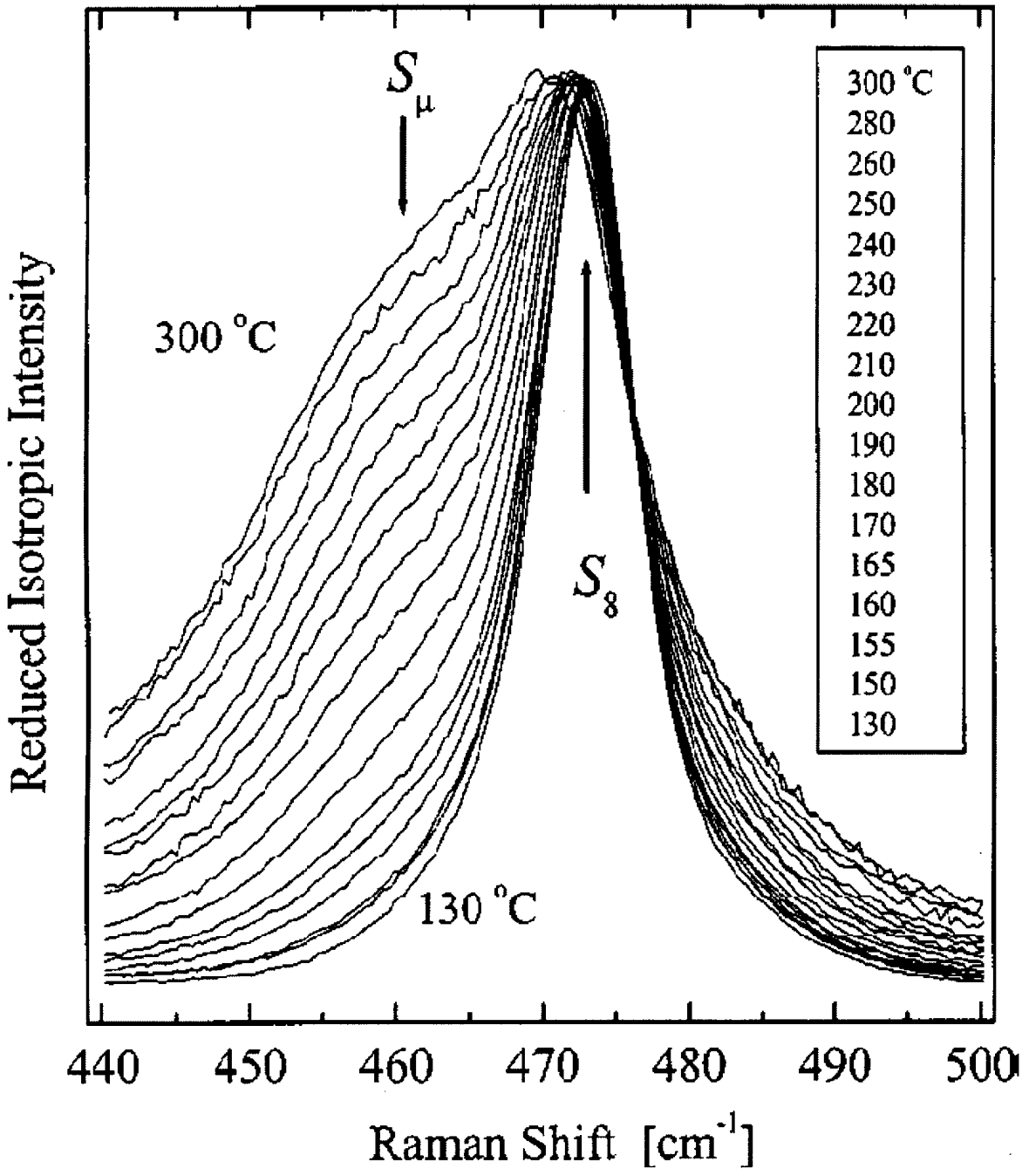

Figure 3.12: The representative reduced isotropic Raman spectra of liquid sulfur. Only the high-frequency spectral region is shown (~440–500 cm^{-1}) where the vibrational modes at 461 and 472 cm^{-1} are located. The latter is characteristic of the symmetric-stretch vibrational frequency of *S*8 and the former is a manifestation of the same type of vibrations of *S*μ chains. The arrows denote the positions of these vibrational modes (from Kalampounias et al., 2003c).

Figure 3.13 shows the Raman spectra of both the polymerized and non- polymerized regions in the sample quenched from 726°C (in 20 seconds) and carefully sectioned.

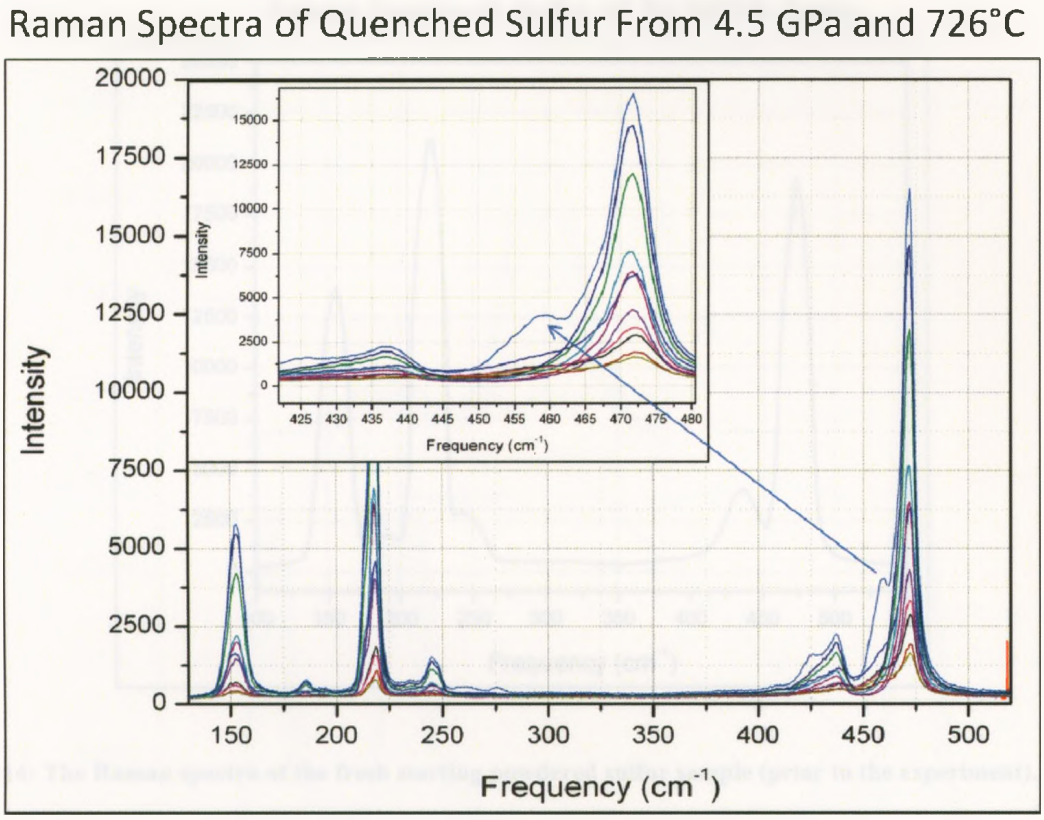

Figure 3.13: The Raman spectra of both the polymerized and non-polymerized regions of the quenched sample (the same sample, ten different spots) for the experiment at 4.5 GPa and 800°C, duration ~20 s. The polymerized regions exhibit strong peak shift around 461 cm^{-1}. The arrow points to such shift.

For a relative comparison, the Raman spectra of crystalline sulfur sample of 99.9995% used in the experiments are shown in the (Figure 3.14). There is a clear absence of the peak at 461 cm^{-1} and general peak shifting observed in polymerized samples.

Additionally, three runs were conducted at 800°C and 3.5 GPa (Figure 3.15), 4.0 GPa (Figure 3.16) and 4.5 GPa (Figure 3.13), respectively to try to assess the extent of polymerization as a function of pressure and temperature.

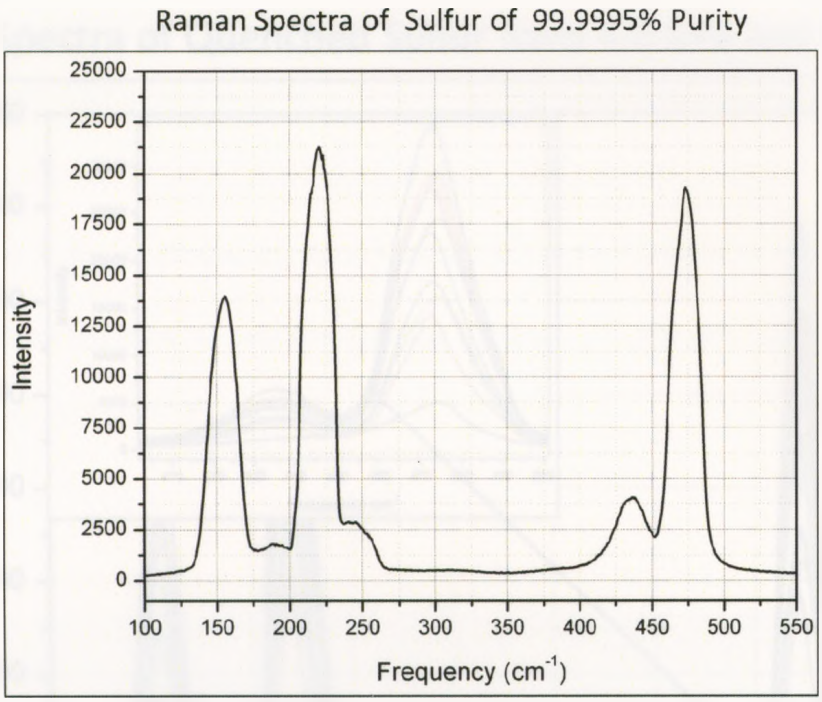

Figure 3.14: The Raman spectra of the fresh starting powdered sulfur sample (prior to the experiment).

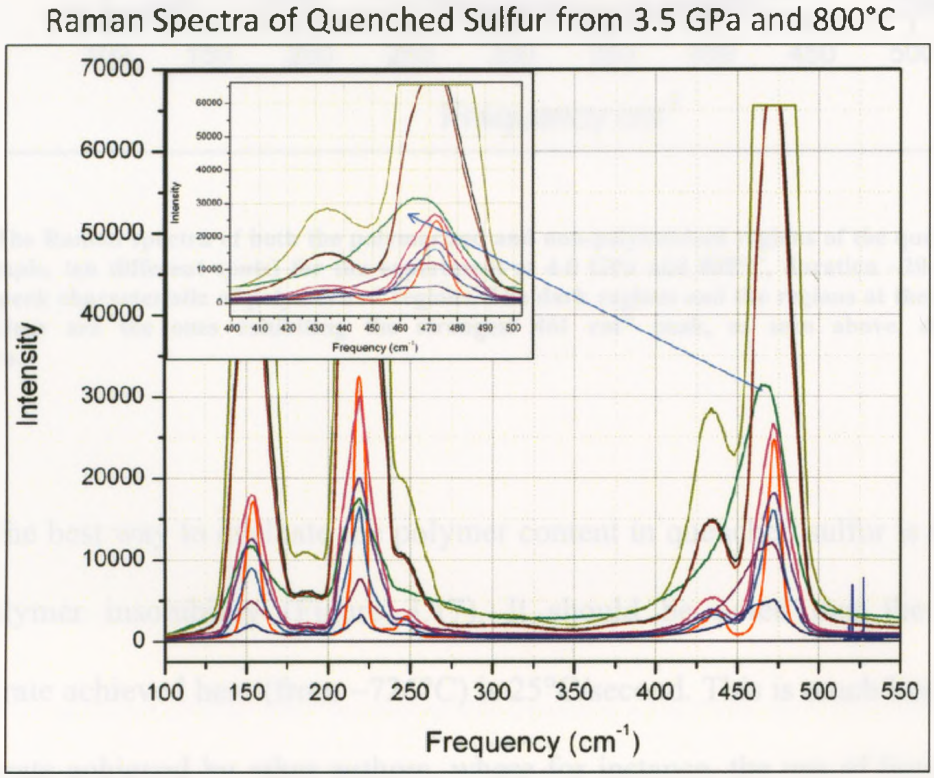

Figure 3.15: The Raman spectra of both the polymerized and non-polymerized regions of the quenched sample (the same sample, ten different spots) for the experiment at 3.5 GPa and 800°C, duration ~20 s. The arrow points to the peak characteristic of polymerized regions. The dark regions and the regions at the bottom of the sample container are the ones exhibiting the strongest 461 cm^{-1} peak, as seen above, due to strong polymerization.

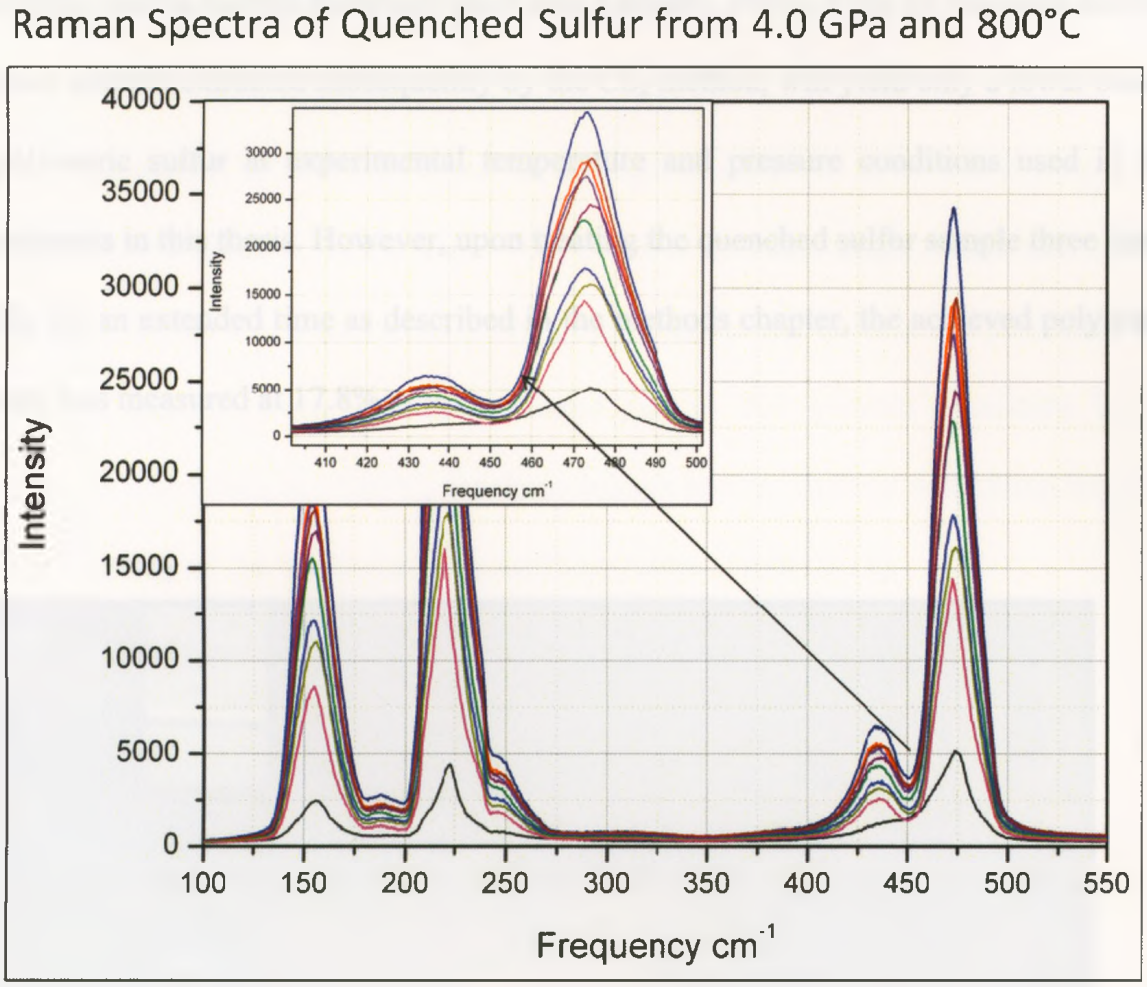

Figure 3.16: The Raman spectra of both the polymerized and non-polymerized regions of the quenched sample (the same sample, ten different spots) for the experiment at 4.0 GPa and 800°C, duration ~20 s. The arrow points to the peak characteristic of polymerized regions. The dark regions and the regions at the bottom of the sample container are the ones exhibiting the strongest 461 cm^{-1} peak, as seen above, due to strong polymerization.

However, the best way to evaluate the polymer content in quenched sulfur is use of CS_2, due to polymer insolubility (Figure 3.17). It should be noted that the maximum quenching rate achieved here (from ~726°C) is 25°C/second. This is much lower than the quenching rate achieved by other authors, where for instance, the use of liquid nitrogen on liquid sulfur at atmospheric pressure may yield a cooling rate of ~10^5 °C/second (Kalampounias et al., 2003c). Since the quenching rate here is much lower than

quenching rates achieved elsewhere (Koh and Klement, 1970), it can be expected that the polymer content extracted subsequently by the CS_2 method, will yield only a lower bound of polymeric sulfur at experimental temperature and pressure conditions used in the experiments in this thesis. However, upon treating the quenched sulfur sample three times in CS_2 for an extended time as described in the methods chapter, the achieved polymeric content was measured at 17.8%.

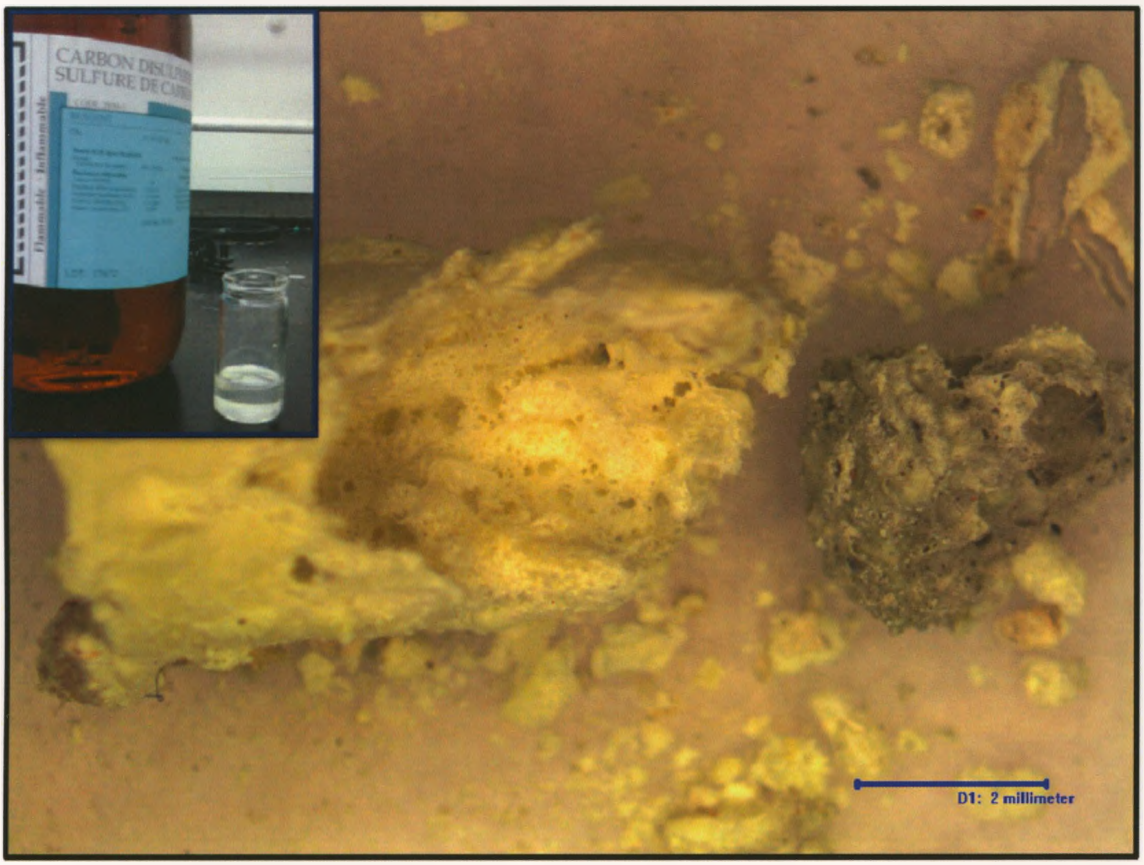

Figure 3.17: The recovered polymer after the sample was treated in a CS_2 bath. Inset: the sample in the CS2 bath.

3.3 Density Driven Phase Separation and Phase Equilibrium at Around 726°C

As indicated earlier in this chapter, the darker regions observed in sectioned samples of sulfur quenched from 4.5 GPa and ~726°C differ in size, shape, color and spatial arrangement within a cell and are directly proportional to the time. It has been observed that as the samples were kept for a longer (up to 300 seconds maximum in the experiments here) time at ~726°C, the deep reddish-brown material will clump together and start settling on the bottom of the sample container (Figure 3.18).

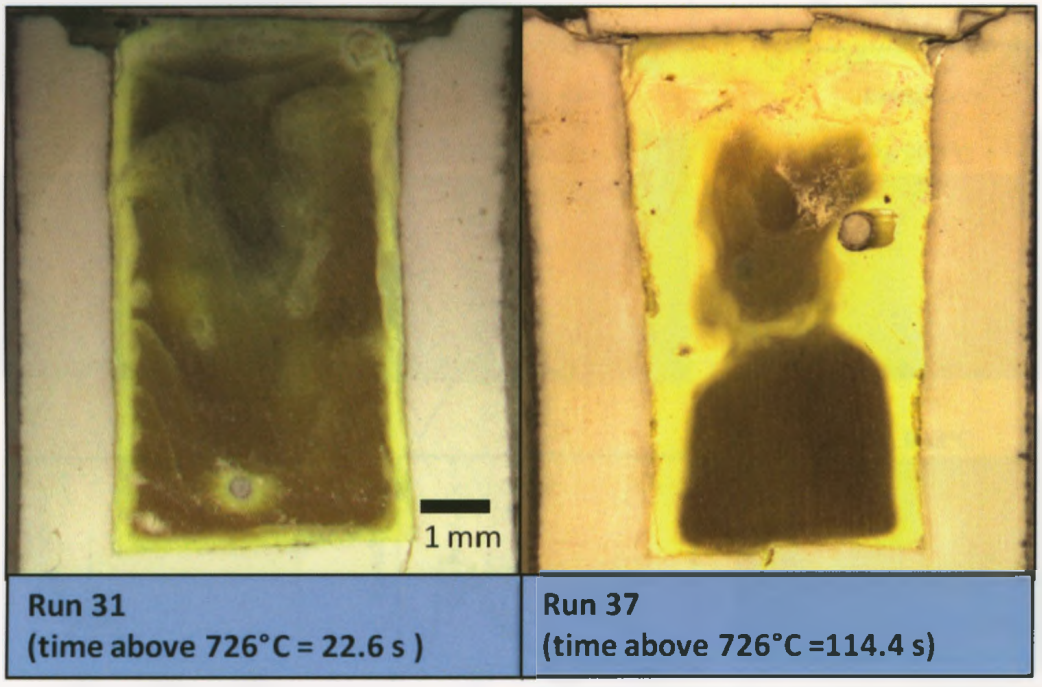

Figure 3.18: Photograph showing a density driven phase separation as a function of time. Left: polymerized dark material spread throughout the sample at t = 22.6 s. Right: Clustering and amalgamation of the polymerized dark material toward the bottom and middle of the container after 114.4 s.

This phenomenon is not new and it is essentially the same process as observed in density driven phase separations in Al_2O_3-Y_2O_3 melt, supercooled water and in low and high density amorphous ices (McMillan et al., 2007 and references therein). However, the clearest parallel to what is seen here has been reported by Katayama et al. (2004) where they used x-ray radiography of phosphorus under 1 GPa and 1000°C, and observed clear density driven phase separation in liquid phosphorus under those conditions (Figure 3.19).

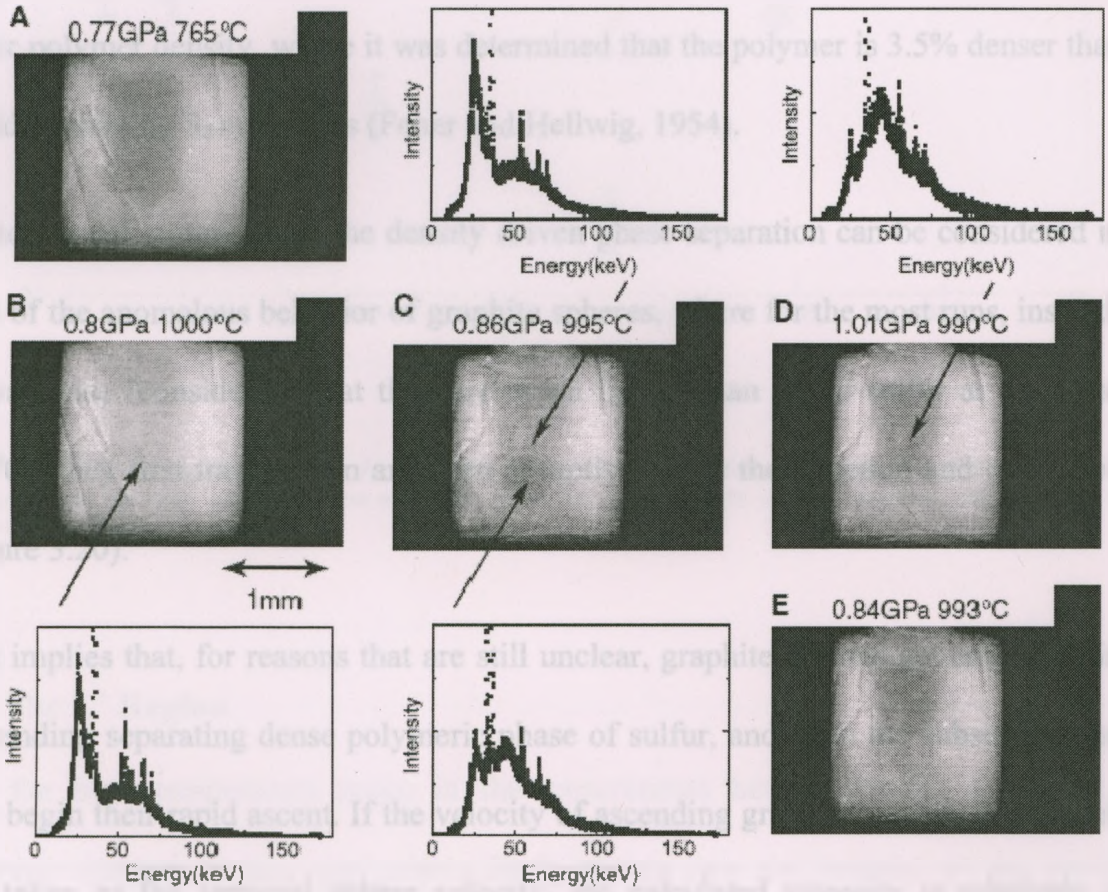

Figure 3.19: Radiographs for phosphorus at various pressures and temperatures. Insets indicate x-ray diffraction patterns measured at the positions indicated by the arrows. (A) Black P at 0.77 GPa and 765°C. (B) Low-density fluid phosphorus (LDFP) at 0.8 GPa and 1000°C. (C) A drop of high-density liquid phosphorus (HDLP) in LDFP at 0.86 GPa and 995°C upon compressing. (D) The sample space filled with HDLP at 1.01 GPa and 990-C. (E) A drop of HDLP in LDFP at 0.84 GPa and 993°C upon decompressing. The x-ray aperture was restricted by the anvils. Sharp lines in the radiographs are probably due to textures in the sample container (from Katayama et al., 2004).

This phenomenon has been suggested for sulfur, selenium and tellurium by Brazhkin et al. (2005), however this is the first time that such phenomenon has been visually observed and more importantly documented in liquid sulfur. While two distinct phases can be unambiguously distinguished in quenched sulfur from 4.5 GPa and around 726°C, there is an indication of a third phase; however, that will take additional investigation to confirm such a claim with absolute confidence. Additionally, the Raman spectra showed the polymerization of the settling denser dark region in quenched liquid sulfur. Further reinforcement of the aforementioned observation stems from the measurement of the sulfur polymer density, where it was determined that the polymer is 3.5% denser than the liquid containing S_8 molecules (Feher and Hellwig, 1954).

An additional argument for the density driven phase separation can be considered in the light of the anomalous behavior of graphite spheres, where for the most runs, instead of a buoyant rise (considering that they are much lighter than liquid sulfur at 4.5 GPa and 726°C), they first travel down and then abruptly change the direction and travel upward (Figure 3.20).

This implies that, for reasons that are still unclear, graphite spheres get entrapped in the descending separating dense polymeric phase of sulfur, and upon the subsequent escape they begin their rapid ascent. If the velocity of ascending graphite spheres is extrapolated and taken as the terminal sphere velocity, the calculated viscosity is relatively close (within the factor of three) to the values derived from velocities of the BN spheres.

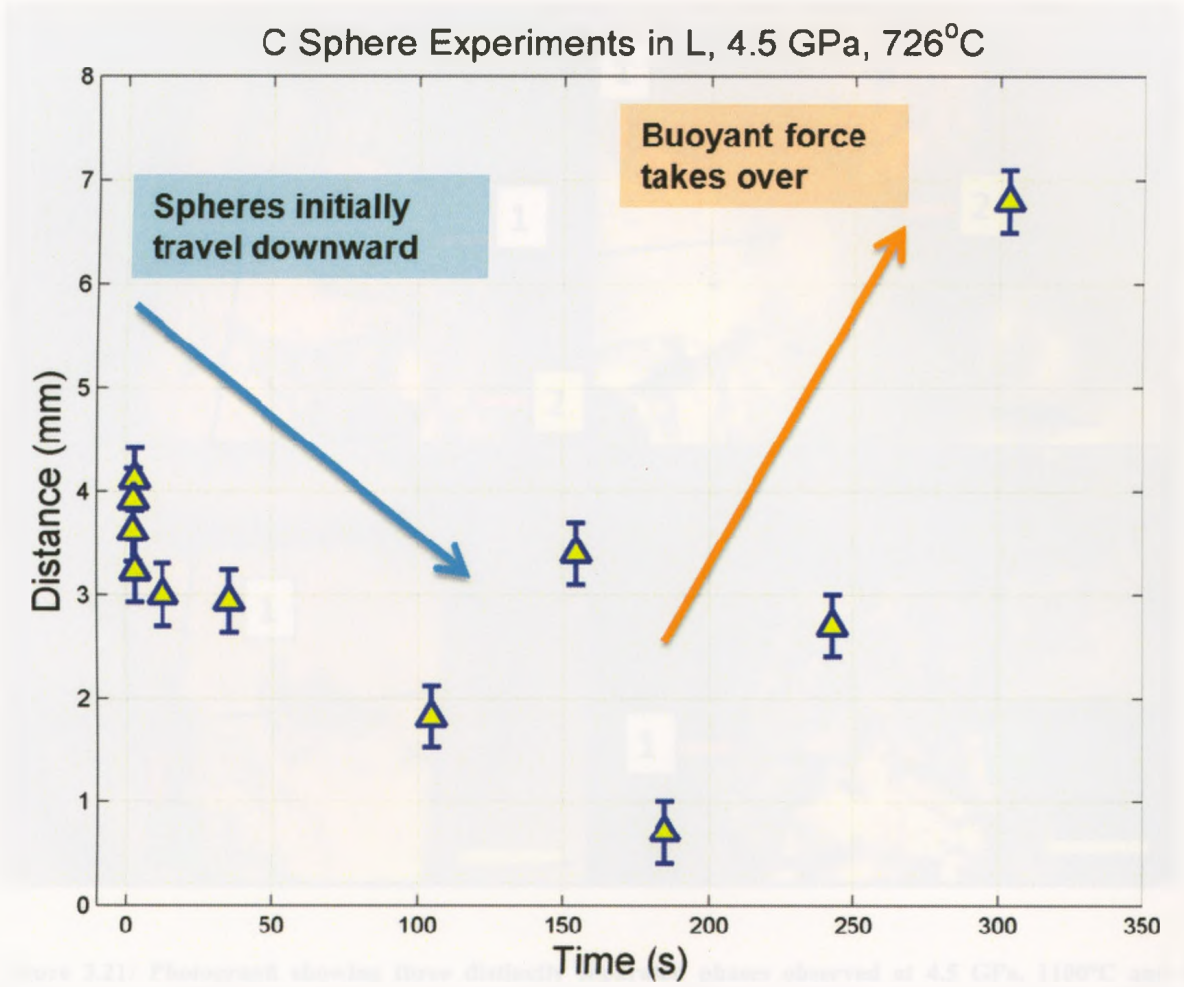

Figure 3.20: Plot of distance vs. time for graphite spheres. Initially, a downward trend is observed (denoted by the arrow on the left), which changes abruptly, after the spheres begin a rapid buoyant rise (denoted by the arrow on the right).

3.4 The L' Region

For the high temperature range in the experiments here (~1100°C, L'-liquid), the situation appears much more clear. Dark regions are not present in the sectioned quenched samples; however, three distinctly separated phases have been observed (Figure 3.21).

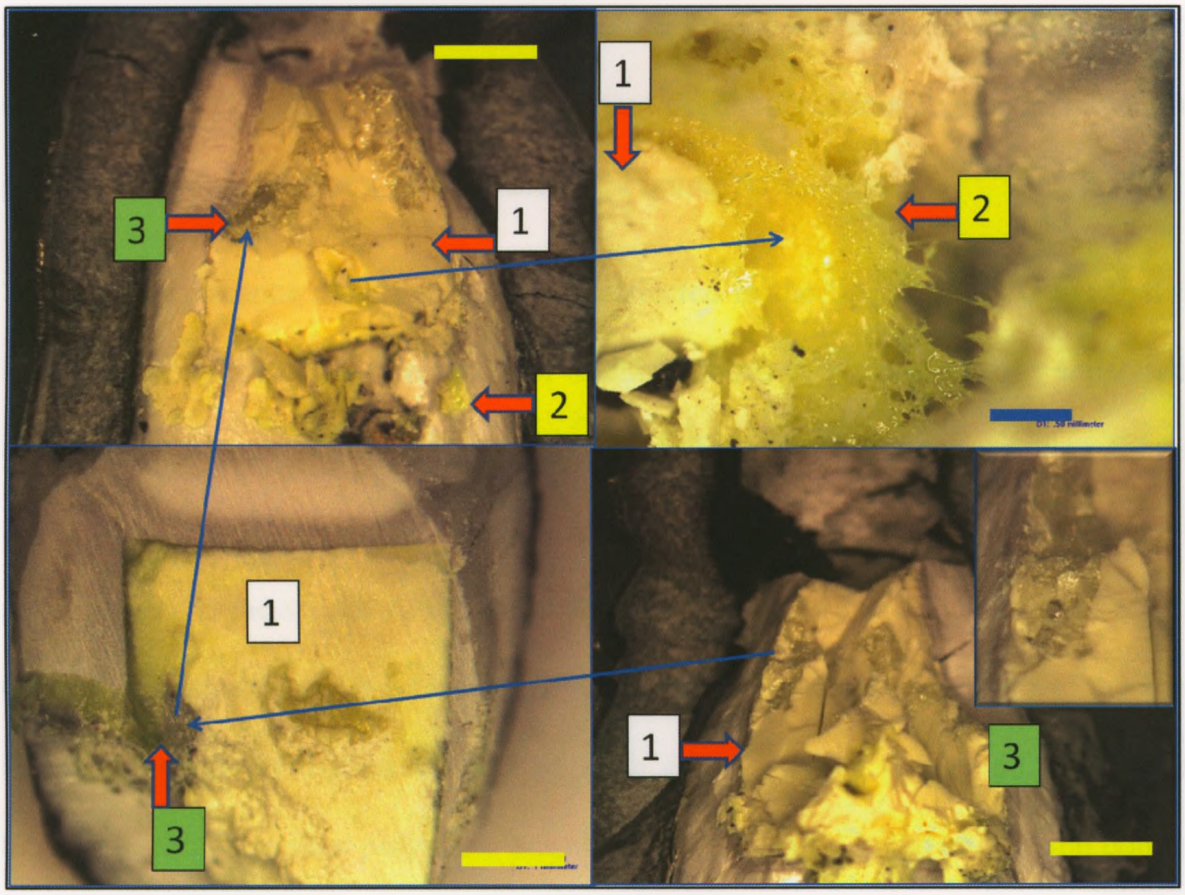

Figure 3.21: Photograph showing three distinctly separated phases observed at 4.5 GPa, 1100°C and ~ 20 seconds, in two different samples. Arrows connect the same phases in different spatial orientations. Yellow bar denotes 1 mm scale and the blue bar denotes 0.5 mm scale. The numbers correspond to different phases. Detailed explanation is given in the text.

In the recovered sample, the first phase (1) is a whitish-yellow, hard and brittle, and appears as a crystalline phase, visually estimated to comprise a maximum of 40% by volume, in all quenched samples. The second phase (2) is bright yellow, almost jelly-like, rubbery and stretchy in texture, containing a large number of vesicles and bubbles. This is clearly the polymer as per Vezzoli et al. (1969b). By volume, this phase is estimated at around 50% or more. The third phase (3) (5-10 % by volume) is greenish, translucent and almost glass like in appearance and it hardens as a function of time at experimental temperature.

However, if the sample is quenched immediately upon reaching the target temperature, the third phase remains soft and rubbery in texture, almost mimicking the aforementioned polymer (for more pictures, see Appendix 1, Figures A1.8 – A1.10).

The true significance of this discovery is reflected in the fact that this is the first time such phenomenon of the presence of multiple distinct phases, clearly separated, is observed in the atomic (one-component) liquid. Thus, the questions resulting from this are at which point "unmixing" happens and what is the driving mechanism behind this phenomenon. If the spatial arrangement of these phases is considered, it can be seen that the crystalline brittle phase is located primarily on the outer and upper parts of the sample indicating relatively lighter density of such phase relative to the polymeric phase. Consequently, the yellow polymeric phase is found generally in the middle and bottom of the sample. Interestingly, at the beginning of cube/sample sectioning, the polymeric phase exerts such volumetric expansion and pressure on the surrounding quenched sample, that it causes structural disintegration of the container cell and the cube. The "green phase" can be observed frequently at the external boundary of the sample in the midsection region and in small clusters. The spatial arrangement of the observed phases within the sectioned sample container is determined to be a direct function of the densities of the specific phases.

3.5 Liquid-Liquid Phase Transition

From the observations and results reported here, it is evident that liquid-liquid transitions occur in liquid sulfur at high pressures in both the L and L' regions. The nature of such

transitions is not immediately clear and it needs to be resolved with more clarity. The assumption has been made here that the liquid-liquid transitions in sulfur are second order transitions (Vezzoli, 2004; Monaco et al., 2005), because of specific heat and acoustic anomalies, and as such by the definition, should be endothermic (Currell et al. 1975; Scopigano et al., 2007). While the heating rates employed in these experiments are high compared to the ones used by other authors, (36°C/min vs. 2°C/min) (Vezzoli et al., 1969b), an attempt was made to simulate a differential thermal analysis (DTA) experiment, essentially by plotting dT/dt vs. T obtained instrumentally. Considering the high heating rate, the signals obtained are noisy and the only obvious and clear phase change is at the melting point. The main reason for this is that melting is a first order phase transition, exhibiting discontinuous changes in thermodynamic parameters. Second order phase transitions are not discontinuous in the first derivative of the Gibbs free energy with pressure and temperature, but are discontinuous in the second derivative, and consequently they are more difficult to detect by a crude simulated DTA method. Nevertheless, the signal was to some extent smoothed by applying the moving average filter in Matlab computational software. The obtained result is illustrated in Figure 3.22 (also see Appendix 1, Figures A1.3 – A1.7).

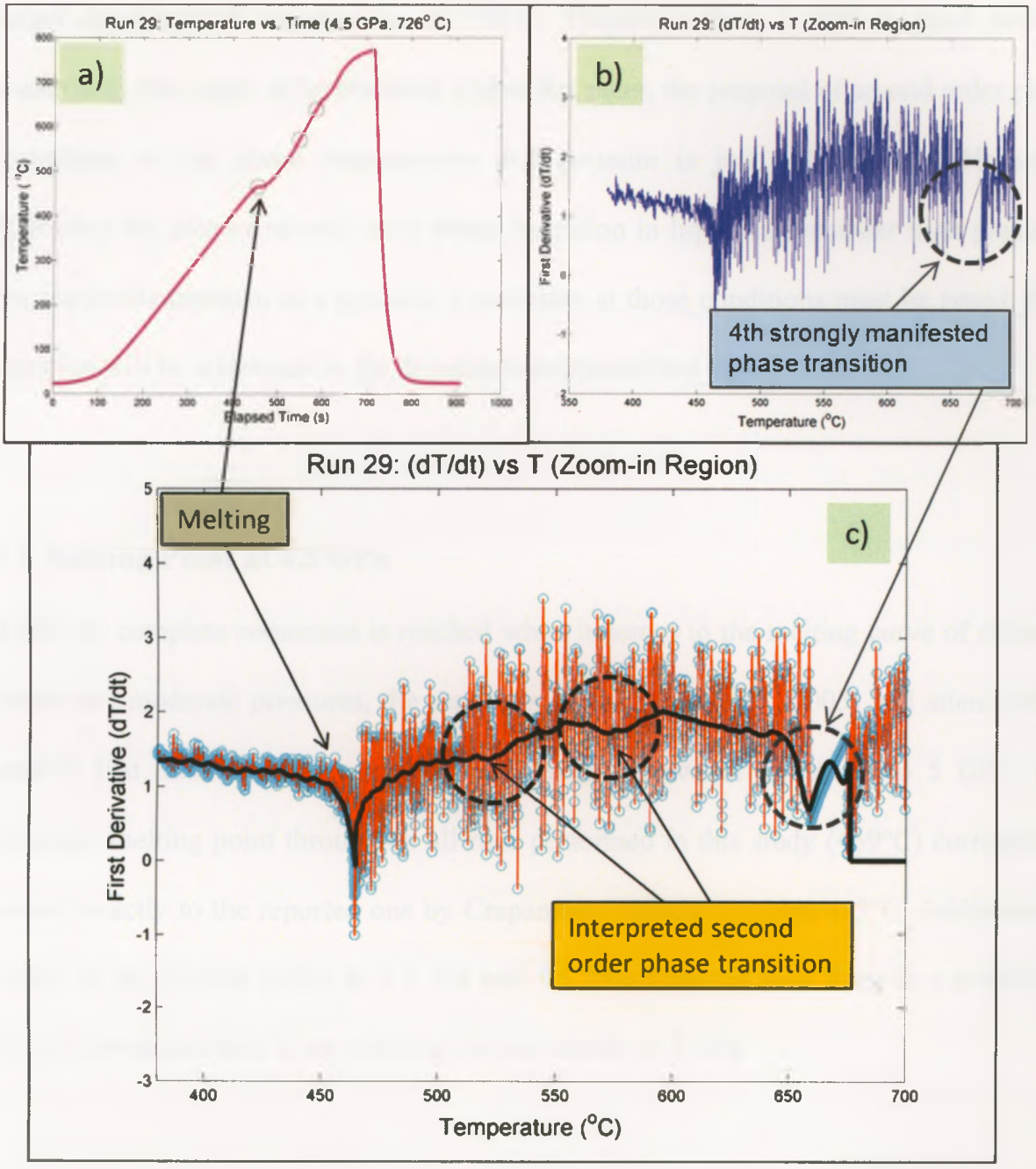

Figure 3.22: a) Temperature vs. time signal recorded using Pt/Pt-10%Rh thermocouple with an obvious signal indicative of melting at about 460°C; b) Plot of dT/dt vs T (scattered and difficult to interpret signal); c) The black line represents the smoothened signal after applying the moving average filter, superimposed over the original scattered signal (dT/dt vs T).

Based on the aforementioned method, the averaged temperature for the first potential second order phase transition from all runs, is at (573±42)°C and for the second one (651±25)°C. The fourth phase transition was not analyzed, because of its proximity to the

target experimental temperature of 726°C. However, there is still a great deal of uncertainty that needs to be resolved, and at this point, the proposal of second order phase transitions at the given temperatures and pressure is just a hypothesis. However, following the idea of second order phase transition in liquid sulfur under high pressure, the inevitable question of a possible λ-transition at those conditions must be posed. This question will be addressed in the discussion section of this thesis.

3.6 Melting Point at 4.5 GPa

While no complete consensus is reached when it comes to the melting curve of sulfur at lower and moderate pressures, the recent work by Crapanzano (2005) had attempted to resolve that dilemma by reanalyzing the melting curve of sulfur up to 5 GPa. The averaged melting point throughout all runs performed in this study (469°C) corresponds almost exactly to the reported one by Crapanzano (2005) to within ± 5°C. Additionally, based on the melting points at 3.5, 4.0 and 4.5 GPa obtained here, there is a possibility that the abrupt minima in the melting curve exists at ~4.5 GPa.

4. Discussion

The viscosity values obtained from the experiments in this thesis are presented with confidence, within the specified margin of error; however it is evident that bulk modulus and the thermal expansion coefficient of sulfur need to be refined. Consequently, it would be desirable to further refine the results of sulfur viscosity at 4.5 GPa and across the L-L' phase transition using the synchrotron radiography method using a Pt sphere.

Based on the obtained viscosity results from this study, it is clear that viscosity of liquid sulfur decreases with increasing temperature. At 4.5 GPa, and ~726°C, corresponding to liquid L, viscosity is more than a factor of two higher than in liquid L', at about 1100°C and at the same pressure. The effect of the L-L' transition is not clear at the moment. Coincidently, the values of viscosity that Terasaki et al. (2004) obtained in the vicinity of the melting curve, one measurement in L, just before L-L' transition and the other measurement in L', exhibit a similar ratio as the results obtained here. Therefore, based on this information, it is not clear at this moment if the decrease in viscosity observed in this study should be attributable completely to the temperature effect or to the phase transition. In that context, it is useful to recall that the major phase transitions in liquid sulfur under high pressure, generally between the L, L' and L'' liquids, are closely analogous to the first order phase transitions, and mirror those in terms of discontinuous behavior in thermodynamic parameters (Brazhkin and Lyapin, 2003).

However, Terasaki et al. (2004) observed that viscosity of liquid sulfur in the vicinity of the melting curve decreases with pressure, which is interesting in itself as it mimics the behavior of metallic liquids (Terasaki et al., 2001) at high pressure, and aluminosilicates mentioned earlier. It should also be noted that similar behavior of selenium viscosity

under pressure, and along its melting curve was observed by Brazhkin et al. (2007). Consequently, the atypical decrease in sulfur viscosity with pressure in addition to the decrease of the viscosity with increasing temperature reported in this thesis may by extension contribute to further illuminate the viscosity of the outer core as indicated in the opening chapter of this thesis. Funakoshi (2010) measured viscosity of liquid Fe-S up to 9.4 GPa and 2023K using synchrotron radiography. He reported that viscosity of liquid Fe-S remains constant with increasing pressure and it decreases gradually with temperature, which is consistent with previous studies. However, the most relevant conclusion made by Funakoshi (2010) was that the addition of sulfur may not have a serious impact on viscosity of the Earth's outer core. Based on the behavior and values of viscosity of liquid sulfur with increasing pressure and temperature observed by Terasaki et al. (2004) and in this thesis, it can be argued that the presence of sulfur in the outer core will not have an appreciable effect on the viscosity of the outer core.

Moreover, Terasaki at al. (2004) reported no appreciable effect of the λ-transition on the viscosity measurements. Here, the author is inclined to agree with such assessment even as a significant polymer content has been recovered from experimental temperatures and pressure in the experiments conducted in this thesis. However, one should not rush to a conclusion dismissing the possibility of the λ-transition based on the circumstantial and limited evidence stated above. On the contrary, there seems to be a significant body of evidence, more subtle than not, that points toward the existence of the λ-transition under high pressure. This thesis will present this hypothesis exclusively and in the following paragraphs, argument and the evidence will be presented to prove the existence of the λ-transition under high pressure.

For that purpose, let us recall an interesting peculiarity observed throughout the experiments here. In the liquid L, it takes well over one hundred and fifty seconds (refer to Tables 3.5 – 3.8 in the Results section) for the BN sphere to move 0.5 mm, between the melting temperature of sulfur and the instrumentally observed temperature of 726°C. Yet the same sphere moves upward more than 5mm in just over 70 seconds at the temperature of ~726°C. Moreover to illustrate the point additionally, from experiments (from the melting point to 1100°C) in L' liquid, it takes ~89 seconds for a BN sphere, at accelerated heating rate to move ~3.5 mm from the original starting position. While it must be acknowledged that the sphere takes time to accelerate to its terminal velocity from its starting position, there is still significant discrepancy when the extrapolated velocity is considered based on the viscosity values taken from Terasaki et al. (2004) along the melting curve. This directly implies that the sphere encounters a temperature region at 4.5 GPa, where very viscous liquid exists, which impedes the expected rate of the buoyant sphere rise. Moreover the experiments (Terasaki et al., 2004) that yielded those values were taken at 515°C at 3.2 GPa and 593°C at 5.14 GPa. From the heating vs. time plots, the second phase transition following the melting, averaged across all runs, occurs at 4.5 GPa and (573±42)°C. A third phase transition appears at the same pressure and at (651±25)°C. Thus, it can be reasoned that the Terasaki et al. (2004) measurements were slightly below the first phase transition at 4.5 GPa and 573C, which from herein will be proposed as the pressure suppressed λ-transition and referred to as such. However, before full explanation is given for the previous statement, it is useful to consider some essentials.

It has been shown that the high viscosity of sulfur, at atmospheric pressure and above the λ-transition is directly proportional to the polymer chain length (Touro and Wiewiorowski, 1965), where the maximum chain length of about 10^6 atoms is reached at 187°C which in turn corresponds to the highest viscosity value. It can also be recalled that viscosity at such conditions does not depend on the polymer content, rather the polymer continues to increase well beyond 187°C and all the way to the boiling temperature of sulfur (Koh and Klement, 1970), while at the same time viscosity starts to decrease fairly rapidly beyond the temperature of 187°C (Meyer, 1976). If one goes a step further and considers the recovered polymer content from 4.5 GPa and ~726°C, of 17.8 wt%, and additionally considers that based on the relatively slow quenching rate achieved here and already mentioned in the previous text, then the reasoning would imply that the true polymer content at those experimental conditions is much higher and possibly exceeds 20 wt%, based on the comparison of different quenching methods given by Koh and Klement (1970). The importance of quenching rate was also clearly stated by Davis and Hyne (1976). Based on such assumption, and relative to the polymer content in liquid sulfur at atmospheric conditions, and above 187°C, it can be reasonably argued that the experimental temperature in the L-liquid of 726°C is well beyond the proposed λ-transition that exists in the lower temperature regime. The obtained viscosity values are in line with such assumption. A peculiar effect of "geometrical" confinement on the λ-transition and polymerization of liquid sulfur has been observed by Kalampounias et al. (2003a). Using "nanonoporous" sol-gel glasses, which were packed with prepared sulfur powder and subsequently heated under vacuum up to 600°C, and probed by the Raman spectra, they observed profound changes in the structural, dynamical and thermodynamic

properties of liquid sulfur. A critical observation was the decrease in polymer content of the confined samples in comparison with the unconfined samples. Figure 4.1 illustrates a dramatic impact of volumetric confinement on polymerization rate.

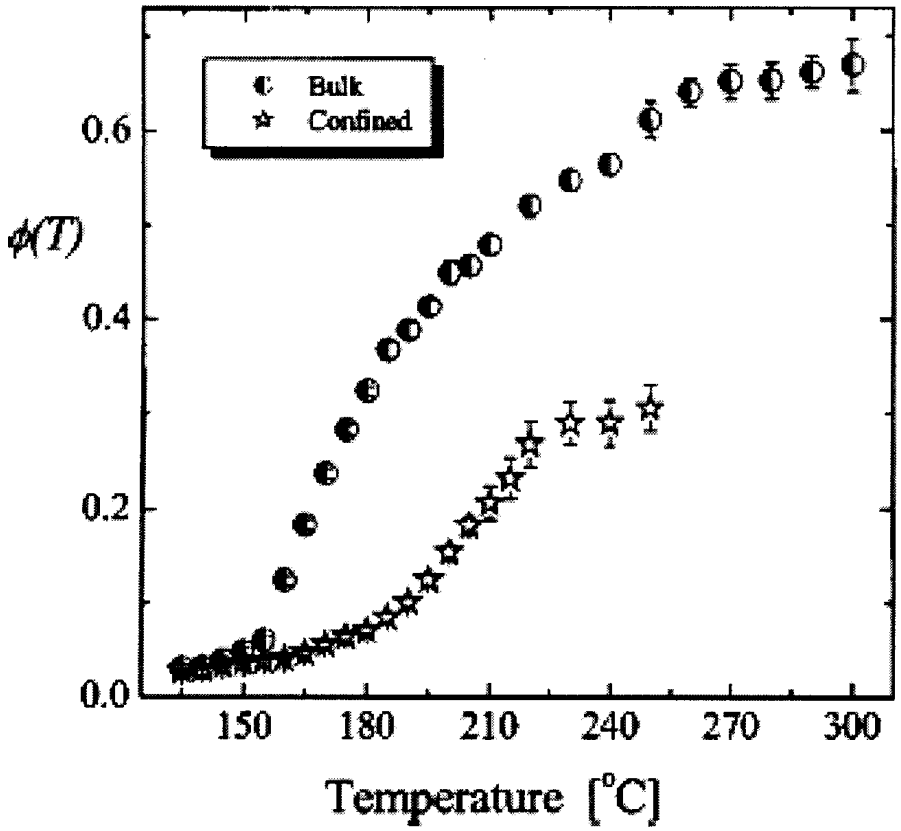

Figure 4.1: Temperature dependence of the extent of polymerization as determined from the relative intensity ratio of the 470- and 460-cm^{-1} vibrational lines. Open stars: confined liquid. Semi solid circles: bulk sulfur. Error bars correspond to two standard deviations (from Kalampounias et al., 2003a).

Moreover, the profound change is evident is the specific heat around the λ-transition, where a sharp jump of C_p is considerably blunted and the λ-transition has been shifted to 174°C instead of 159°C, implying a considerable temperature delay in the polymerization

as shown in the Figure 4.2. Consequently, it can be concluded that the same effect will be observed in the viscosity values.

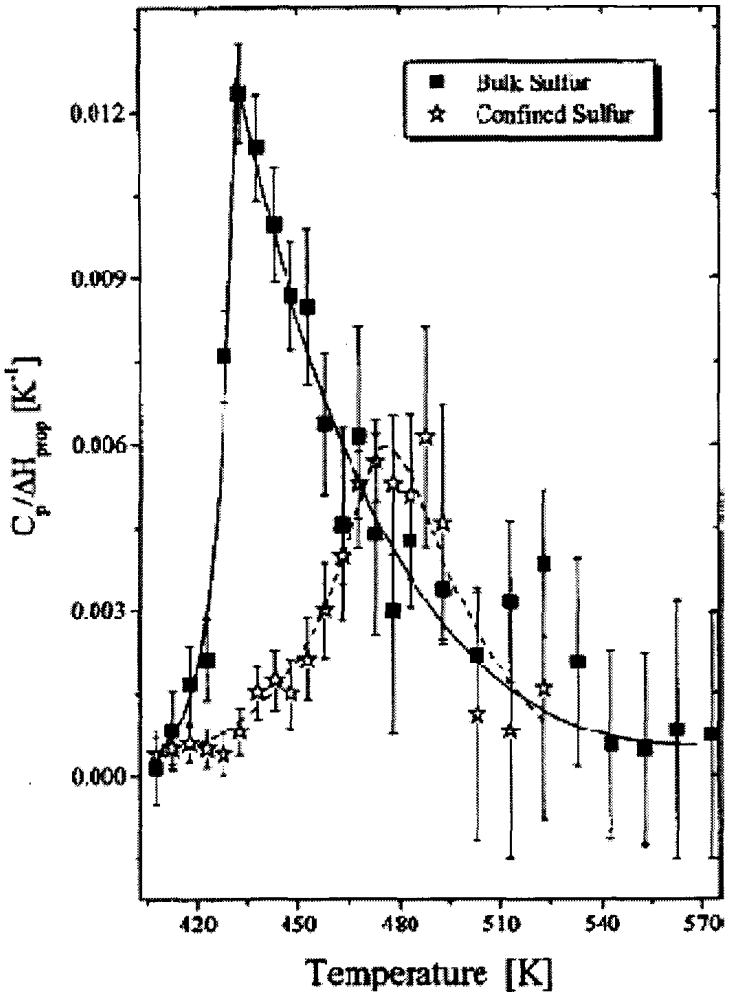

Figure 4.2: Constant pressure heat capacities for bulk (solid squares) and confined (open stars) sulfur. The solid and dashed lines through data points are guides to the eye. The error bars correspond to two standard deviations (from Kalampounias et al., 2003a).

The same results were also confirmed by Andrikopoulos et al. (2011) (Figure 4.3). The Raman spectra they obtained for polymeric sulfur (~460 cm^{-1}) (Figure 4.4) looks strikingly similar to the Raman spectra of polymeric regions in the sectioned samples

obtained from the experiments in this thesis. When these results are used as the analogy and the predictor for the high pressure behavior, context is provided for the observations reported from experiments in the text above.

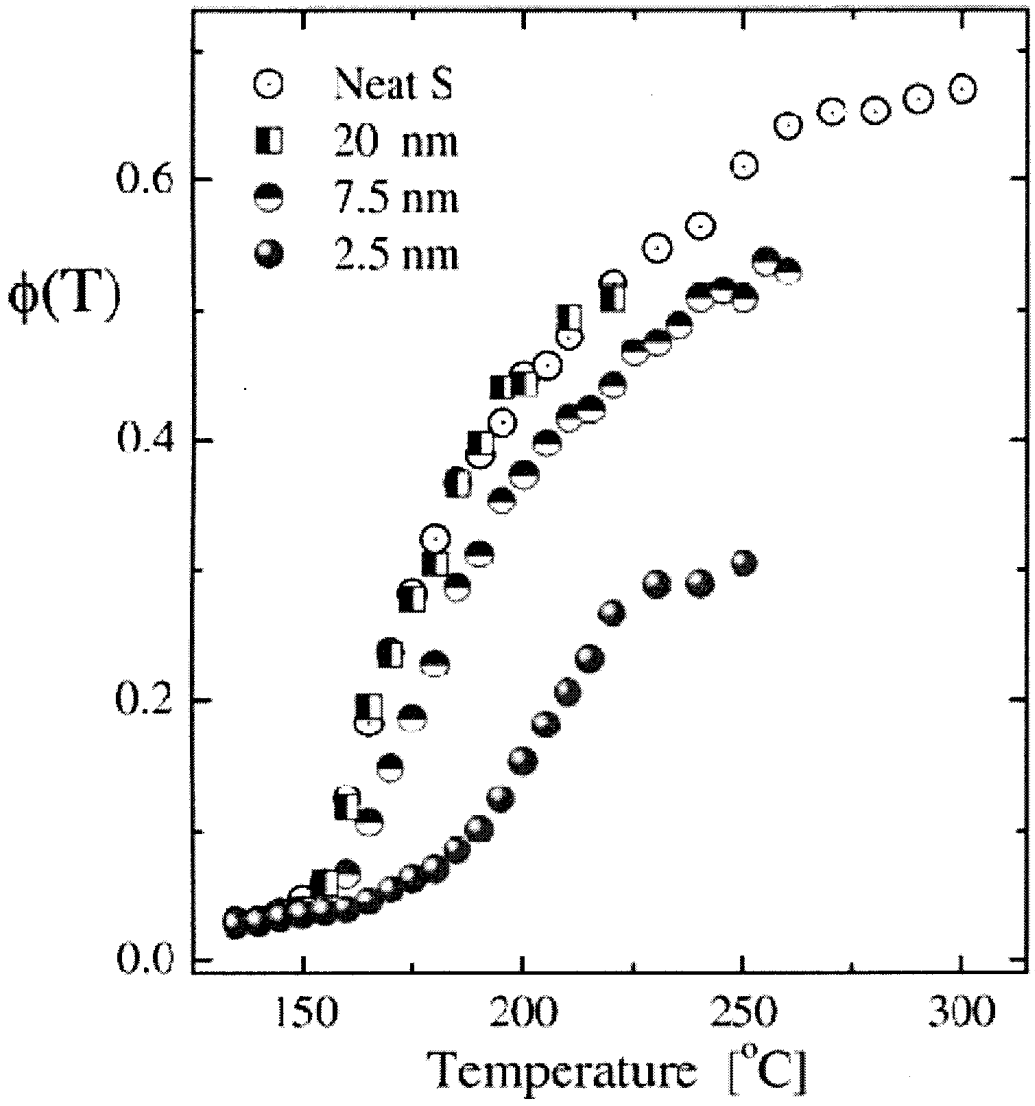

Figure 4.3: Temperature dependence of the sulfur polymer fraction for bulk (Neat S) and confined sulfur (2.5-20 nm) (from Andrikopoulos et al., 2011).

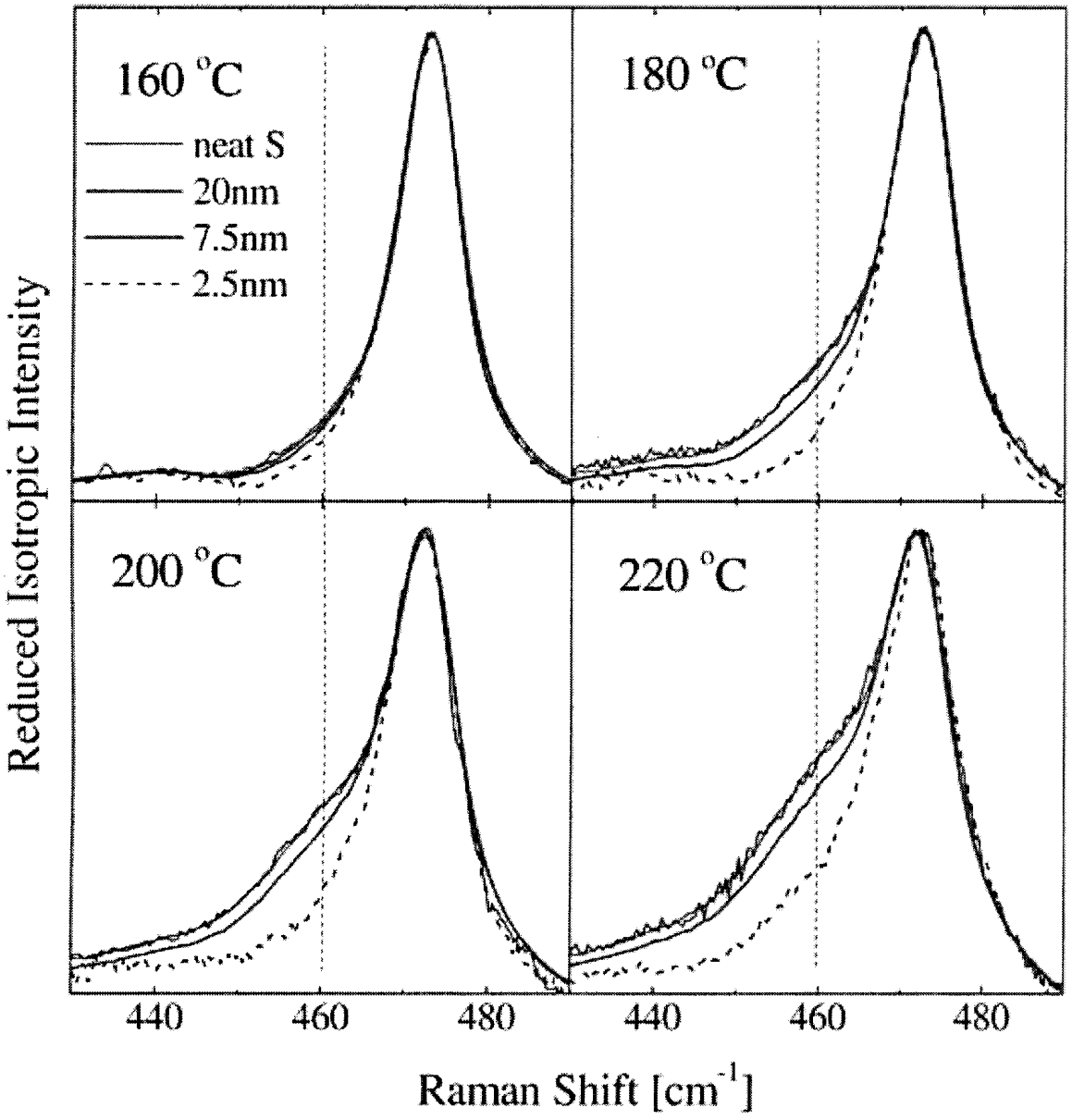

Figure 4.4: Reduced isotropic Raman spectra of bulk and confined liquid sulfur. For each temperature (160°C, 180°C, 200°C and 220°C) representative spectra of the bulk and confined sulfur at various pore sizes are shown. The spectra are normalized with respect to the S_8 peak at ~470 cm^{-1} in order to reveal the relative intensity of the polymer content in each case (from Andrikopoulos et al., 2011).

It can be subsequently predicted that the second order phase transition in liquid sulfur (Vezzoli, 2004), corresponds to a sudden increase in viscosity that occurs under compressed and heated liquid sulfur (e.g. conditions reported in this thesis) will be

severely muted, and may not be clearly identifiable using already established methods such as the DTA. In addition to that, Brazhkin and Lyapin (2003) clearly stated that the temperature increase of 1.3-1.5 times that of the melting temperature will significantly diffuse any anomalies related to the liquid-liquid phase transition. This might be the best explanation why only faint phase transition signal was observed in the plot of dT/dt vs T, after the melting point, as seen in the previous chapter. Notably, most theoretical models of polymerization of liquid sulfur in the past that also touched upon the phenomenon of viscosity increase about the λ-transition, only considered atmospheric pressure conditions in their treatments (Tobolsky and Eisenberg, 1959, Scott, 1965, Kennedy and Wheeler, 1983, Dudowicz et al., 1999). However, long overdue mathematical treatment of compressible models of equilibrium polymerization, has been developed by Artyomov and Freed (2005). They extended the Flory-Huggins-type models of equilibrium polymerization to systems under high pressure with a direct application to liquid sulfur.

This study has shown that polymerization is directly affected by applied pressure because polymer and monomer solutions have different compressibilities and because volumes of unreacted and reacted monomers differ. Additionally, Artyomov and Freed (2005) reported that the change in entropy under pressure, between solutions of unreacted monomers and of polymer chains leads to different volume fractions of vacant sites and consequently, to different densities and compressibility for these systems, where polymer chains are less compressible. However, they concluded, based on their calculations that pressure conditions are conducive to formation of polymers. Furthermore, the most relevant finding reported by Artyomov and Freed (2005), at least in regard to this thesis, is the behavior of specific heat. With increasing pressure, the sharp jump in specific heat

is diminished and it is shifted to higher temperature region along with polymerization temperature. That would mean that the anticipated λ-transition, as proposed in this thesis, is also shifted up in temperature as a result of the pressure effect, and subsequently significantly muted in its manifestation. Coincidently, experimental results showing almost the same phenomenon were obtained by Kalampounias et al. (2003a) and Andrikopoulos et al. (2011), who studied sulfur polymerization under confinement, as discussed in the text above. At this point it should be noted that Boue et al. (1992) hinted that the onset of the λ-transition may be conducive to a phase separation.

Another piece of physical evidence supporting the hypothesis of a major phase transition below 4.5 GPa and below 726°C comes indirectly from unpublished thesis by Heath (1994). He attempted to evaluate viscosity of liquid sulfur at 4.0 GPa and ~500°C and remarkably the BN sphere in his experiments traveled downward in contrast to the results obtained here. To test the proposed hypothesis here, bulk modulus and thermal expansion coefficients used to evaluate density of sulfur and BN in this thesis, were applied to the conditions in Heath's experiments and it is evident that that BN is still less dense than liquid sulfur, contrary to what he observed. That implies that at some point before 4.5 GPa and 726°C, there is a jump in density of sulfur as a result of the phase transition, rather than a gradual increase predicted by Birch-Murnaghan equation of state (BM-EOS). In fairness it should be noted that Heath (1995) did not employ bulk modulus of sulfur or BN in his study, and had a different analytical approach in evaluating liquid sulfur viscosity under pressure.

Admittedly, while the above evidence is subtle and circumstantial, it clearly points to the existence of a muted λ-transition under the pressure and consequently toward the liquid-

liquid phase transition at 4.5 GPa and below 726°C. It appears that the older evidence for the merging of the λ-transition with the melting curve under pressure (0.07-0.08GPa) (Vezzoli et al., 1969) may not be entirely accurate. A logical supposition can be made then that more likely, the λ-transition closely trails the melting curve in the low pressure region, possibly up to 1 GPa, and consequently it starts deviating into the higher temperature region, as it can be expected from the above presented evidence.

However the true nature of the liquid-liquid phase transition in liquid sulfur has to be addressed more comprehensively, and while the hypothesis in the text above about the second order phase transition is based on the experimental data of Monaco et al. (2005) and Scopigno et al. (2007) under the atmospheric pressure conditions, high pressure conditions need to be treated separately, with an inclusion of the data from the above noted studies. Notably, if the presence of high frequency relaxations along with low frequency relaxations using acoustic studies is observed at high pressures and temperatures, that will be clear evidence of the second order phase transition in liquid sulfur at high temperatures and pressures (Monaco et al. 2005; Scopigno et al. 2007). Additionally, if a jump in viscosity is observed below 726°C, as hypothesized in this thesis, then according to classical Navier-Stokes hydrodynamics, that would be an indication of a second order phase transition. The reason for that is obvious since the behavior of sound absorption (equation 1.1) characteristic of a second order phase transitions is directly dependent on value of viscosity (Kozhevnikov et al., 2003b).

Coming back to the question of liquid-liquid phase transitions and distinct phase separations, one should recall that it was established in recent years that the liquids of any composition exist in several differently structured nano-phases (Vezzoli, 2004), and that

there exists a non-homogenous local configuration with a short range nano-ordering. While the theory suggests that liquid-liquid phase transitions will exist in any liquid because of specific symmetry-selective interactions and bond ordering, and because of locally favored structures that result from many body interactions (Tanaka, 2000 and references therein), the full dynamics of mechanisms that lead to "unmixing", phase clustering and subsequent density driven phase separation, observed in the experiments in this thesis remains unclear. An excellent review of the topic and recent progress is given in McMillan et al. (2007) including the examination of density driven phase separations. However, more critical assessment of this topic is beyond the scope of this thesis and a further study of the problem should include the exceptional phenomenon observed here. While a distinct phase separation was observed optically, Y_2O_3-Al_2O_3 (Figure 4.5), it was never observed in a single component atomic liquid such as sulfur, hence a great significance of the results reported here. For comparison, Figure 4.6 (also see Appendix 1, Figures A1.8 – A1.9) shows three phases observed here, quenched from 1100°C and 4.5 GPa.

Finally, one should recall that Brazhkin and Lyapin (2003) stated the following: "... *however there are virtually no substances for which it would be possible to study experimentally the transitions between pairs of stable liquids... and corresponding amorphous phases*". It is evident that is not the case any longer as it was shown in this thesis. It should be emphasized that the observed phase separations are highly time dependent. This means that a more distinct separation of the "unmixed" phases will occur if the experiment is left at a target temperature for longer amount of time.

Figure 4.5: Larger samples of Y_2O_3–Al_2O_3 glasses formed by high-*T* melting in a Xe lamp thermal imaging furnace, and quenched by passing the molten droplets through a Pt wire grid. Here, the polished sample shows coexisting low density area (LDA) (top left) and the high density areas (HDA) matrix regions. The glassy polymorphs have different mechanical properties, resulting in a higher quality of polish for the LDA sample (from McMillan et al., 2007)

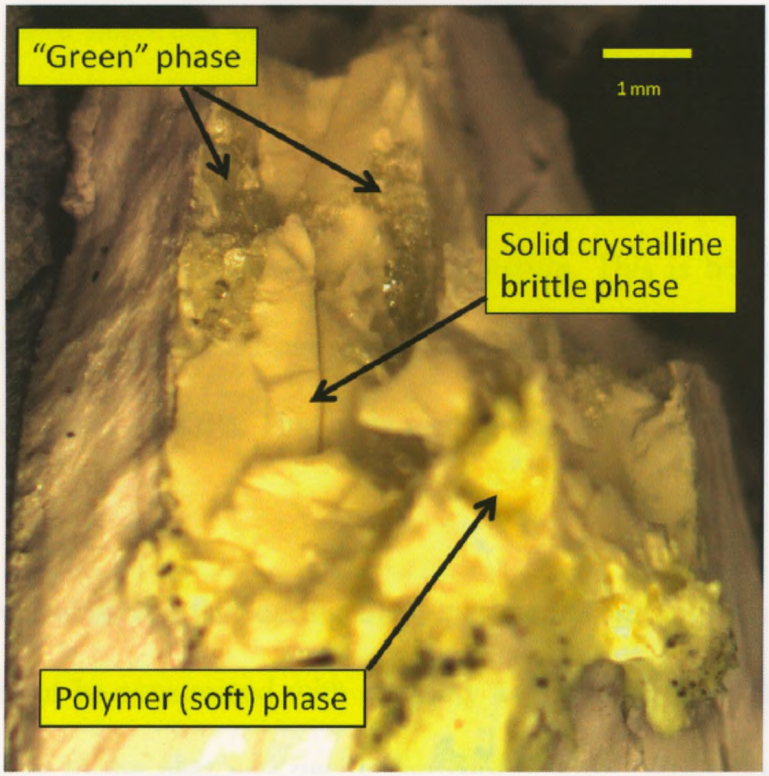

Figure 4.6: "Opened" sample quenched from 1100°C, showing 3 distinct phases.

However, if the viscosity of liquid sulfur below 726°C and 4.5 GPa is found to be very high as proposed, that will entail that liquid sulfur in that temperature and pressure regime cannot be treated as a Newtonian fluid any longer. It will mean that liquid sulfur at those conditions will need to be treated as a viscoelastic liquid (Monaco et al., 2005). In the past, studies have established that if viscosity is to be evaluated for a viscoelastic liquid by means of the falling sphere method, in order to obtain accurate results, a series of mathematical corrections would need to be made (Gottlieb, 1979; Cho et al., 1984; Valladares et al., 2003). For more experimental and theoretical approaches of evaluating viscosity in viscoelastic non-Newtonian fluids by the falling sphere method, the following publications provide excellent reviews (Fabris et al. 1999; Harlen, 2002; Chung and Vaidya, 2010; Song, 2010).

However, a few more important observations need to be discussed. First, based on the Raman data obtained from samples subjected to 800°C, at 3.5, 4.0 and 4.5 GPa, and specifically on the polymer peak intensity (Kalampounias et al., 2003b), it is possible to see that the polymer content is higher at lower pressure. This is because the polymer content increases with temperature and at 3.5 GPa 800°C is much further above the melting curve than it is at 4.5 GPa. That goes well in line with issues discussed earlier in this chapter.

Additionally, it was observed that during the experimental heating, the recorded signal for melting could not be constrained with certainty as the obtained melting temperature from one experiment to the next was oscillating significantly. While the averaged value for the melting point across all the experiments is in excellent agreement with the experimentally constrained phase diagram by Crapanzano (2005), (Figure 4.7). The

melting points obtained at 3.5, 4.0 and 4.5 GPa in this thesis are indicative of a sharp minima in the melting curve (Figure 4.7). The existence of such minima would explain large oscillations in the melting point observed throughout experiments as a result of the pressure uncertainty.

Before concluding this chapter, it is important to note that solid sulfur in a high pressure range (~4.5 GPa) is a direct analogue (because of it helical structure) of polymeric species observed above the melting curve. This clearly indicates a direct influence of a solid on short and perhaps medium range liquid structures as observed by Secco and Schloessin (1989) in liquid Fe, and recently in sulfur by Crapanzano (2005).

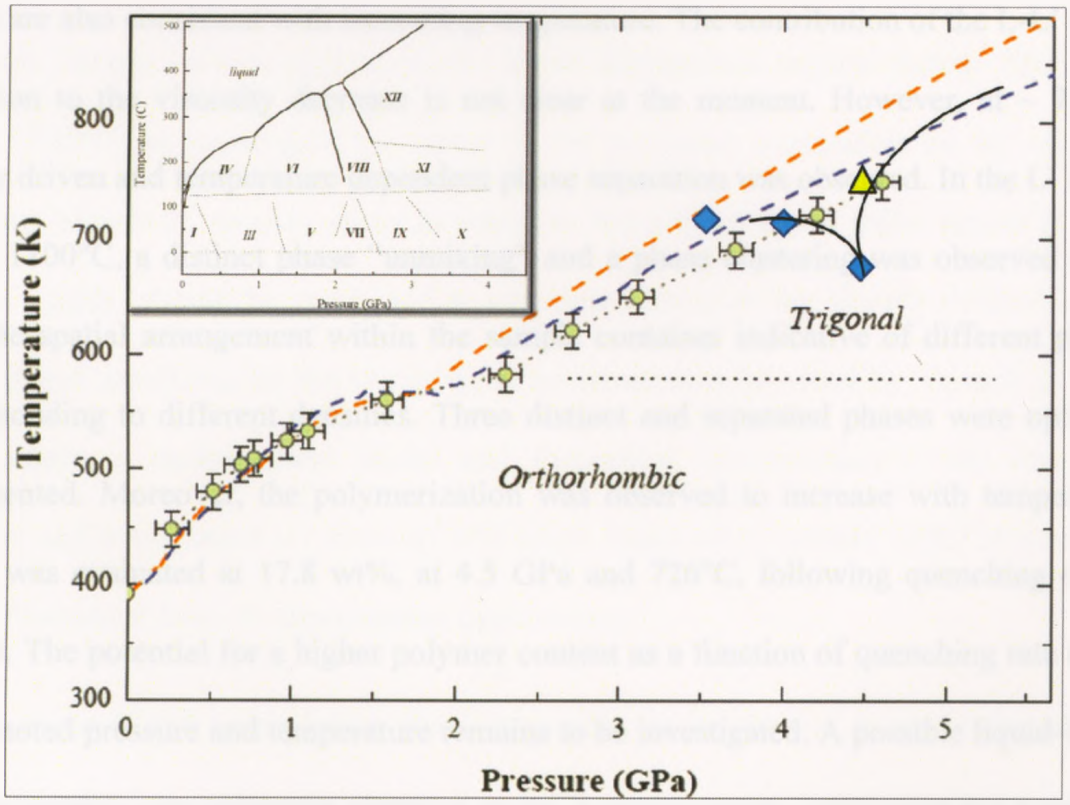

Figure 4.7: The phase diagram of sulfur up to 5.5 GPa. The melting curve with round data points and error bars is from Crapanzano (2005). The yellow triangle is the value for the melting point averaged over all runs in the experiments here (with a TC on the bottom of the container and corrected for the thermal gradient), where blue diamonds are measured values (temperature vs. time plot) of the melting points at 3.5, 4.0 and 4.5 GPa (thermocouple in the middle of the container and corrected for the temperature gradient). Inset comes from Vezzoli (1970) and it is meant to illustrate the complexity of sulfur phases up to 3.5 GPa.

5. Conclusion and Future Research

5.1 Conclusion

The viscosity of liquid sulfur at 4.5 GPa and at 726°C and 1100°C was investigated by the falling sphere and quenching method using a 1000 ton cubic anvil press at the University of Western Ontario. The recovered samples were analyzed optically, by μXRD and Raman spectra, as well as by the CS_2 solution method. For the L-liquid at 726°C, the viscosity was determined to be 0.140 ± 0.023 Pa·s and in the liquid L' at 1100°C, the viscosity was determined to be 0.050 ± 0.006 Pa·s. These results are consistent with previously obtained values by Terasaki et al. (2004). Moreover, such values are also consistent with increasing temperature. The contribution of the L-L' phase transition to the viscosity decrease is not clear at the moment. However, at ~ 726°C, density driven and temperature dependent phase separation was observed. In the L' liquid and at 1100°C, a distinct phase "unmixing" and a phase clustering was observed along with the spatial arrangement within the sample container indicative of different phases corresponding to different densities. Three distinct and separated phases were optically documented. Moreover, the polymerization was observed to increase with temperature and it was evaluated at 17.8 wt%, at 4.5 GPa and 726°C, following quenching of the sample. The potential for a higher polymer content as a function of quenching rate at the above noted pressure and temperature remains to be investigated. A possible liquid-liquid phase transition was indirectly observed in the L region below 726°C, and the existence of the pressure muted λ-transition, shifted to a higher temperature, significantly above the melting curve is hypothesized. It is evident that further research is needed to elucidate

properties of liquid sulfur at high pressures and temperatures, and consequently a range of new research topics is suggested.

5.2 Future Research

Even after a long history of investigation of solid and liquid sulfur, there remains an extensive potential for new research, with implications ranging from material to planetary sciences. Several immediate and specific research topics have been identified and are reported here, with emphasis on the ability to investigate those within the capacity of high pressure and temperature lab at the University of Western Ontario.

Viscosity should be investigated in the lower temperature regime (below 726°C and above ~580°C) to investigate the effect of the proposed λ-transition on the viscosity behavior. Moreover, an easy study to compare viscosity of liquid sulfur across B, C, D and E liquids, should be conducted to elucidate effects of the already defined liquid-liquid phase transitions on the viscosity, as proposed and theorized by Vezzoli (1969b). Additionally, a mathematical model and theoretical interpretation of the effects of pressure and temperature on viscosity and chain length of polymeric sulfur is needed to give a theoretical basis to experimental observations.

The question of the liquid-liquid phase transition, its nature and dynamics around 4.5 GPa and in the L-liquid region should be investigated by acoustical methods (Monaco et al., 2005; Scopigno et al., 2007) and by DTA, to determine a potential existence of the new liquid phase (F - a potentially new liquid phase following the E liquid in Vezzoli (1969b)) as the evidence in this thesis points to. For that purpose, a high resolution

electrical resistivity study would be also desirable, because of structural and electrical properties among different phases.

Polymerization, as a function of pressure and temperature, needs to be investigated, in addition to quantifying the polymer along the melting curve, throughout the pressure range up to 5 GPa.

Additionally, defining thermal expansion of polymer sulfur along with its compressibility would be essential because of its distinct properties, noted earlier in the text.

Finally, a direct influence of the solid structure on a short and medium range effects in liquid needs to be determined with more resolution as a direct extension of previous studies which noted the existence of such phenomenon.

References

Abowitz, G. (1977) The Compressibility of Liquid Sulfur, Selenium and Tellurium, Scripta Metallurgica, Vol. 11, pp. 353-359

Abrahams, S. C. (1955) The Crystal and Molecular Structure of Orthorhombic Sulfur, Acta Crystalolographica, Vol. 8, pp. 661

Albe, K. (1997) Theoretical study of boron nitride modifications at hydrostatic pressures, Physical Review B, Vol. 55, No. 10, pp. 6203-6210

Alvarenga, D. A. Grimsditch, M. Susman, S. and Rowland, S. C. (1996) L-Transition in Liquid Sulfur by Brullouin Scattering, Journal of Physical Chemistry, Vol. 100, pp. 11456-11459

Anderson E. M., Greer S. C. (1988) The Liquid-Liquid Phase Diagram of Sulfur + Biphenyl, Journal of chemical Physics, Vol. 88, pp. 2666-2671

Andrikopoulos, K. S. Kalampounias, A. G. and Yannopoulos, S. N. (2011) Confinment effects on Liquid-Liquid Transitions: Pore Size Dependence of Sulfur Living Polymerization, Soft Matter, Vol.7, pp. 3404-3411

Anisimov, M.A. Kugel, K.I. and Lisovskaya, T. Y. (1987) Thermodynamics of the Phase Transition in Liquid Sulfur and Sulfur Solutions, High Temperature, Vol. 25, pp. 165-173

Artyomov, M. N. and Freed, K. (2005) Compressible Models of Equilibrium Polymerization, Journal of Chemical Physics, Vol. 123, pp. 194906 1-194906 13

ASM International Materials Properties Database Committee (2002) ASM Ready Reference: Thermal Properties of Metals, #06702G, Cverna, F. (Editor) ASM International, Materials Park, Ohio, USA, www.asminternational.org

Baak, T. (1965) Sulfur - a New High Pressure Form, Science, Vol.148, pp. 1220

Bacon, R. and Finelli, R. (1943) The Viscosity of Sulfur, Journal of American Chemical Society, Vol. 65, Issue 4, pp. 639-648

Bacon, R. F. and Finelli, R. (1942) Purification of Sulfur, Industrial and Engineering Chemistry, Vol. 34, No.9, pp. 1043-1048

Baker, E. H. and Davey, T. G. (1978) Conductivity measurements on liquid sulfur, Journal of Material Science, Vol. 13, pp. 1951-1956

Ballone, P. and Jones, R. O. (2004) Equilibrium polymerization in sulphur: Monte Carlo simulations with a density functional based force field, NIC Symposium, John von Neumann Institute für Computing Series Volume 20

Balog P.S, Secco R.A, Rubie D.C, Frost D.J (2003) Equation of state of liquid Fe-10 wt% S: implications for the metallic cores of planetary bodies. Journal of Geophysics Research 108(B2):2124

Balog, P. S. Secco, R. A. and Rubie, D. C. (2001) Density Measurments of Liquids at High Pressure: Modification to the Sink/Folat Method by Using Composite Spheres, and Application to Fe-10Wt%S, High Pressure Research, Vol. 21, pp. 237-261

Beckmann, E., C. Platzmann, Z. (1918) Schwefel als klyoskopisches Lösungsmittel, Zeitschrift für anorganische und allgemeine Chemie, Vol. 102, Issue 1, pp. 201-214, doi; 10.1002/zaac.19181020111

Biermann, C. Winter, R. Benmore, C. and Egelstaff, P. A. (1998) Structural and Dynamic Properties of Liquid Sulfur Arround the L-transition, Journal of Non-Crystalline Solids, Vol. 232-234, pp. 309-313

Birch, F. (1952) Elasticity and constitution of the Earth's interior, Journal of Geophysics Research, Vol. 57, pp. 227–286

Blasklee, O., Proctor, D., Seldin, E., Spence, G. and T. Weng (1970) Elastic Constants of Compression-Annealed Pyrolytic Graphite, Journal of Applied Physics, Vol. 41, 3373

Block S. and Piermarini, G. J. (1973) The melting curve of sulfur to 300°C and 12 kbar. High Temperatures-High Pressures, Vol. 5, pp. 567

Boudiombo J., Baehr, O. Boudrioua, A., Thevenin, P, Loulergue, J. C. and Bath, A. (1997) Modes of propagating light waves in thin films of boron nitride deposited by plasma enhanced chemical vapor deposition, Materials Science Engineering, B46 96–98

Boue, F. Ambroise, J. P. Bellissent, R. and Pfeuty, P. (1996) Equilibrium Polymerization of Liquid Sulfur from Small Angle Neutron Scattering of Sulfur Solutions, Journal of Physics I France, Vol. 2, pp. 969-980

Bouroushian, M. (2010) Electrochemistry of Metal Chalcogenides, Monographs in Electrochemistry, Springer-Verlag Berlin Heidelberg, Ch. 1, pp. 1-56

Brazhkin, V. V. and Lyapin, A. G. (2003) High Pressure Phase Transformations in Liquids and Amorphous Solids, Condensed Matter, Vol. 15, pp. 6059-6084

Brazhkin, V. V. Funakoshi, K. Kanzaki, M. and Katayama, Y. (2007) Nonviscous Metalic Liquid Se, Physical Review Letters, Vol. 99, pp. 245901 1 -245901 4

Brazhkin, V. V. Popova, S. V. and Voloshin, R. N. (1999) Pressure-Temperature Phase Diagram of Molten Elements: Selenium, Sulfur and Iodine, Physica B, Vol. 265, pp. 64-71

Brazhkin, V. V. Voloshin, R. N. Popova, S. V. and Umnov, A. G. (1991) Nonmetal-Metal Transition in Sulfur Under High Pressure, Physics Letters A, Vol. 154, Issues 7-8, pp. 413-415

Bridgman, P. W. (1938) Rough Compressibilities of Fourteen Substances to 45,000 Kg/Cm, Proceedings of the American Academy of Arts and Sciences, Vol. 72, No. 5, pp. 207-225

Bridgman, P. W. (1945) The Compression of Twenty-One Halogen Compounds and Eleven Other Simple Substances to100,000 kg/cm, Proceedings of the American Academy of Arts and Sciences, Vol. 76, No. 1, pp. 1-7

Brizard, M. Megharfi, M. and Verdier, C. (2005) Absolute Falling-Ball Viscometer: Evaluation of Measurement Uncertainty, Metrologia, Vol. 42, pp. 298-303

Brooks, R. F. Dinsdale, A. T. and Quested, P. N. (2004) The Measurment of Viscosity of Alloys – a Review of Methods, Data and Models, Measurement Science and Technology, Vol. 16, pp. 354-362

Bundy, F.P. (1961) Effect of pressure on emf of thermocouples, Journal of Applied Physics, Vol. 32, Issue 3, pp. 483-488

Campbell, J. A. (2009), Sulfur Content of Planetary and Protoplanetary Cores, American Geophysical Union, Fall Meeting, Abstract no. MR43B-1878

Campbell, J. A., Seagle, T. C., Heinz, L. D., Shen, G., Prakapenka, B. V. (2007), Partial Melting in the Iron-Sulfur System at High Pressure: A Synchrotron X-ray Diffraction Study, Physics of the Earth and Planetary Interiors 162, p.119–128

Canfield, D.E. (2001) Biogeochemistry of sulphur isotopes. In: Valley, J.W., Cole, D.R. (Eds.), Stable Isotope Geochemistry. In: Reviews in Mineralogy and Geochemistry, vol. 43, pp. 607–636

Canfield. D.E., Raiswell, R. (1999) The evolution of the sulfur cycle, American Journal of Science, Vol. 299, pp. 697–723

Cataldo, F. (1997) A study on the structure and properties of polymeric sulfur, Die Angewandte Makromolekulare Chemie, Vol. 249, No. 4348, pp. 137-149

Cates, M. E. (1987) Theory of the Viscosity of Polymeric Liquid Sulfur, Europhysics Letters, Vol. 4, Issue 4, pp. 497-502

Chen J, Weidner DJ, Wang L, Vaughan MT, Young CE (2005) Density measurements of molten materials at high pressure using Synchrotron X-ray radiography: melting

volume of FeS. In: Advances in high-pressure technology for geophysical applications, Elsevier B. V., 1st Ed., Chapter 9, pp. 185-194, ISBN: 0-444-51979-3

Chen, J. and Yu, T. (2008). Constraints of Sulfur Influence on Bulk Modulus of Liquid Fe. American Geophysical Union, Fall Meeting, Abstract no. MR43A-1801

Cho, Y. I. Hartnett, J. P. and Lee, W. Y. (1984) Non-Newtonian Viscosity Measurments in the Intermediate Shear Rate Range With the Falling-Ball Viscometer, Journal of Non-Newtonian Fluid Mechanics, Vol. 15, pp. 61-74

Chung, J. B. and Vaidya, A. (2010) On the Slow Motion of a Sphere in Fluids with Non-Constant Viscosities, International Journal of Engineering and Science, Vol. 48, pp. 78-100

Crandall, P. B. (1970) Sphere Grinder Improvement, Reviews of Scientific Instruments, Vol. 41, No. 12, pp. 1895-1896

Crapanzano, L (2005) Polymerization of Sulfur: Structural and Dynamical Aspects, PhD Thesis, Joseph Fourier-Grenoble I University (available online since 2008)

Crapanzano, L. Crichton, W. A. Monaco, G. Bellissent, R. and Mezourar, M. (2005) Alternating Sequence of Ring and Chain Structures in Sulfur at High Pressure and Temperature, Nature, Vol. 4, pp. 550-552

Crichton, W. A. Vaughan, G. B. M. and Mezouar, M. (2001) In Situ Solution of Helical Sulfur at 3 GPa and 400°C, Z. Kristallography, Vol. 216, pp. 417-419

Currell, B. R. Williams, A. J. Mooney, A. J. and Nash, B. J. (1975) Plasticization of Sulfur, In: New Uses of Sulfur, (Ed. West, J.) American Chemical Society, Washington, DC

Davis, C. S. and Hyne, J. B. (1976) Thermomechanical Analysis of Elemental Sulfur: The Effects of Thermal History and Ageing, Thermochemica Acta, Vol. 15, pp. 375-385

Deaton, B. C. and Blum, F. A. (1965) Properties of Group VI B Elements Under Pressure. I. Melting Curves of S, Se, and Te, Physical Review, Vol. 137, A1131-A1138

Degtyareva, O. Gregoryanz, E. Somayazulu, M. Dera, P. Mao, H-K, and Hemley, R. (2005) Novel Chain Structures in Group VI elements, Nature, Vol. 4, pp. 152-155

Degtyareva, O. Hernandez, E. R. Serrano, J. Somayazulu, M. Mao, H-K. Gregoroyanz, E. and Hemley, *R. J. (2007) Vibrational Dynamics and Stability of the High Pressure* Chain and Ring Phases in S and Se, The Journal of Chemical Physics, Vol. 126, pp. 084503 1-084503 11

Descotes, L. Bellisent, R. Pfeuty, P. and Dianoux, A. J. (1993) Dynamics of Liquid Sulfur Around the Equilibruium Polymerization Transition, Physica A, Vol. 201, pp. 381-385

Doi, T. (1963) Physio-Chemical Properties of Sulfur, 1. Pressure Effects on Viscosity of Liquid Sulfur, The Review of Physical Chemistry of Japan, Vol. 33, No. 2, pp. 41-52

Donohue, J. (1974) The Structures of the Elements, Wiley, New York, pp. 324

Dreibus G, Waenke H (1985) Mars, a volatile-rich planet. Meteoritics 20:367–381

Dudowicz, J. Freed, K. and Douglas, J. F. (1999) Lattice Model of Living Polymerization: Basin Thermodymamics Properties, Journal of Chemical Physics, Vol. 111, (15), pp. 7116-7130

Eckert, B. and Steudel, R. (2003) Molecular Spectra of Sulfur Molecules and Solid Sulfur Allotropes, Topics in Current Chemistry, Vol. 31, pp. 231-298

Eckert, B., Schumacher, R. Jodl. J. H. and Foggi, P. (2000) Pressure and Photo Induced Phase Transitions in Sulfur Investigated by Raman Spectroscopy, High Pressure Research, Vol. 17, pp. 113-146

Eichler, J. Uibel, K and Lesniak, C. (2010) Boron Nitride (BN) and Boron Nitride Composites for Aplication Under Extreme Conditions, Advance in Science and Technology, Vol. 65, pp. 61-69

Eisenberg, A. (1963) Equilibrium Polymerization Under Pressure: The Case of Sulfur, The Journal of Chemical Physics, Vol. 39, pp.1852-1856

Eisenberg, A. (1968) The Viscosity of Liquid Sulfur. A Mechanistic Reinterpretation, Macromolecules, Vol. 2, No. 1, pp. 44-48

Espeau, P. and R. Céolin (2007) Density of molten sulfur in the 334–508K range, Thermochimica Acta, Vol. 459, pp. 127-129

Faber, T. E. (1995) Fluid Dynamics for Physicists, Cambridge University Press; 1st edition, pp. 472, ISBN: 0521429692

Fabris, D. Muller, J. S. and Liepmann, D. (1999) Wake Measurements for a Flow Arround a Sphere in a Viscoelastic Fluid, Physics of Fluids, Vol. 11, No. 12, pp. 3599-6612

Fairbrother, F, Gee, G. and Merrall, T. (1955) Polymerization of Liquid Sulfur, Journal of Polymer Science, Vol. 16, (82), pp. 459-469

Farquhar, J., Wing, B.A. (2003) Multiple sulfur isotopes and the evolution of the atmosphere. Earth and Planetary Science Letters 213, 1–13

Feher, F., Goerler, G. P., Lutz, H. D. (1971) Beitrage zur Chemie des Schwefels. 108. Schmelzwarme und spezifische Warme des flüssigen Schwefels. Einfluß von Verunreinigungen, Journal of Inorganic and General Chemistry, Vol. 382, (2), pp. 135-148

Feher. F. and Hellwig, E. (1954) Silicium, Schwefel, Phosphate, Colloq. Sek. Anorganic Chemistry, International Union Reine Angew. Chem., Muencster, Vol. 95

Feng, S. Graham, A. L. Reardon, P. T. Abbott, J. and Mondy, L. (2006) Improving Falling Ball Tests for Viscosity Determination, Journal of Fluids Engineering, Vol. 128, pp.157-163

Flemming, R.L., Salzsauler, K.A., Sherriff, B.L. and Sidenko, N.V. (2005) Identification of scorodite in fine-grained, high-sulfide, arsenopyrite mine-waste using micro X-ray diffraction (μXRD), The Canadian Mineralogist, Vol. 43, pp. 1243-1254

Fuchizaki, K., Nakamichi, T., Saitoh, H., and Y. Katayama (2008) Equation of state of hexagonal boron nitride, Solid State Communications, Vol. 148, pp. 390-394

Fujihisa, H. Akahama, Y. Kawamura, H. Yamawaki, H. Sakashita, M. and Yamada, T. (2004) Spiral Chain Structure of High Pressure Selenium-II' and Sulfur-II from Powder X-ray Diffraction, Physical Review B, Vol. 70, pp. 134106 1-134106 4

Funakoshi, Ken-Ichi, (2010), In Situ Viscosity Measurments of Liquid Fe-FeS Alloys at High Pressures, High Pressure Research, Vol. 30, No.1, pp.60-64

Gee, G. (1952) The Molecular Complexity of Sulfur in the Liquid and Vapour, Trans. Faraday Society, Vol. 48, pp. 515-529

Geller, S. (1967) Pressure Induced Phases of Sulfur, Science, Vol. 152, pp. 644-646

Getting, I. C. and Kennedy, G. C. (1970) Effect of Pressure on the emf of Chromel-Alumel and Platium-Platinum 10%Rhodium Thermocouples, Journal of Applied Physics, Vol. 41, No. 11, pp.4552-4563

Godec, Y. Le , Martinez-Garcia, D. , Mezouar, M. , Syfosse, G. , Itié, J. -P. and Besson, J. -M.(2000) Thermoelastic behaviour of hexagonal graphite-like boron nitride, High Pressure Research, Vol. 17, Issue 1, pp. 35-46

Gottlieb, Moshe, (1979) Zero-Shear-Rate Viscosity Measurments for Polymer Solutions by Falling Ball Viscometry, Journal of Non-Newtonian Fluid Mechanics, Vol. 6, pp. 97-109

Greer, S. C. (1998) Physical Chemistry of Equilibrium Polymerization, Journal of Physical Chemistry B, Vol. 102, pp. 5413-5422

Hafner, W., Kritzenberger, J., Olijnyk, H. and A. Wokaun (1990) Phase transitions in crystalline sulfur at p>8 GPa, observed by Raman spectroscopy in a diamond anvil cell, A. High Pressure Res., Vol. 6, Issue 1, pp. 57-75

Hanfland, M., Beister, H., Syassen, K. (1989) Graphite under pressure: Equation of state and first-order Raman modes, Physical Review B, Vol. 39, Issue 17, 12598–12603

Happel, J. and Brenner, H. (1973) Low Reynolds Number Hydrodynamics: Leyden, Noordhoff, p. 555

Harlen, O. (2002) The Negative Wake Behind a Sphere Sedimenting Through a Viacoelastic Fluid, Journal of Non-Newtionian Fluid Mechanics, Vol. 108, pp. 411-430

Harris, R. E. (1970) Molecular Composition of Sulfur, J. Phys. Chem., Vol. 74, Issue 16, pp. 3102-3111, doi: 10.1021/j100710a014

Hauck, A. S., Aurnou, M. J. and Dombard, J. A. (2006), Sulfur's impact on core evolution and magnetic field generation on Ganymede, Journal of Geophysical Research, Vol. 111

Heath, R. D. (1995) Viscosity and Density of Liquid Sulfur at High Pressures and Temperatures: Implication for the Earth's Outer Core and Volcanism on Io, BSc master Thesis, University of Western Ontrario

Hicks, T. L. and Secco, R. A. (1997) Dehydration and Decomposition of Pyrophyllite at High Pressures: Electrucal Conductivity and X-Ray Diffraction Studies to 5 GPa, Canadian Journal of Earth Sciences, Vol.34, pp. 875-882

Hosokawa, S., Matsuoka, T., and Tamura, K. (1994) Optical Absorption Spectra of Liquid Sulfur Over a Wide Absorption Range, Journal of Physics: Condensed Matter, Vol.6, pp. 5273-5282

Ishikawa, T., Tsuchiya, T. (2010) New high-pressure phase of Fe3S predicted from first-principles calculation, American Geophysical Union, Fall Meeting 2010, abstract #DI41A-1934

Ito, E. (2007) Theory and practice-multianvil cells and high-pressure experimental methods. In: Price, G.D., Schubert, G. (Eds.), Treatise on Geophysics, Vol. 2. Elsevier, Amsterdam, pp. 197e230.

Ivin, K. J. (1974) In ReactiVity, Mechanism, and Structure in Polymer Chemistry; Jenkins, A. D., Ledwith, A., Eds.; John Wiley: New York, p 514

Janotti, A. and S.-H. Wei, D.J. Singh (2001) First-principles study of the stability of BN and C, Physical Review B, 64, 174107

Kalampounias, A. G. Andrikopoulos, K. S. and Yannopoulos, S. N. (2003a) "Rounding" of the Sulfur Living Polymerization Transition Under Spatial Confinement, Journal of Chemical Physics, Vol. 119, (14), pp. 7543-7553

Kalampounias, A. G. Andrikopoulos, K. S. and Yannopoulos, S. N. (2003c) Probing the Sulfur Polymerization Transition in Situ With Raman Spectroscopy, Journal of Chemical Physics, Vol. 118, No. 18, pp. 8460-8467

Kalampounias, A. G. Kastrissios, D. Th. And Yannopoulos, S. N. (2003b) Structure and Vibrational Modes of Sulfur Around the L-Transition and the Glass-Transition, Journal of Non-Crystalline Solids, Vol. 326 and 327, pp. 115-119

Karamanev, D. G. (2001) The Study of Free Rise of Buoyant Spheres in Gas Reveals the Universal Behavior of Free Rising Rigid Spheres in Fluid in General, International Journal of Multiphase Flow, Vol. 27, pp. 1479-1486

Katayama, Y. (1996) Density measurements of non-crystalline materials under high pressure and high temperature. High Press Research, 14, 383–391

Katayama, Y., Inamura, Y., Mizutani, T., Yamakata, M., Utsumi, W., and Shimomura, O. (2004) Macroscopic Separation of Dense Fluid Phase and Liquid Phase of Phosphorus, Science, Vol. 306, pp. 848-851

Kennedy, S. and Wheeler, J. C. (1983) On the Density Anomaly in Sulfur at the Polymerization Transition, Journal of Chemical Physics, Vol. 78, (3), pp. 1523-1527

Kern, G., Kresse, G. and Hafner, J. (1999) Ab initio calculation of the lattice dynamics and phase diagram of boron nitride, Physical Review B, Vol. 59, Issue 13

Kim, E. and C. Chen (2004) Calculation of bulk modulus for highly anisotropic materials, Physics Letters A, Vol. 326, pp. 442-448

Kirk-Othmer Encyclopedia of Chemical Technology. 4th ed. New York: John Wiley & Sons, 1998, pp. 2240

Koh, J. C. and Klement, W. Jr. (1970) Polymer Content of Sulfur Quenched From the Melt, The Journal of Physical Chemistry, Vol. 74, No. 24., pp. 4280-4283

Koningsberger, D. C. (1971) On the polymerization of sulfur and selenium in the liquid state : an ESR study, Doctoral Dissertation, Technische Hogeschool Eindhoven, The Netherlands, http://repository.tue.nl/109059

Kozhevnikov, V. F. Payne, W. B. Olson, J. K. McDonald, C. L. and Inglefield, C. E. (2004) Physical Properties of Sulfur Near the Polymerization Transition, Journal of Chemical Physics, Vol. 121, (15), pp. 7379-7386

Kushiro, L. (1980) In: R. B. Hargraves (Ed.), Physics of Magmatic Processes, Princeton University Press, p. 92

Larkin, J. A. Katz, J. and Scott, R. L. (1967) Phase Equilibria in Solutions of Liquid Sulfur. II. Experimental Studies in Ten Solvents: Carbon Disulfide, Carbon Tetrachloride, Benzene, Toluene, O-xylene, Naphtalene, Biphenyl, Triphenylmethane, Cis-Descalin, and Trans-Decalin, Journal of Physical Chemistry, Vol. 72, (2) pp. 352-358

Leblanc, G. E., Secco, R. A., Kostic, M. (1999) Viscosity Measurement, In: The Measurement, Instrumentation and Sensors Handbook (Electrical Engineering Handbook), CRC Press, 1st Ed., p. 2630, ISBN: 0849383471

Lelonis D. A. et al (2003) A High Performance Alternative for Solid Lubrication, GE Company Publication No 81506

Lewis, G. N. and Randall, M. (1911) The heat content of the various forms of sulfur, Journal of American Chemical Society, Vol. 3 (3), pp. 476

Lopes, M. C. R. and Spencer, R. J. (2007) Io After Galileo, A new view of Jupiter' Volcanic Moon, Springer; 1 edition, pp. 365. ISBN: 3540346813

Lowitzer, S., Winkler, B., and M. Tucker (2006) Thermoelastic behavior of graphite from in situ high-pressure high-temperature neutron diffraction, Physical Review B, Vol. 73, 214115

Luo, H. and Ruoff, A. L. (1993) X-ray Diffraction Study of Sulfur to 32 GPa: Amorphisation at 25 GPa, Physical Riview B, Vol. 48, No. 1, pp. 569-572.

Luo, H., Desgreniers, S., Vohra, Y. K., and Ruoff, A. (1991) High Pressure Optical Studies on Sulfur up to 121 GPa: Optical Evidence for Metalization, Physical Review Letters, Vol. 67, No. 21, pp. 2998-3001

Luo, H., and A. Ruoff (1994) L. X-Ray Diffraction Study of Sulfur to 212 Gpa, In: High-Pressure Science and Technology-1993; Schmidt, S. C., Shaner, J. W., Samara, G. A., Ross, M., Eds.; AIP Press: New York, 1994

Lynch R. and H. Drickamer (1966) Effect of High Pressure on the Lattice Parameters of Diamond, Graphite, and Hexagonal Boron Nitride, Journal of Chemical Physics, Vol. 44, Issue 1, pp. 181

MacKnight, W. J. Poulis, J. A., Massen, C. H. (1967) Effect of Sπ on the Polymerization of Liquid Sulfur and the Nature of Sπ, Journal of Macromolecular Science: Pure and Applied Chemistry A., Vol. 1, Issue 4, 699-705

Mason, B. (1966) Composition of the Earth, Nature, Vol.211 pp. 616–618

Matsushima, T. (1959) The viscosity of liquid sulfur, Science reports of the Research Institutes, Tohoku University. Series A, Physics, Chemistry and Metallurgy, Vol. 11, pp. 474-481

McMillan, P. F. and Wilding, M. C. (2009) High Pressure Effects on Liquid Viscosity and Glass Transition Behavior, Polymorphic Phase Transitions and Structural Properties of Glasses and Liquids, Journal of Non-Crystalline Solids, Vol. 355, pp. 722-732

McMillan, P. F. Willson, M. Wilding, M. C. Daisengerger, D. Mezouar, M. and Greaves, G. N. (2007) Polyamorphism and Liquid-Liquid Phase Transitions: Chalenges for Experiment and Theory, Journal of Physics: Condensed Matter, Vol.19, p.41

Métrich, N. and C.W. Mandeville (2010) Sulfur in Magmas, Elements, Vol. 6, pp. 81-86

Meyer, B (1976) Elemental Sulfur, Chemical Reviews, Vol. 76, No. 3, pp. 367-388

Meyer, B. Oommen, T. V. and Jensen, D. (1971) The Color of Liquid Sulfur, The Journal of Physical Chemistry, Vol. 75, No. 7, pp. 912-917

Mojzsis, J. Stephen, (2007), Precambrian Ophiolites and Related Rocks, Edited by Martin J. van Kranendonk, R. Hugh Smithies and Vickie C. Bennett, Developments in Precambrian Geology, Vol. 15 (K.C. Condie, Series Editor)

Monaco, G. Crapanzano, L. Bellissent, R. Crichton, W. Fioretto, D. Mezouar, M. Scarponi, F. and Verbeni, R. (2005) Rubberlike Dynamics in Sulphur Above the L-Transition Temperature, Physical Review Letters, Vol. 95, pp. 255502 1-255502 4

Murthy, R.V. and Hall, H.T. (1970) The chemical composition of the Earth's core: Possibility of sulphur in the core, Physics of the Earth and Planetary Interiors, Vol. 2, pp. 276–282

Nagamori, M (1969) Density of molten Ag–S, Cu–S, and Ni–S systems. Transactions of the Metallurgical Society of the American Institute of Mechanical Engineers, AIME 245:1897–1902

Nagata,K., Nishio, T., Taguchi, H., and Miyamoto, Y. (1992) Raman Spectra and X-Ray Diffraction of Sulfur Under High Pressure, Japanese Journal of Applied Physics, Vol. 31, pp. 1078-1084

Nasch, P.M., Steinemann, S.G. (1995) Density and thermal expansion of molten manganese, iron, nickel, copper, aluminum and tin by means of the gamma-ray attenuation technique, Physics and Chemistry of Liquids, 29:43–58

Nehb, W. and K. Vydra (2006) Sulfur, In: Ullmann's Encyclopedia of Industrial Chemistry, Wiley-VCH Verlag GmbH & Co. KGaA, pp. 64

Nishida, K. Ohtani, E. Uradawa, S. Suzuki, A. Sakamaki, T. Terasaki, H. and Katayama, Y. (2011). Density Measurement of Liquid FeS at High Pressures Using Synchrotron X-ray Absorption, American Mineralogist, Volume 96, pp. 864-868

Nishida, K., Terasaki, H, Ohtani, E. and A. Suzuku (2008) The effect of sulfur cintent on density of the liquid Fe-S at high pressure, Physics and Chemistry of Minerals, Vol. 35, pp. 417-423

Ohmoto, H., Goldhaber, M.B., 1997. Sulfur and carbon isotopes. In: Barnes, H.L. (Ed.), Geochemistry of Hydrothermal Ore Deposits, 3rd ed. John Wiley & Sons, New York, pp. 517–611

Ohtani, E. Suzuki, A. Ando, R. Urakawa, K. Funakoshi, K. and Katayama, Y. (2005) Viscosity and Density Measurements of Melts and Glasses at High Pressure and Temperature by Using the Multi-Anvil Apparatus and Synchrotron X-Ray Radiation, Ch. 10, Advances in High Pressure Technology for Geophysical Applications, Edited by: Wang, T. Duffy, T. S. Shen, G. and Dobrzhinetskaya, L. F., Elsevier B. V.

Olson, J. K. Moodie, C. B. Kozhevnikov, V. F. and Taylor, P. C (2002) Acoustical Impedance of Sulfur Near the Polymerization Transition, International Journal of Thermophysics, Vol. 25, (5) pp. 1429-1436

Ono, S., Oganov, A. R., Brodholt, J. P., Vočadlo, L., Wood, I. G., Lyakhov, A., Glass, C. W., Côté, A. S., Price, G. D. (2008) High-pressure phase transformations of FeS: Novel phases at conditions of planetary cores, Earth and Planetary Science Letters, Vol. 272, Issues 1-2, pp. 481-487

Ooi, N., Rairkar, A. and J. B. Adams (2006) Density functional study of graphite bulk and surface properties, Carbon, Vol. 44, pp. 231-242

Orgzall, I. and Lorenz, B. (1994) On the Formation of Photoinduced High Pressure Phases in Sulfur Below 10 GPa, High Pressure Research, Vol. 13, pp. 215-224

Patel, H. and Borst, L. B. (1971) First-Order Lambda Transition in Sulfur, Journal of Chemical Physics,Vol. 54, 822, doi: 10.1063/1.1674925

Paukov, E. I. and Tonokov, E, Yu. (1965a) The Melting Curve of Sulfur up to 11 000 KG/CM2, Journal of Applied Mechanics and Technical Physics, No. 4, pp. 172-1747

Paukov, I. E. Tonkov, E. Y.and Mirinski, D. S. (1965b) Phase diagram of sulphur at high pressure. Doklady Akademii Nauk, SSSR., Vol.164, pp.588

Poirier, J.P. (1988) Transport properties of liquid metals and viscosity of the Earth's core, Geophysical Journal International, 92, pp. 99–105

Poirier, J.P. (1994) Light elements in the Earth's outer core- a critical review, Physics of Earth Planetary Interior, Vol. 85, pp. 319-337

Powell, E. and Eyring, H. (1943) The Properties of Liquid Sulfur, Journal of American Chemical Society, Vol. 65, Issue 4, pp. 648-654

Rempe, J. l. and Wilkins, S. C. (2005) High Temperature Thermocouples For in-Pile Applications, The 11th International Topical Meeting on Nuclear Reactor Thermal-Hydraulics (NURETH-11), Popes Palace Conference Center, Avignon, France,10/02/2005,10/06/2005

Rettig, S. J. Trotter, J. (1987) Refinement of the structure of orthorhombic sulfur, alpha-S8, Acta Crystalographica, C43, pp.2260-2262

Ringwood, A.E. (1977) Composition of the core and implications for the origin of the Earth, Geochemical Journal, Vol. 11, pp. 111-135.

Ruiz-Garcia, J. Anderson, E. M. and Greer, S. C. (1989) Sheer Viscosity of Liquid Sulfur Near the Polymerization Temperature, Journal of Physical Chemistry, Vol. 93, pp. 6980-6983

Ryan, M P. and James Y.K. B (1987) The viscosity of synthetic and natural silicate melts and glasses at high temperatures and 1 bar (10 p5 s Pascals) pressure and at higher pressures, US Geological Survey Bulletin 1764, Denver, CO, 1st Ed., p. 563

Rydberg, H., Dion, M., Jacobson, N., Schroder, E., Hyldgaard, P., Simak, S. I., Langreth, D. C., and B. I. Lundqvist (2003) Van derWaals Density Functional for Layered Structures, Physical Review Letters, Vol. 91, No. 12, pp. 126402:1-4

Sakaguchi, Y. and Tamura, Y. (2007) Laser-Induced Pattern Formation in Liquid Sulfur, European Physics Journal, E. 22, pp. 315-324

Sands, D. (1965) The Crystal Structure of Monoclinic Sulfur, Journal of the American Chemical Society, Vol. 87, 6, pp.1395-1396

Sanloup C, Guyot F, Gillet P, Fiquet G, Mezouar M, Martinez I.(2000) Density measurements of liquid Fe–S alloys at high-pressures. Geophysics Research Letters, 27(6):811–814

Sata, N., Ohfuji, H., Hirose, K., Kobayashi, H., Ohishi Y. and N. Hirao (2008) New high-pressure B2 phase of FeS above 180 GPa, American Mineralogist, Vol. 93, No. 2-3, pp. 492-494

Saunders, G. A., Yogurtcu, Y. K., Macdonald, J. E. and G. S. Pawley (1986) The elastic behaviour of orthorhombic sulfur under pressure, Proceedings of the Royal Society of London, Series A, Mathematical and Physical Sciences, Vol. 407, No. 1833, pp. 325-342

Schenk P. W. and U. Thümmler (1959) Sπ und die Schwefelschmelze, Zeitschrift für Elektrochemie, Berichte der Bunsengesellschaft für physikalische Chemie, Vol. 63, Issue 8, pp 1002-1005

Schenk, P. W. (1955) Zur Kenntnis der Schwefelmodifikationen, Zeitschrift für anorganische und allgemeine Chemie, Vol. 280, Issue 1-3, pp. 1-23

Schloessin, H. and Lenson, P. F. (1989) Meaurement and Moddelling of the Temperature Field in High-Pressure and High-Temperature Experiments in Cubes with Internal Heating, High Temperature-High Pressures, Vol. 21, pp. 275-285

Schmeiser, J. W. Zanotto, E. D. and Fokin, M. V. (2005) Pressure Dependance of Viscosity, The Journal of Chemical Physics, Vol. 122, pp. 074511 1 - 074511 11

Schmidt, M., H.-D. Block (1967) Occurrence of Cyclododecasulfur in Sulfur Melts, Angewandte Chemie International Edition, Vol. 6, Issue 11, pp. 955-956

Scopigno, T., Yannopolous, S.N., Scarponi, F., Andrikopoulos, K.S., Fioretto, D., Ruocco, G. (2007) Origin of the λ transition in liquid sulfur, Physical review Letters, Vol. 99

Scott, R. L. J. (1965) Phase Equilibria in Solutions of Liquid Sulfur. I. Theory, Journal of Physical Cjemistry, Vol.69, No.1 pp.261-361

Scwartz, M. (1956), 'Living' Polymers, Nature, Vol. 178, pp.1168-1169

Seal, R.R., II, (2006) Sulfur isotope geochemistry of sulfide minerals. In: Vaughan, D.J. (Ed.), Sulfide Mineralogy and Geochemistry. In: Reviews in Mineralogy and Geochemistry, vol. 61, pp. 633–677

Secco R.A, Rutter M.D, Balog P.S, Liu H, Rubie D.C, Uchida T, Frost D, Wang Y, Rivers M, Sutton SR (2002) Viscosity and density of Fe–S liquids at high pressures. J. Phys. Condensed Matter 14:11325–11330

Secco, A. R. (1994) Load Cycling and Pressure Efficiency in a Large Volume Cubic Press, AIP Conference Proceedings, Vol. 309, pp. 1593-1596

Secco, R. A. and H.H. Schloessin (1989) The electrical resistivity of solid and liquid Fe at pressures up to 7 GPa, Journal of Geophysical Research, Vol. 94, No. B5, pp. 5887-5894

Semlyen, J. A. (1971) Equilibrium ring concentrations and the statistical conformations of polymer chains: Part 6. Freezing point of liquid sulphur, Polymer, Vol. 12, Issue 6, 383-388

Shen, G., Wang, Y., Prakapenka, V., Benmore, C. J., Alp, E. E., Ding, Y., and Yang, W. (2010) High-Pressure Research at the Advanced Photon Source, Synchrotron Radiation News, Vol. 23, (3), pp. 32-38

Shieh, R. S. (2011) Personal communication with Dr. Sean Shieh

Smith A. and W. B. Holmes (1905) On amorphous sulphur: III. The nature of amorphous sulphur and contributions to the study of the influence of foreign bodies on the behavior of supercooled melted sulphur, Journal of the American Chemical Society, Vol. 27, Issue 8, 979-1013, doi: 10.1021/ja01986a008

Solozhenko, V. L., Will, G., and F. Elf (1995) Isothermal compression of hexagonal graphite-like boron nitride up to 12 Gpa, Solid State Communications, Vol. 96, No. 1, pp. 1-3

Solozhenko, V.L. and T. Peun (1997) Compression and thermal expansion of hexagonal graphite-like boron nitride up to 7 Gpa and 1880 K, Journal of Physics and Chemistry of Solids, Vol. 58, No. 9, pp. 1321-1323

Solozhenko V.L. and E.G. Solozhenko (1999) On the compressibility of graphite-like boron nitride, Journal of Superhard Mater, 21, pp. 83–84

Solozhenko V.L., and E.G. Solozhenko (2000) On the compressibility of graphite, Journal of Superhard Mater, Vol. 22, pp. 79–80

Song, D. Gupta, K. R. and Chhabra, R. P. (2010) Efffects of Shear Thining and Elasticity in Flow Around a Sphere in a Cylindrical Tube, COMSOL Conference, Boston, Ma.

Steudel, R. (2003) Liquid sulfur, Topics in Current Chemistry, Vol. 230, pp. 81-116

Steudel, R., Eckert, B. (2003) Solid Sulfur Allotropes, Topics in Current Chemistry, Vol.230, pp. 1-79

Sumer (1955) On Compressibility of Sulfur, Bulletin of the Turkish Physical Society, No. 23

Susse, C. Epain, R. and Vodar, B. (1964) Compte Rendu Physique, Vol.258, pp. 45138

Tanaka, Hajime, (2000) General View of a Liquid-Liquid Phase Transition, Physical Review, Vol. 62, No. 5, pp. 62-76

Templeton, L. K. Templeton, D.H. Zalkin, A. (1976) Crystal Structure of Monoclinic Sulfur, Inorganic Chemistry, Vol. 15, pp. 1999-2001

Terasaki, H. Kato, T. Funakoshi, K, Suzuki, A. and Urakawa, S. (2004) Viscosity of Sulfur Under High Pressure, Journal of Physics: Condensed Matter, Vol. 16, pp. 1707-1714

Terasaki, H. Kato, T. Urakawa, S. Funakoshi, K. Suzuki, A. Okada, T. Maeda, M. Sato, J. Kubo, T. and Kasi, S. (2001) The Effects of Temperature, Pressure, and Sulfur

Content on Viscosity of the Fe-FeS Melts, Earth and Planetary Science Letters, Vol. 190, pp. 93-101

Tinker, D., Lesher, C.E., Baxter, G.M., Uchida, T. and Y. Wang (2004) High-pressure viscometry of polymerized silicate melts and limitations of the Eyring equation, American Mineralogist, Vol. 9, pp.1701-1708

Tobolsky, A. V. and Eisenberg, A. (1959) Equilbrium polymerization of Sulfur, Journal of American Chemical Society, Vol. 81 (4), pp. 780-782

Tobolsky, A. V. and Eisenberg, A. (1962) Transition Phenomenon in Equilibrium Polymerization, Journal of Colloid Science, Vol. 17, pp. 49-65

Touro, F. J. and Wiewiorowski, T. K. (1966) Viscosity-Chain Length Relationship in Molten Sulfur System, The Journal of Physical Chemistry, Vol. 70, No. 1, pp. 239-241

Tuinstra, F. (1967) Structural Aspects of the Allotropy of Sulfur and the Other Divalent Elements, Waltman, Delft., PhD Thesis

Uchida T., Wang, Y., Rivers, M. L., Sutton, S. R., Weidner, D. J., Vaughan, M. T., Chen ,J., Li, B., Secco, R. A., Rutter, M. D. and H. Liu (2002) A large-volume press facility at the Advanced Photon Source: diffraction and imaging studies on materials relevant to the cores of planetary bodies, Journal of Physics: Condensed Matter, Vol. 14, No 44, pp. 11517-11523

Usselman, T.M. Experimental approach to the state of the core: part I. The liquidus relations of the Fe-rich portion of the Fe-Ni-S system from 30 to 100 kb, Journal of the American Society for Information Science and Technology, 275 (1975) 278-290

Vaidya, S. N. and Kennedy, G. C. (1971) Compressibility of 22 Elemental Solids to 45 KB, Journal of Physical Chemistry: Solids, Vol. 33. pp. 1377-1389

Valladeres, R. M. Goldstein, P. Stern, C. and Calles, A. (2003) Simulation of the Motion of a Sphere Through a Viscous Fluid, Revista Mexicana De Fisica, Vol. 49, No. 2, pp. 166-174

Vezolli, G. C. (2004) Nano-Structures and Phase Transitions in the Liquid Phase of Metallic and Non-Metallic Elements, NSTI-Nanotech, Vol. 1, pp. 239-242

Vezzoli, G. C. and Zetto, R. J. (1970) The Ring – Chain High-Pressure Polymorphic Transformation in Sulfur and the Accompanying Change From Insulating to Modest Semiconducting Behavior, Inorganic Chemistry, Vol. 9, No. 11, pp. 2478-2484

Vezzoli, G. C. Dachille, F. and Rustom, R. (1969a) The Melting Curve of Sulfur up to 31 kbars, Inorganic Chemistry, Vol. 8, No. 12, pp.2658-2661

Vezzoli, G. C. Dachille, F. and Rustom, R. (1969b) High Pressure Studies of Polymerization of Sulfur, Journal of Polymer Science, Part A-1, Vol. 7, 1557-1566

Vezzoli, G. C. Dachille, F. and Rustom, R. (1969c) Sulfur Melting and Polymorphism Under Pressure: Outline of Fields for 12 Crystalline Phases, Science, New Series, Vol. 166, No. 3902, pp. 218-221

Vezzoli, G. C. Kisatsky, P. J. Doremus, L. W. and Walsh, P. J. (1976) Optical and Electrical Effects During Polymerization and Depolymerization in Liquid Sulfur: Indications for the Nonuniformity Model for Covalent Liquids, Applied Optics, Vol. 15, (2), pp. 327-339

Viswanath, D. S. Ghosh, T. K. Prasad, D. H. Dutt, N. V. K. and Rani, K. Y. (2007) Viscosity of Liquids, Springer, Derdrecht, The Netherlands, 1st Ed. p. 676, ISBN-10: 1402054815

Ward K. B. and Deaton, B. C. (1967) Properties of Group VIB Elements Under Pressure. III Phase Diagram Studies of Various Forms of Sulfur, Physical Review, Vol.153, 947-951

West, E. D. (1959) The Heat Capacity of Sulfur From 25 to 450°, the Heats and Temperature of Transition and Fusion, Journal of American Chemical Society, Vol. 81, (1), pp. 29-37

Wheeler, J. C. and P. Pfeuty (1981) The $n \rightarrow 0$ vector model and equilibrium polymerization, Physical Review A, Vol. 24, No. 2, pp. 1050-1062

Wheeler, J. C. Kennedy, S. J. and Pfeuty, P. (1980) Equilibrium Polymerization as a Critical Phenomenon, Physical Review Letters, Vol. 45, No. 22, pp. 1748-1752

Wiewiorowski, T. K., A. Parthasarathy, B. L. Slaten, (1968) Molten sulfur chemistry V. Kinetics of chemical equilibration in pure liquid sulfur, Journal of Physical Chemistry, Vol. 72, Issue 6, 1890-1892, doi: 10.1021/j100852a005

Wiewiorowski, T. K., F. J. Touro (1966) Molten Sulfur Chemistry I. Chemical Equilibria in Pure Liquid Sulfur, Journal of Physical Chemistry, Vol. 70, Issue 11, pp. 3528-3531

Winter, R. Bodensteiner, T. Szornel, C. Egelstaff, P. A. (1988) The Structural Properties of Liquid and Quenched Sulfur, Journal of Non-Crystalline Solids, Vol. 106, pp. 100-103

Yoder CF, Konopliv AS, Yuan DN, Standish EM, Folkner WM (2003). Fluid core size of mars from detection of the solar tide, Science, 300:299–303

Yoshioka, A. and Nagata, K. (1995) Raman Spectrum of Sulfur Under High Pressure, Journal of Physical Chemistry, Vol. 56, No. 3/4, pp. 581-584

Yu, P., Wang, W. H., Wang, R. J., Lin, S. X., Liu, X. R., Hong, S. M. and H. Y. Bai (2009) Understanding exceptional thermodynamic and kinetic stability of amorphous sulfur obtained by rapid compression, Applied Physics Letters, Vol. 94, 011910

Zhao, Y. X., and I. L. Spain (1989) X-ray diffraction data for graphite to 20 GPa, Physics Review B, Vol. 40, Issue 2, pp. 993-997

Zhao, Y., R. B. Von Dreele. D. J. Weidner, and D. Schiferl, (1997), P-V-T Data of Hexagonal Boron-Nitride hBN and Determination of Pressure and Temperature Using Thermoelastic Equation of State of Multiple Phases, High Pressure Research, 62, 1-18

Zheng, K. M. and Greer S. C. (1992) The Density of Liquid Sulfur Near the Polymerization Temperature, Journal of Chemical Physics, Vol. 96, Issue 3, pp. 2175-2182

Appendix 1

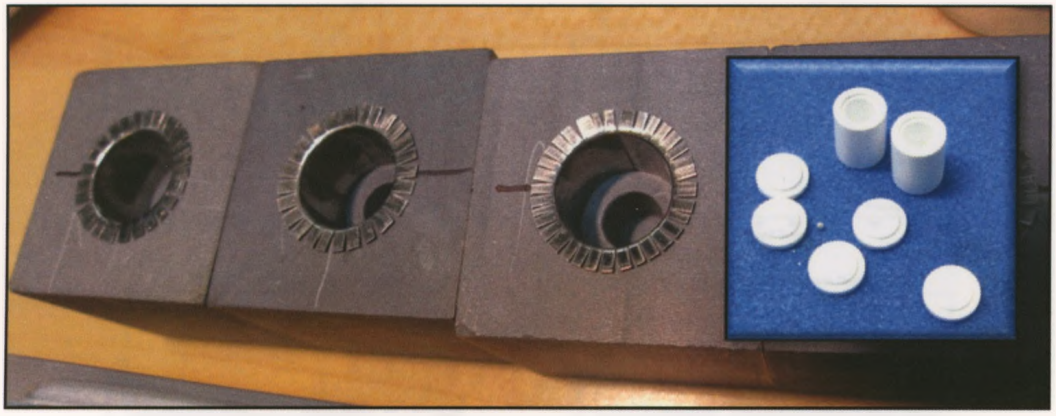

Figure A1.1: Pyrophyllite cubes during preparation. Inset: sample containers prior to packing.

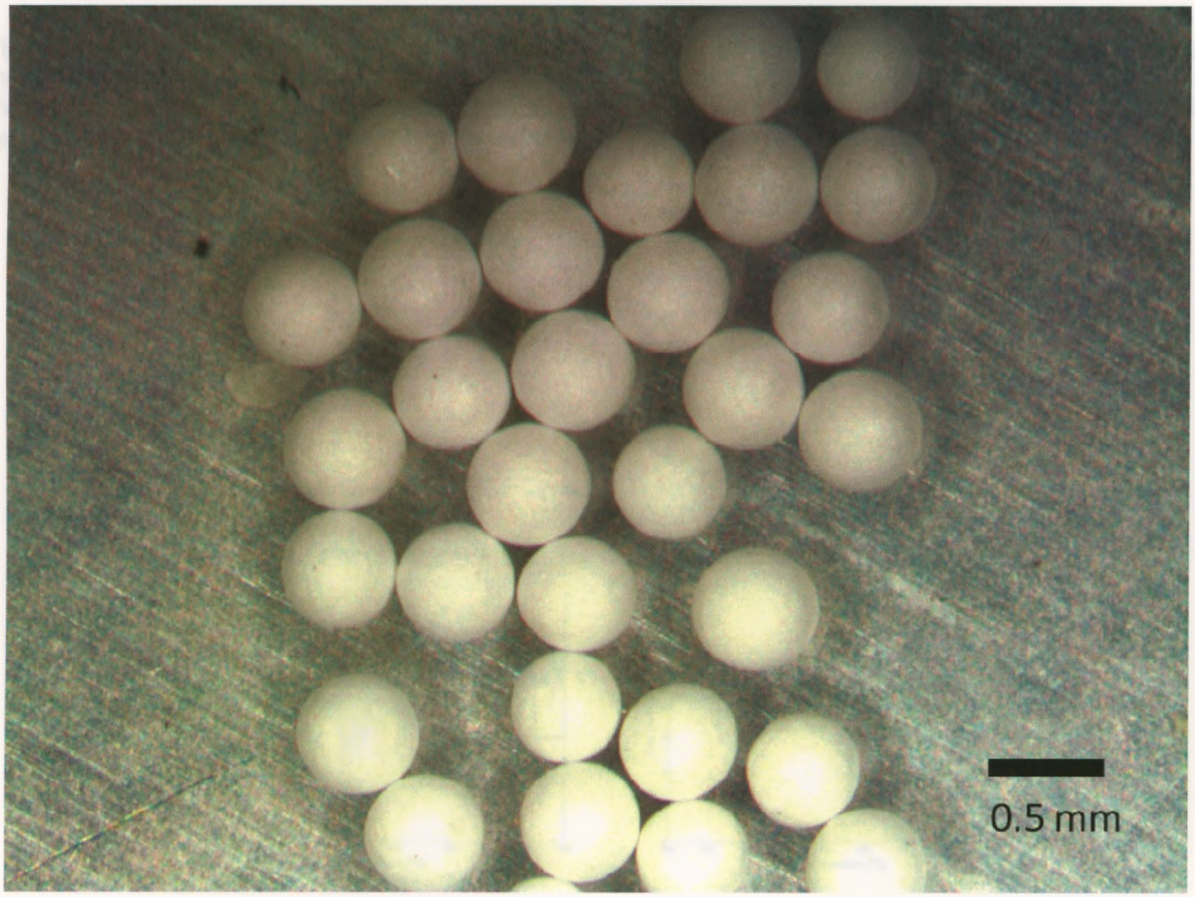

Figure A1.2: Photograph showing fabricated BN spheres shown for size uniformity.

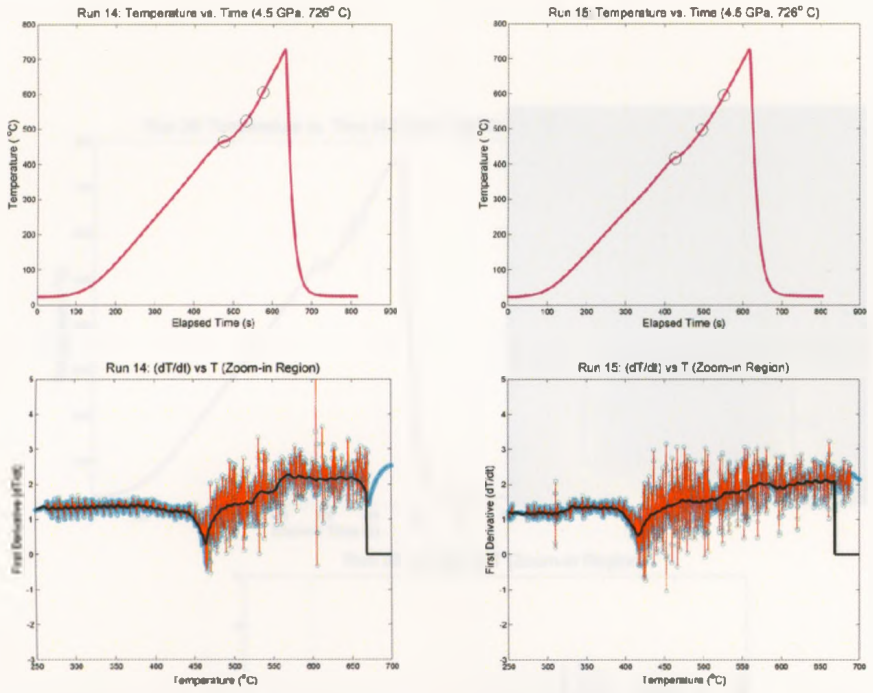

Figure A1.3: Temperature vs. time plots with dT/dt vs T plots for selected runs, to illustrate the deviation of the recorded melting signal, possibly as a result of a sharp minima at 4.5 GPa and pressure uncertainty around it. Notably, the heating rate was the same for all these experiments, and all other parameters such as the container geometry and the TC placement were kept experimentally constrained to ensure repeatability of results.

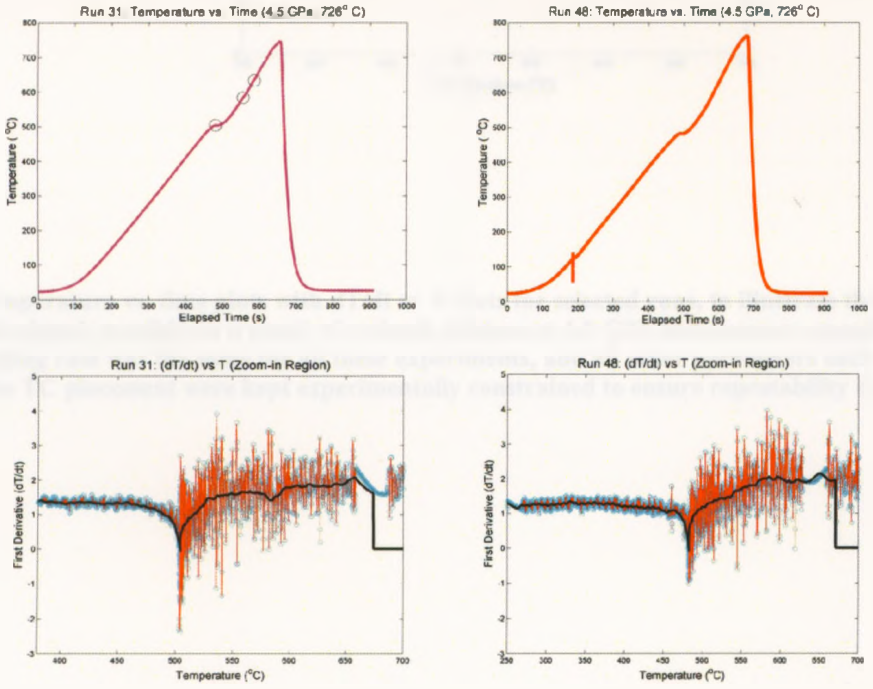

Figure A1.4: Temperature vs. time plots with dT/dt vs T plots for selected runs, to illustrate the deviation of the recorded melting signal, possibly as a result of a sharp minima at 4.5 GPa and pressure uncertainty around it. Notably, the heating rate was the same for all these experiments, and all other parameters such as the container geometry and the TC placement were kept experimentally constrained to ensure repeatability of results.

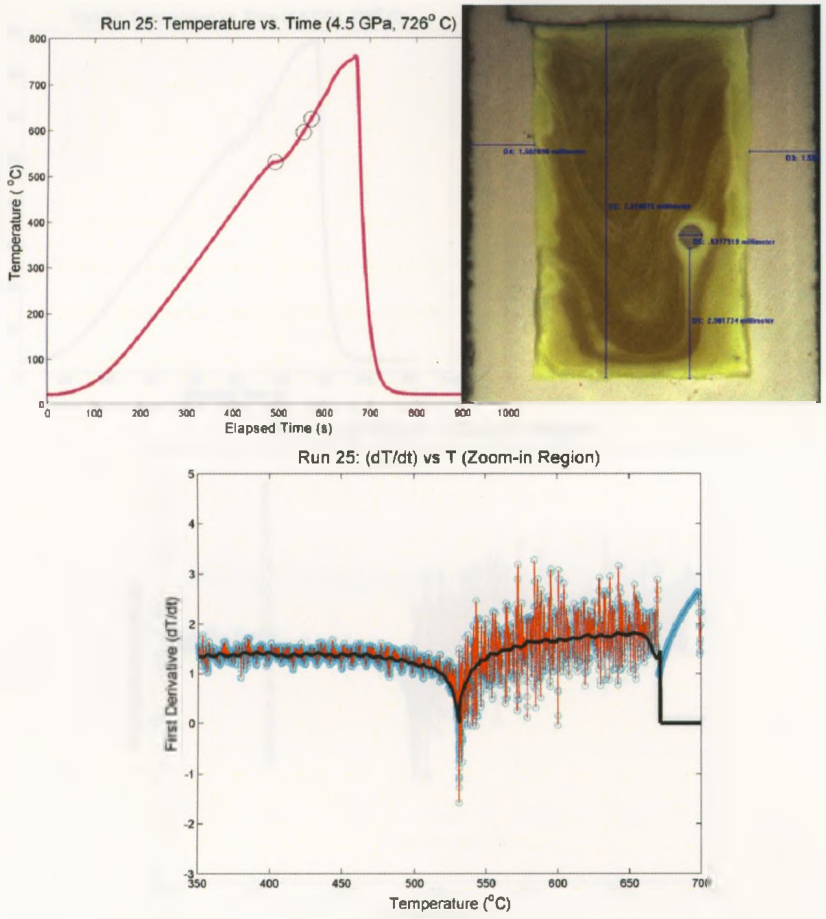

Figure A1.5: Temperature vs. time plots with dT/dt vs T plots for selected runs, to illustrate the deviation of the recorded melting signal, possibly as a result of a sharp minima at 4.5 GPa and pressure uncertainty around it. Notably, the heating rate was the same for all these experiments, and all other parameters such as the container geometry and the TC placement were kept experimentally constrained to ensure repeatability of results.

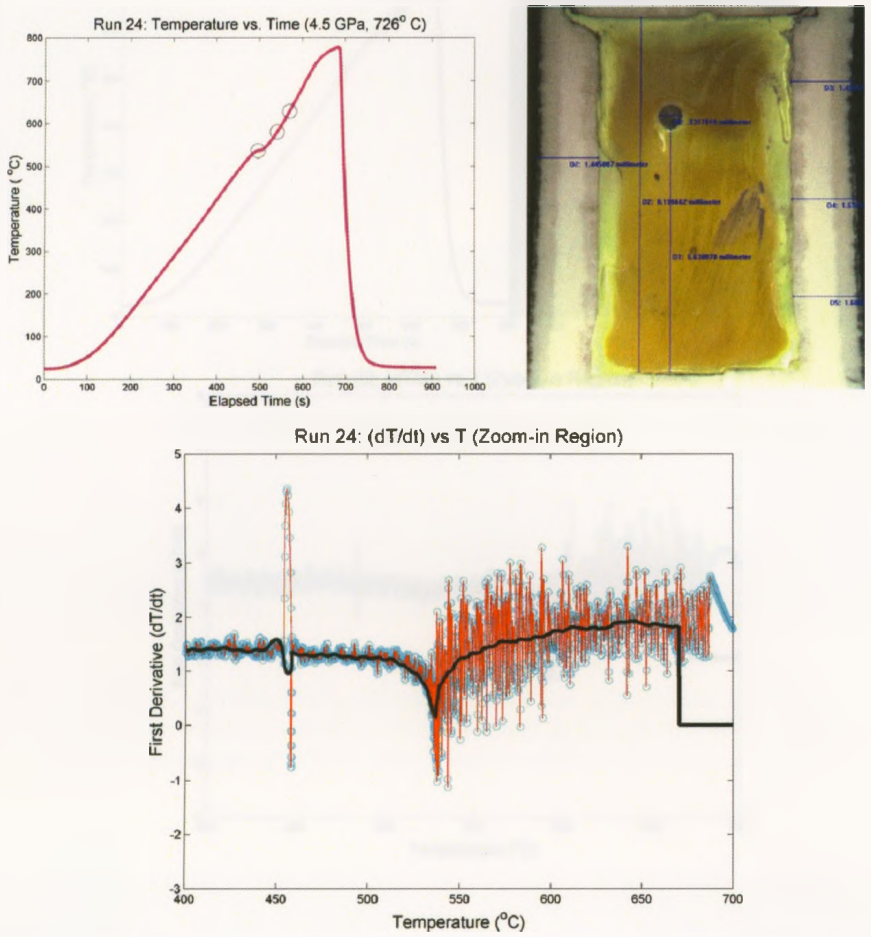

Figure A1.6: Temperature vs. time plots with dT/dt vs T plots for selected runs, to illustrate the deviation of the recorded melting signal, possibly as a result of a sharp minima at 4.5 GPa and pressure uncertainty around it. Notably, the heating rate was the same for all these experiments, and all other parameters such as the container geometry and the TC placement were kept experimentally constrained to ensure repeatability of results.

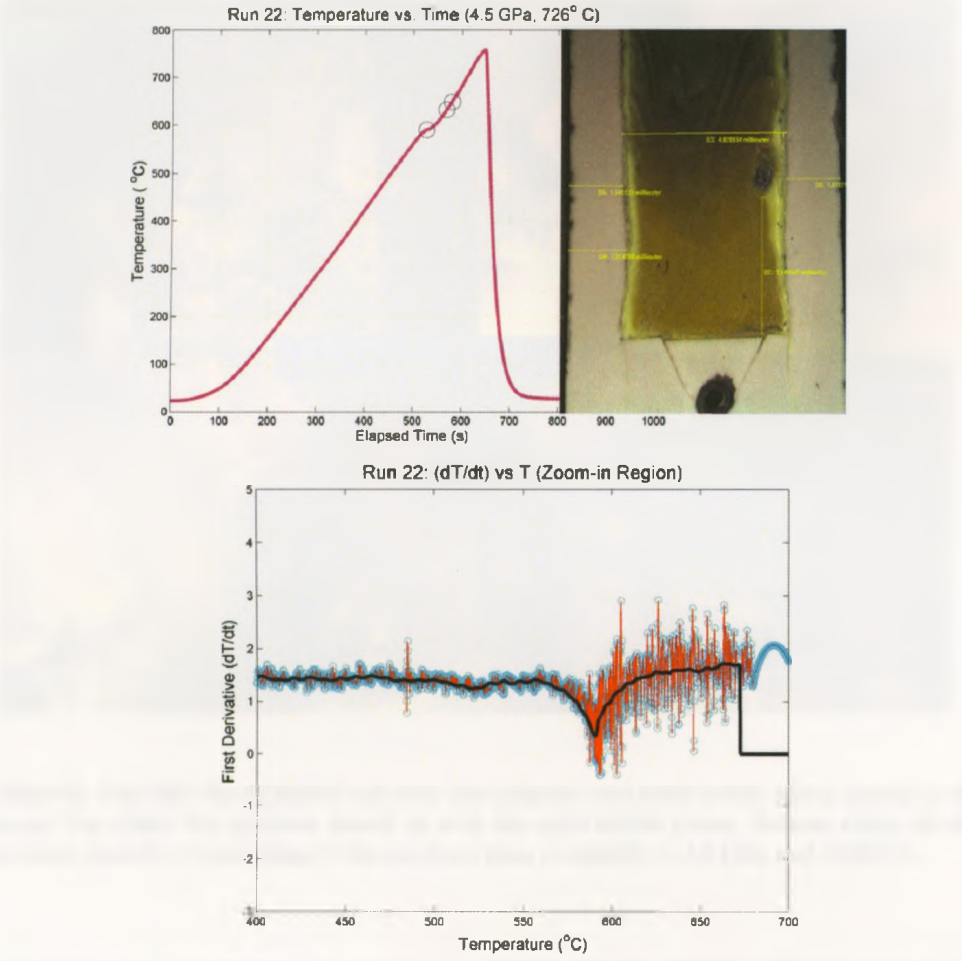

Figure A1.7: Temperature vs. time plots with dT/dt vs T plots for selected runs, to illustrate the deviation of the recorded melting signal, possibly as a result of a sharp minima at 4.5 GPa and pressure uncertainty around it. Notably, the heating rate was the same for all these experiments, and all other parameters such as the container geometry and the TC placement were kept experimentally constrained to ensure repeatability of results.

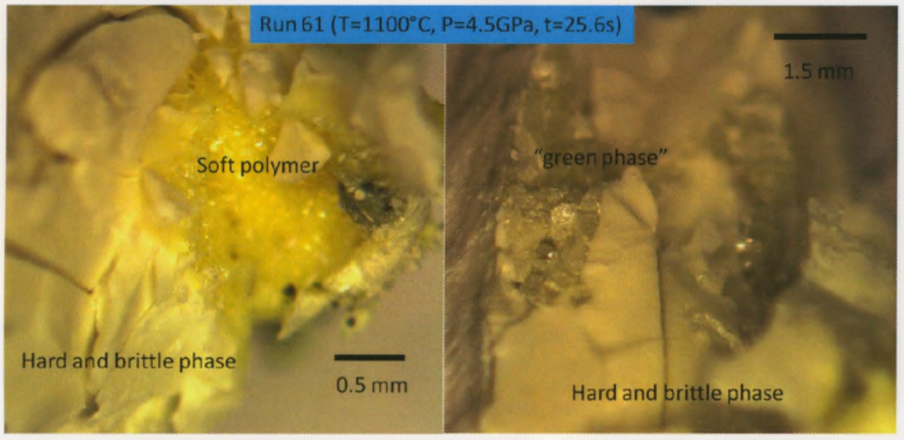

Figure A1.8: Photograph showing a clear separation of the distinct phases after 25.6 seconds. On the left there is clear separation of the hard and brittle phase and the polymer. On the right, there is a clear delineation between solid brittle and "green phase".

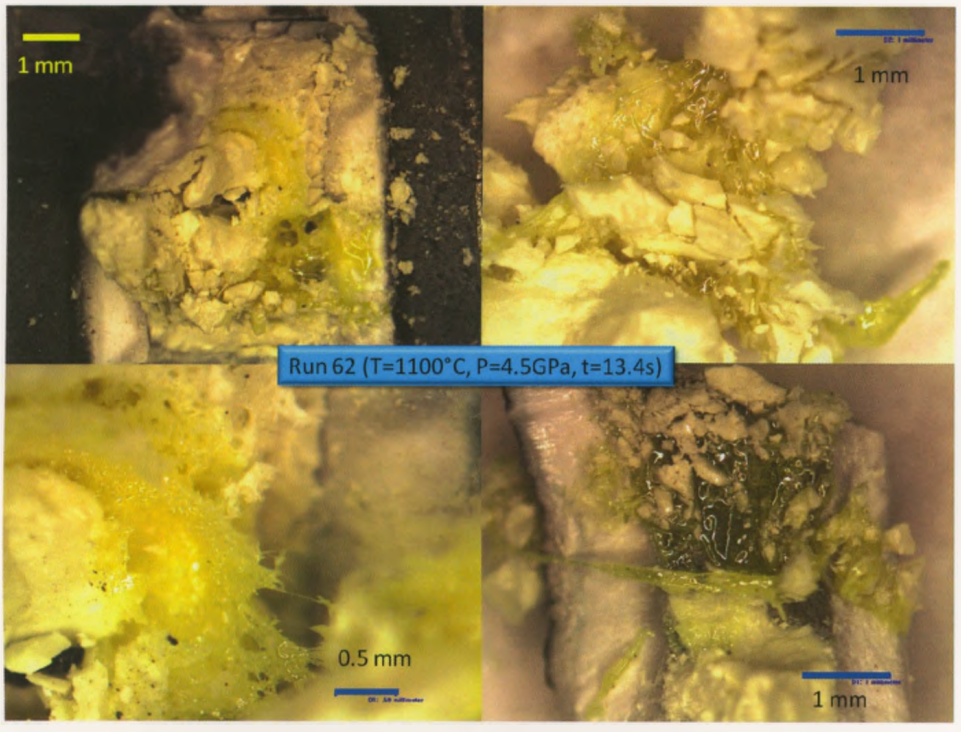

Figure A1.9: Run 65: Top left: the exploded cell with the polymer and solid brittle phase mixed in. Bottom left: polymer close-up. Top right: the polymer mixed in with the solid brittle phase. Bottom right: all three phases mixed together (note that the "green phase" did not have time to solidify at 4.5 GPa and 1100°C).

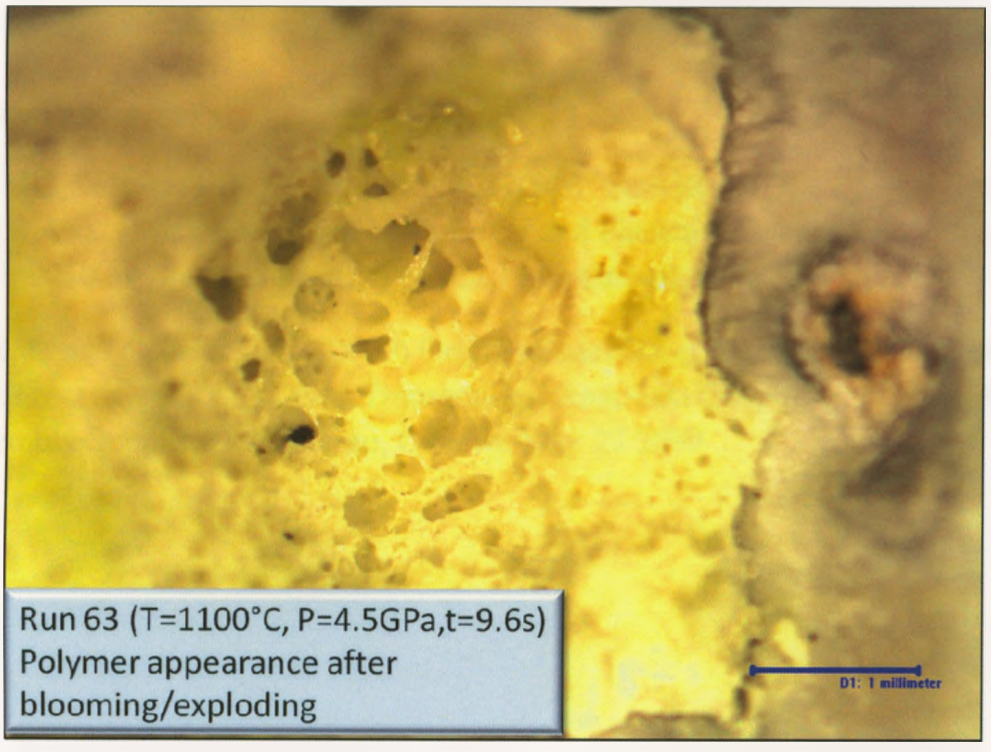

Figure A1.10: Photograph showing polymer appearance after the "explosion" (a violent expansion upon "opening" the cube).